

REDOX-ACTIVE LIGANDS AND CONDUCTING POLYMERS IN THE
ELECTROCHEMICAL CONTROL OF REACTIVITY

by

IVAN LORKOVIC

B.S., Grinnell College, Grinnell, Iowa
(1989)

SUBMITTED TO THE DEPARTMENT OF CHEMISTRY IN PARTIAL
FULFILLMENT OF THE REQUIREMENTS FOR THE DEGREE OF DOCTOR OF
PHILOSOPHY

at the

MASSACHUSETTS INSTITUTE OF TECHNOLOGY

February 1995

©Massachusetts Institute of Technology 1995

Signature of Author _____

Department of Chemistry
January 9, 1995

Certified by _____

Mark S. Wrighton
Thesis Supervisor

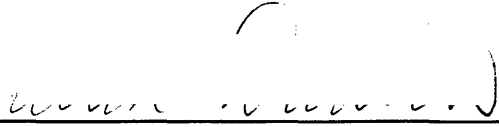
Accepted by _____

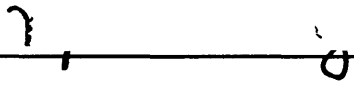
Dietmar Seyferth
Chairman, Departmental Committee on Graduate Students

Science
MASSACHUSETTS INSTITUTE OF TECHNOLOGY

FEB 11 1995

This doctoral Thesis has been examined by a Committee of the Department of
Chemistry as follows:

Professor Alan Davison  _____ Chairman

Professor Mark S. Wrighton  _____ Thesis Supervisor

Professor Richard R. Schrock  _____

Professor Christopher C. Cummins  _____

REDOX-ACTIVE LIGANDS AND CONDUCTING POLYMERS IN THE
ELECTROCHEMICAL CONTROL OF REACTIVITY

by

IVAN LORKOVIC

Submitted to the Department of Chemistry on January 9, 1994 in partial fulfillment of the
requirements for the Degree of Doctor of Philosophy in Chemistry

Abstract

Chapter 1.

Transition metal complexes of redox-active ligands are briefly reviewed. Important parameters in achieving redox control of reactivity are discussed, and the ligands used in this thesis compared with the properties of others in the literature.

Chapter 2.

The chelating ligand, 1,1'-bis(diphenylphosphino)-cobaltocene (dppc) is used as an electrochemically tunable ligand for altering electrophilicity of the carbonyl carbon in metal carbonyl complexes. The Re carbonyl complexes $[\text{Re}(\text{CO})_{4-n}(\text{CH}_3\text{CN})_n\text{dppc}]^{2+/+}$, $n = 0$ (*cis*), 1 (*fac*), 2 (*cis,cis*), and $[\text{fac-Re}(\text{CO})_3(\text{NCO})\text{dppc}]^{+/0}$ were prepared and characterized in both states of charge indicated. Single crystal X-ray crystallography was performed for both states of charge of $[\text{Re}(\text{CO})_4\text{dppc}]^{2+/+}$ with the oxidized and reduced forms crystallizing in the monoclinic space groups $C2/c$ and $P2_1/c$, respectively. The most pronounced structural difference between the two forms is the Cp-Co distance, which is 0.09 Å longer for the reduced form. Cyclic voltammetry shows that $E_{1/2}$ for the Co(III)/Co(II) couple is 200-400 mV more positive for coordinated dppc than for the free ligand. For each CO substituted, $E_{1/2}$ becomes ~100 or 200 mV more negative for substitution by CH_3CN or NCO^- , respectively. Solution IR spectroscopy shows that ν_{CO} for the oxidized form of each species is typically $\sim 15 \text{ cm}^{-1}$ higher than for the reduced form, but the number and relative intensities of the carbonyl absorptions is the same. In every redox pair the oxidized species has higher reactivity with respect to nucleophilic attack at the carbonyl carbon. In CH_3CN at 25.0 °C, $[\text{fac-Re}(\text{CO})_3(\text{CH}_3\text{CN})\text{dppc}]^{+2}$ reacts with amine-N-oxides $(\text{CH}_3)_3\text{NO}$, N-methylmorpholine-N-oxide, and $(\text{CH}_3)_2(\text{C}_6\text{H}_5)\text{NO}$ ~200 times faster than $[\text{fac-Re}(\text{CO})_3(\text{CH}_3\text{CN})\text{dppc}]^{+}$ to form $[\text{cis,cis-Re}(\text{CO})_2(\text{CH}_3\text{CN})_2\text{dppc}]^{+2/+}$, while $[\text{cis-Re}(\text{CO})_4\text{dppc}]^{+2}$ reacts with N_3^- 5400 times faster than $[\text{cis-Re}(\text{CO})_4\text{dppc}]^{+}$ to form $[\text{fac-Re}(\text{CO})_3(\text{NCO})\text{dppc}]^{+/0}$, with $\Delta\Delta H^\ddagger = 3-4$ kcal/mole in both cases. The ionic strength and dielectric strength dependence of the reactivity of $[\text{Re}(\text{CO})_4\text{dppc}]^{2+/+}$ towards N_3^- were assayed to investigate electrostatic contributions to the attenuation of reactivity of $[\text{Re}(\text{CO})_4\text{dppc}]^{2+/+}$ towards N_3^- caused by reduction of the dppc ligand.

Chapter 3.

The redox-active hydrogenation catalyst precursors $[\text{Rh}(\text{dppc})\text{NBD}]^{2+/+}$ (NBD=Bicyclo[2.2.1]hepta-2,5-diene, dppc = 1,1'-bis(diphenylphosphinocobaltocene), $\mathbf{1}_{\text{ox}}/\mathbf{1}_{\text{red}}$, $[\text{Rh}(\text{omdppf})\text{NBD}]^{2+/+}$ (omdppf = 1,1'-bis(diphenylphosphino)octamethylferrocene), $\mathbf{3}_{\text{ox}}/\mathbf{3}_{\text{red}}$, $[\text{Ir}(\text{dppc})(\text{COD})]^{2+/+}$ (COD = cycloocta-1,5-diene), $\mathbf{5}_{\text{ox}}/\mathbf{5}_{\text{red}}$, and $[\text{Ir}(\text{omdppf})(\text{COD})]^{2+/+}$, $\mathbf{6}_{\text{ox}}/\mathbf{6}_{\text{red}}$, have been synthesized and characterized by UV-Vis, NMR and electrochemistry. Single crystal X-ray crystallography was performed for $\mathbf{1}_{\text{red}}$ which crystallized in the orthorhombic space group

P212121 with R and $R_w = 6.2$ and 7.7% , respectively. **1** and **3** react with H_2 in acetone to give the “catalysts” $[Rh(dppc)(acetone)_n]^{2+/+}$, $2_{ox}/2_{red}$, and $[Rh(omdppf)(acetone)_n]^{2+/+}$, $4_{ox}/4_{red}$, respectively. 1_{ox} and 1_{red} catalyze NBD hydrogenation at roughly the same rate. 2_{red} catalyzes the hydrogenation and isomerization of olefins and ketones 1-2 orders of magnitude faster than 2_{ox} , while 2_{ox} catalyzes the hydrosilation of olefins and ketones about an order of magnitude faster than 2_{red} . All reaction rates are 0.5 order or less in catalyst, except for the hydrogenation of NBD. **1**, **3**, **5**, and **6** catalyzed olefin hydrogenation in CH_2Cl_2 , with both states of charge having the same rate within a factor of 2, the oxidized form of every redox pair being the more durable catalyst. 4_{ox} is reduced in acetone by H_2 and Et_3SiH to 4_{red} , which also catalyzes olefin hydrogenation and ketone hydrosilation. Preliminary results in the electrocatalytic oxidation of Et_3SiH by **4** are discussed.

Chapter 4

The reaction of electrode-confined polyaniline with trifluoroacetic anhydride in acidified acetonitrile giving insulating and electroinactive trifluoroacetylated polyaniline has been studied by electrochemistry, reflectance IR, and microelectrochemistry. Variation of electrochemical potential from 0.2 V (reduced, most reactive) to 0.6 V (oxidized by 0.5 electrons per repeat unit, unreactive) vs SCE allows control of the reaction rate. Reaction of trifluoroacetic anhydride with aniline oligomers *N*-phenylphenylenediamine and *N,N'*-diphenylphenylenediamine gave *N*-trifluoroacetylation products exclusively, exhibiting positive shifts in oligomer oxidation potential of > 0.5 V, with terminal amines reacting considerably faster than internal amines. Reflectance IR following the potential dependent growth of CO and CF_3 peaks for macroelectrode films of polyaniline treated with trifluoroacetic anhydride showed similar potential dependence of reactivity as conductivity measurements during trifluoroacetylation of polyaniline derivatized microelectrode arrays. Polyaniline trifluoroacetylation was accompanied by narrowing but no shifting of the potential window of electroactivity and conductivity, and eventual elimination of all conductivity. Trifluoroacetylation of polyaniline terminal amines, rapid at all potentials, does not detectably affect conductivity. IR through polyaniline electrodeposited onto optically transparent Au electrodes shows that essentially complete loss of polyaniline electroactivity occurs when $\approx 25\%$ of nitrogens are trifluoroacetylated. Electroactivity and conductivity of trifluoroacetylated polyaniline may be recovered by hydrolysis in $K_2CO_3/CH_3OH/H_2O$ solution to regenerate polyaniline.

Thesis Supervisor: Mark S. Wrighton

Title: Provost and CIBA-Geigy Professor of Chemistry

Acknowledgements

First I would like to acknowledge my coworkers for the work in this thesis, Ron Duff and Chris McCoy. Ron did a lot of the work reported in Chapter 3, and daily discussions with him were invaluable in determining what to do next and even more importantly, how to do it. As my thesis writing predecessors have noted, Ron is indispensable in the upkeep of most of the equipment in the laboratory. Ron also has an almost Shakespearean capacity to invent words. Chris McCoy did most of the work in Chapter 4. He has exquisite touch. Chris was also a great source of encouragement to me, especially the night and morning before orals propositions were due, when he taught me how to use Chemdraw. Godspeed in moving out to Palo Alto, Chris.

The Stubbe group, in particular Marty Bollinger and Wei Wu, should be acknowledged for providing stopped-flow instrumentation used for the rate measurements in Chapter 2.

Before the big move to the Wrighton group, Jon Bloch and I became close friends and continue to be. I hope he takes that job out at Sandia. Those calm, cold, bright days at Killington.

While in the Wrighton group, I had two perfect office mates. Tayhas Palmore, who approached lab work with the attitude and dress of a Commando (and she had *mellowed out*) and Dave Albagli "Al Davebagli", whose love for chemistry was hilarious at times; only to Dave could "10 grams of happiness" consist of a pure cobalticinium salt. Eric Wollman was a great help in my getting started, and later gave me the opportunity to work on some organic photochemistry. During my years in this lab I also had the pleasure of meeting Chuck Christ, who straightened me out when I needed it (more than once), and showed me how to catch a frisbee between my legs, Tim Oyer, who ran my first marathon with me, Chris Hable, who ran my second and third marathons with me, Doris Kang, who is pretty funny when she wants to be, and Steve Colbran, with whom it was great fun to do and discuss chemistry. Cheers!. My old roommates Dan Frisbie, who turned out to be a fantastic coworker and remained a good friend (that Stirling engine was cool). and Jon Come, who would drag me out of bed and give me a ride on the back of his bike like his little brother to morning ball, only to tackle me every time I had an open layup. Eric Lee's appreciation for the finer things in life was quite a relief. Eric has this talent.... Sam Gerritz appeared somewhere along the line and reminded me who I was, and made the middle few years here very bearable, and ran with Colin and me on his first marathon. I look forward to seeing him and his in the future. Just stay away from Updike. I'm going to miss Joel Gwynn, Colin Wolden and Annie Helgason, who have been good friends, and even better skiing partners. I wish Larry (I hope you keep calling them like you see them, I promise not to be so touchy when I'm finished with this thing), Maria, and Laura, good luck in finishing, although I'm sure they won't need it. Good luck also to Hiro Iwasaki, Albert Folch i Folch, Chris Peters, and Chris Weder. Helen! Thanks for all those warm fuzzies, and all that food (staggering amounts), too. More recently Joel Freundlich and Mike Fickes from the other labs up here in Building 6 have become good friends, and with them I've continued to explore the beautiful Boston metro area on foot. Moonrise over the Charles...

I have been lucky enough to see my family, my sister Maja, cousin Sonia, and mother Tatjana, and brother Radoslav on a regular basis while here in school. Lucky for Rad he had a place to crash in Cambridge.

Finally, I would like to thank Mark for taking me on 4 and a half years ago. I will look back on my situation here as ideal. You can't really ask for much more than a good project, good facilities (except for the lack of NIR capability in the department), and an unlimited budget. Most importantly, although it is sometimes harrowing, I am continuing to learn to respect and make the most of my freedom.

Biographical Note

Ivan Lorkovic was born November 29, 1966 in Minneapolis, Minnesota to Hrvoje and Tatjana Lorkovic, who had recently immigrated with their daughter Maja and older son, Radoslav from Zagreb, Croatia (Yugoslavia) via Tübingen and London. He grew up in Iowa City, Iowa, attending Hoover Elementary, South East Junior High, and City High School. He attended college at Grinnell in Grinnell, Iowa, where he was initiated to research in organometallic chemistry by Professor Rich Biagioni, whose rigorous teaching style suited him, and where he was encouraged to pursue chemistry as a career. He matriculated at MIT in the Physical Chemistry Division. After a year during which the seminars he enjoyed the most were the Inorganic ones he wasn't supposed to attend, he switched degree programs, joining the laboratory of Mark Wrighton, whose energy and applications oriented research program interested him, in Inorganic Chemistry. After four and a half years of thinking of different ways to contort ferrocene and cobaltocene, his liking for chemistry has survived. He is moving on to do more research on the west coast.

To my mother, Tatjana

Table of Contents

ABSTRACT.....	3
ACKNOWLEDGEMENTS	5
BIOGRAPHICAL NOTE.....	6
DEDICATION	7
TABLE OF CONTENTS	8
LIST OF FIGURES.....	10
LIST OF SCHEMES.....	13
LIST OF TABLES.....	14
CHAPTER 1 INTRODUCTION	15
Overview of Transition Metal Complexes with Redox-Active Ligands	16
References	22
CHAPTER 2 USE OF THE REDOX-ACTIVE LIGAND 1,1'-BIS(DIPHENYL- PHOSPHINO)COBALTOCENE TO REVERSIBLY ALTER METAL CARBONYL ELECTROPHILICITY	25
Introduction.....	26
Experimental.....	30
Results and Discussion.....	36
References	69
CHAPTER 3 USE OF REDOX-ACTIVE 1,1'-BIS(DIPHENYLPHOSPHINO)- METALLOCENE LIGANDS TO REVERSIBLY ALTER THE RATE OF RHODIUM(I) CATALYZED HYDROGENATION, HYDROSIL- ATION, AND ISOMERIZATION OF OLEFINS AND KETONES ..	72
Introduction.....	73
Experimental.....	76
Results and Discussion.....	83
References	116
CHAPTER 4 THE POTENTIAL DEPENDENT NUCLEOPHILICITY OF POLYANILINE	119
Introduction.....	120

Experimental.....	122
Results and Discussion.....	127
References.....	156

LIST OF FIGURES

Number	Page
<u>Chapter 2</u>	
Figure 1. Ortep diagram of 2_{ox} (a) and 2_{red} (b) with ellipsoids drawn at the 35% probability level. In (b) ellipsoids without octant shading represent carbon atoms, all of which were refined only isotropically.	38
Figure 2. UV/Visible spectral changes, acquired using stopped flow techniques, showing the reaction of 2_{red} (0.08 mM) with N_3^- (2 mM) to form 4_{red} (top) and reaction of 3_{red} (0.08 mM) with $(CH_3)_3NO$ (5 mM) to form 5_{red} (bottom) in CH_3CN at 25.0 °C showing that upon substitution of CO for less π -acidic ligands such as CH_3CN or NCO^- , the cobaltocene-based absorbance undergoes a hypsochromic shift. Presence of isosbestic points demonstrates absence of secondary reactions.....	48
Figure 3. Solution IR spectra in the carbonyl region for 2 , 3 , 4 and 5 , showing that the spectrum of the reduced form of all species is identical to the oxidized form except that all absorptions for the reduced species are $\sim 15\text{ cm}^{-1}$ lower in energy.	51
Figure 4. Eyring plot for the temperature-dependent rate of reaction between TMANO and 3_{ox} (open circles, left y-axis) and between TMANO and 3_{red} (filled circles, right y-axis) showing that reduction of the redox-active ligand induces an increase in the activation enthalpy of nucleophilic attack at the carbonyl carbon atom of 3	54
Figure 5. Eyring plot for the temperature dependent rate of reaction between N_3^- and 2_{ox} (open circles, left y-axis) and between N_3^- and 2_{red} (filled circles, right y-axis) showing that reduction of the redox-active ligand induces an increase in the activation enthalpy of nucleophilic attack at the carbonyl carbon atom of 2	59
Figure 6. Ionic strength dependence of the reaction between N_3^- and 2_{ox} (open circles) and N_3^- and 2_{red} (filled circles). Shown as solid line segments are ionic strength dependences for a bimolecular reaction between a cation and an anion and between a dication and an anion predicted by the Debye-Hückel Limiting Law in a medium having a dielectric strength of 36.7 at 25.0 °C.	62
Figure 7. Dielectric strength dependence of the reaction between N_3^- and 2_{ox} (open circles) and N_3^- and 2_{red} (filled circles) at 25.0 °C. For this figure the dielectric strength is decreased by addition of C_2H_5CN , and it is assumed that the dielectric strength of the mixture is linearly dependent on the volume percent of C_2H_5CN . The best fit slopes for 2_{ox} and 2_{red} are 354 and 321, corresponding to $d_{ab} = 3.16\text{ \AA}$ and 1.74 \AA respectively.	65
<u>Chapter 3</u>	
Figure 1. Ortep Diagram of 1_{red} shown with 35% probability ellipsoids. The carbon atoms, showing only principle ellipses, were refined only isotropically.	84

- Figure 2.** Hydrogenation of norbornadiene in acetone at 20.0 °C at a total pressure (H_2 + acetone) of 870 torr, catalyzed by 1_{ox} (3.6 mM, [NBD] = 0.23 M) and 1_{red} (4.5 mM, [NBD] = 0.58 M), followed by GC/MS. 90
- Figure 3.** Plot of the log of cyclohexene hydrogenation rate versus log of catalyst concentration in acetone at 20.0 °C catalyzed by 1_{ox} and 1_{red} 94
- Figure 4.** Hydrogenation of cyclohexane in acetone at 20.0 °C catalyzed by 4_{red} 96
- Figure 5.** Progress of the hydrogenation of cyclohexene in acetone at 20.0 °C catalyzed by a solution of 2 prepared from 0.044 mmol of 1_{red} . At 65 min and 125 min, 0.044 mmol of Fc^*PF_6 and cobaltocene are added, respectively. 98
- Figure 6.** Progress of the hydrogenation/isomerization of 1-pentene to pentane and cis and trans 2-pentene in acetone at 20.0 °C catalyzed by a solutions of 2_{red} prepared from 0.013 mmol of 1_{red} (top) and 2_{ox} prepared from 0.0095 mmol of 1_{ox} (bottom). After 146 min, 0.013 mmol of cobaltocene is added to the solution containing 2_{ox} and after 201 min 0.013 mmol of Fc^*PF_6 is added to the same solution.....100
- Figure 7.** Plot of the the log of isopropoxytriethylsilane formation rate on the concentration of 2_{ox} and 2_{red} at 20° C. with $[Et_3SiH] = 0.57$ M, showing 1/2 order dependence on $[2_{ox}]$108
- Figure 8.** Progress of the hydrosilation of neat acetone at 20.0° C catalyzed by 2 , prepared from 0.038 mmol of 1_{ox} . At 65 and 125 min, 0.038 mmol of cobaltocene and Fc^*PF_6 are added, respectively.110

Chapter 4

- Figure 1.** Cyclic voltammetry of polyaniline deposited onto flat gold electrodes ($\Gamma = 1 \times 10^{-6}$ moles of aniline cm^{-2}) before and after exposure to trifluoroacetic anhydride. The electrode at the top was held at 0.2 V vs SCE during exposure to trifluoroacetic anhydride while the bottom electrode was poised at 0.5 V vs SCE.129
- Figure 2.** Cyclic voltammetry and I_D - V_G characteristics for polyaniline deposited onto three adjacent electrodes on a microelectrode array before and after treatment of the derivatized array with 1.0 M trifluoroacetic anhydride in 0.2 M F_3CCO_2H / 0.1 M $LiClO_4$ / CH_3CN132
- Figure 3.** Reflectance IR spectra for electrodeposited polyaniline on flat Au electrodes over the course of exposure to 1.0 M trifluoroacetic anhydride in 0.2 M F_3CCO_2H / 0.1 M $LiClO_4$ / CH_3CN . The top electrode was poised at 0.2 V vs SCE, while the bottom electrode was poised at 0.4 V vs SCE. Spectral changes corresponding to nitrogen trifluoroacetylation can be seen in both spectra.135
- Figure 4.** Evolution of $-\log(R/R_0)$ for the reaction of polyaniline on Au electrodes with trifluoroacetic anhydride while poised at different potentials. The carbonyl band "absorbance" is shown as normalized to the absorbance of the unchanging polyaniline 818 cm^{-1} band.137
- Figure 5.** Plot of the rate of CO absorbance growth from Figure 4 versus polyaniline state of charge, in electrons per repeat unit. The polyaniline state of charge was

obtained by averaging the anodic and cathodic current of the dashed CV in Figure 3 integrated to the potentials at which the samples were held. It was assumed that the degree of oxidation after the second anodic wave is 1 electron per repeat unit. The dashed line is a hypothetical reaction rate which is linearly dependent on the polyaniline oxidation state.140

Figure 6. Peak carbonyl stretching frequency for polyaniline treated with trifluoroacetic anhydride as a function of extent of trifluoroacetylation. Data taken from results shown in Figure 4.146

Figure 7. RIR spectra following the hydrolysis of trifluoroacetylated polyaniline on flat Au electrodes, showing the regeneration of polyaniline.153

LIST OF SCHEMES

Number	Page
<u>Chapter 1</u>	
Scheme 1. Other examples of reversibly redox-active ligands.	18
<u>Chapter 2</u>	
Scheme 1. Redox switching of metal carbonyl electrophilicity.	26
Scheme 2. Molecular orbitals involved in a transition metal-CO bond.	27
Scheme 3. Synthesis of 1 , 2 , and 3	36
Scheme 4. Relative reactivity of 3_{ox} and 3_{red} with amine- <i>N</i> -oxides.	56
Scheme 5. Relative reactivity of 2_{ox} and 2_{red} with N ₃ ⁻	57
<u>Chapter 3</u>	
Scheme 1. Activation of Rh(I) reduction catalysts having dppe and omdppf ligands. Redox potentials are relative to E ⁰ (Fc ⁺ /Fc) = 0.39 V vs SCE.	73
Scheme 2. Difference between 1_{ox} and 1_{red} in catalysis of 1-hexene hydrosilation/isomerization.	104
Scheme 3. Catalytic properties of 2_{ox} versus 2_{red}	112
<u>Chapter 4</u>	
Scheme 1. Polyaniline oxidation states in acidic media.	120
Scheme 2. Reactivity of oligoanilines I and II with trifluoroacetic anhydride in 0.2 M trifluoroacetic acid/CH ₃ CN at 25.0 °C.	127
Scheme 3. Polyaniline microelectrochemical transistor.	131
Scheme 4. Proposed reaction sequence of polyaniline with trifluoroacetic anhydride in 0.2 M trifluoroacetic acid/0.1 M LiClO ₄ /CH ₃ CN.	144

LIST OF TABLES

Number	Page
--------	------

Chapter 2

Table 1. Key bond distances and angles in the crystal structures of 2_{ox} and 2_{red}	41
Table 2. Spectroscopic and electrochemical data in CH ₃ CN at 23±3 °C.	43
Table 3. Rate constants and activation parameters for the reaction between 3 and amine-N-oxides ^a in CH ₃ CN (T = 25-39 °C).	53
Table 4. Rate constants and activation parameters for the reaction between 2 and N ₃ ⁻ in CH ₃ CN (T = 25-39 °C).	58

Chapter 3

Table 1. Experimental details of X-ray crystallography of [(dppc)Rh(NBD)] ⁺ [PF ₆] (1_{red}).....	86
Table 2. Key features of the solid state structure of 1_{red}	88
Table 3. Rate data for hydrogenation (P _{total} = 870 torr) catalyzed by 1_{ox} and 1_{red} at 20 °C in acetone.	92
Table 4. Rate data for cyclohexene hydrogenation catalyzed by 1 , 3 , 5 , and 6 at 20 °C in CH ₂ Cl ₂	103
Table 5. Rate data for hydrosilation catalyzed by 2_{ox} and 2_{red} at 20° C.	106

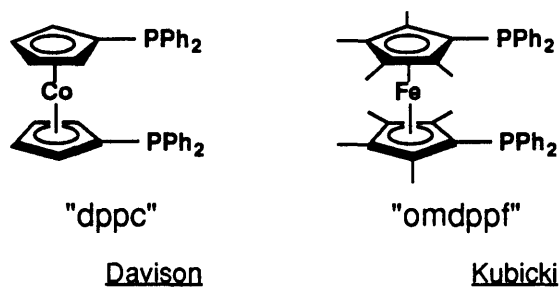
Chapter 4

Table 1. Electrochemistry of I-VI.	148
Table 2. X-Ray Photoelectron Spectroscopy Data for V , VI , and for polyaniline trifluoroacetylated at 0.2 V and 0.5 V vs SCE.	150

Chapter 1

Introduction

This thesis describes the use of electrochemistry to control the reactivity of transition metals and conducting polymers. Chapters 2 and 3 describe the use of redox-active chelating organometallic ligands 1,1'-bis(diphenylphosphino)cobaltocene, dppc,¹ and octamethyl-1,1'-bis(diphenylphosphino)ferrocene, omdppf,² to switch between two discrete states the electron density and reactivity of the metal to which they are bound.



The final chapter describes the state-of-charge dependent nucleophilicity of polyaniline, for which a continuum of charge states and reactivity states exists.

Just as the discovery of buckminsterfullerene, C₆₀, in 1985 sparked an enormous amount of work in the development of its materials chemistry, electrochemistry, superconductivity, ligand properties as cryptand or olefin, and even medicinal properties,³ organometallic chemistry experienced a similar burst of activity with the discovery of ferrocene⁴ and cobaltocenium⁵ in 1951 and 1952, respectively. Like C₆₀, the highly symmetrical ferrocene and cobaltocene enjoy stability in multiple states of charge and have at least one easily accessible redox process (Fe(II)/(III), Co(II)/(III)) which is accompanied by minimal structural change.⁶

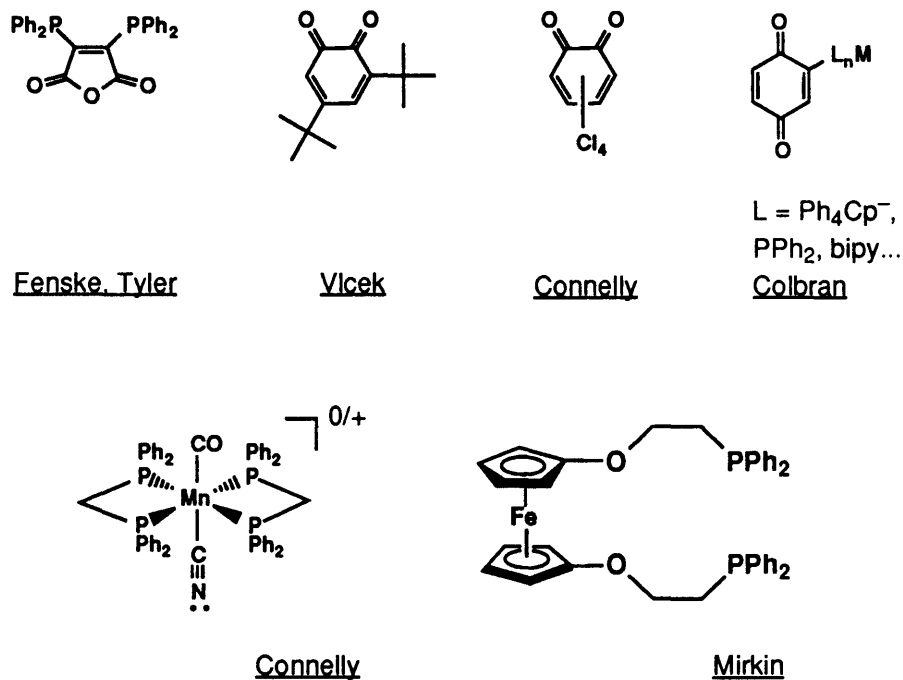
The synthesis and ligand properties of 1,1'-bisphosphinoferrocenes, such as the diphenyl derivative, dppf, were extensively developed by Davison and coworkers during the early 1970s.⁷ Previous workers in the Wrighton group have exploited the reversible electrochemistry of these ligands, and of other ferrocene based ligands, to tune the electron density of transition metals.⁸ The instability of the complexes when oxidized, however,

particularly that of the ferrocenium moiety, precluded isolation and charge-dependent reactivity characterization. Stability problems were overcome using the cobaltocene analogue dppc, which is an 18 electron species when oxidized and relatively robust when reduced, especially when tied up by a metal center, and the permethylated version of dppf, omdppf.

Besides stability in both states of charge, another critical factor in designing redox controllable transition metal complexes is the degree of electronic communication between reactive and redox sites. There are numerous methods for evaluating and quantifying such delocalization. ESR spectroscopy is a useful tool, since a SOMO is almost always formed for one of the states of charge of the assembly. For transition metals possessing nuclear spin or which have other atoms in their coordination sphere with nuclear spin, the magnitude of the hyperfine coupling constant in an ESR experiment indicates what percentage of the SOMO is located on those nuclei. Hush has developed a method based on UV-Vis-NIR spectroscopy to classify polyfunctional species according to the degree of coupling between redox centers based on electronic spectra according to the energy and intensity of charge transfer absorbances.⁹ Weakly interacting centers have low intensity charge transfer absorbances with the absorbance energy related to redox potentials of both centers. Electronic communication also perturbs the electronic properties of the free metal center and free ligand. The change in redox potential of the ligand upon binding is related to the coupling, although depending on the metal/ligand system a positive shift, a negative shift, or no shift at all may be observed. Conversely, and most characteristically for a transition metal carbonyl, and most importantly for the work in Chapter 2, the change in CO stretching frequency ($\Delta\nu_{\text{CO}}$) induced by ligand oxidation or reduction is directly proportional to the degree of communication. As demonstrated in Chapter 2, a relatively small $\Delta\nu_{\text{CO}}$ may lead to a large change in reactivity. All these properties are related. That is, if ESR shows large hyperfine coupling constant for a ligand based SOMO to a metal

nucleus, an intense charge transfer absorbance should be observed in the UV-Vis and, for metal carbonyls, a large positive $\Delta\nu_{\text{CO}}$ should be observed upon ligand oxidation.

Use of redox-active ligands to tune the electronic properties of transition metals is not new. A sampling (by no means exhaustive) of some types of redox-active ligands which have been developed and have seen use in the literature are shown in Scheme 1.



Scheme 1. Other examples of reversibly redox-active ligands.

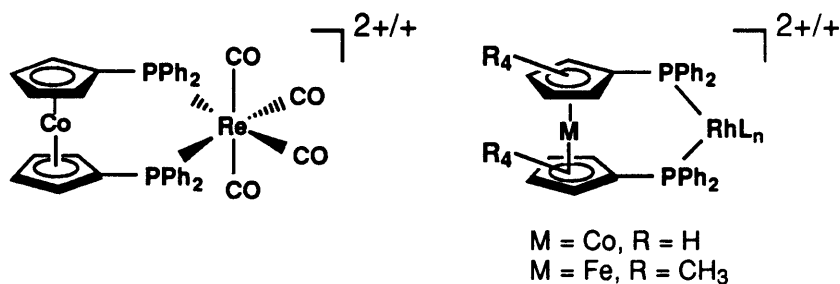
As mentioned above, Miller, Ahmed and Wrighton examined several different tethers of ferrocene to a Re(I)carbonyl chloride metal center and found that the most effective in transferring electron density away from Re by ferrocene oxidation was by direct bonding of a Cp carbon to Re, which induced a 25 cm^{-1} shift in the carbonyl stretching frequencies of the Re. Vlcek¹⁰ has performed many ESR and spectroelectrochemical studies of the commercially available chelating 3,5-*tert*-butylorthoquinones (Scheme 1) on Mn and Re carbonyls and found a high degree of ligand to metal communication, with up

to a $40 \text{ cm}^{-1} \Delta\nu_{\text{CO}}$ per electron, charge transfer absorbances having extinction coefficients greater than $5000 \text{ cm}^{-1}\text{M}^{-1}$, and positive shifts in the quinone/semiquinone/catechol redox potentials of 1.0 to 1.5 V upon ligand binding. Connelly¹¹ has seen similar behavior using orthochloranil as a ligand. Similarly, Fenske¹² has prepared a chelating phosphine based on maleic anhydride, further characterized by Tyler,¹³ which upon coordination to metal carbonyls forms species which have reversible ligand-based oxidations at 0.0 V vs SCE, or 0.7 V more positive than the free ligand, accompanied by $20\text{-}25 \text{ cm}^{-1} \Delta\nu_{\text{CO}}$. Although extinction coefficients were not reported for these species, they all display low energy solvatochromic absorbance (800nm for $\text{L}_2\text{Co}(\text{CO})_3$) when in the reduced state. As will be seen in the following chapter, the chelating dppc ligand on $\text{Re}(\text{CO})_4^+$ is shifted by 0.45 V positive of the free ligand, $\Delta\nu_{\text{CO}}$ observed upon ligand reduction is about 15 cm^{-1} , and the reduced complex shows an absorbance at 560 nm ($1000 \text{ M}^{-1}\text{cm}^{-1}$).

In a somewhat more complex system, Mirkin¹⁴ and coworkers have recently synthesized and structurally and electrochemically characterized Rh(I) complexes of redox-active hemilabile 2-ferrocenyldiphenylphosphinoethane, which upon oxidation change coordination from monomeric bis- O_2P_2 complexes to dimeric ($\eta^6\text{-arene-P}_2$) complexes with dangling oxyferrocenium groups. In this case communication between the redox center and the ligating oxygen renders the oxygen too weakly coordinating. Similarly, Colbran and coworkers, in addition to having studied the oxidation state dependent structure of ferrocenylcarbyne tricobaltnonacarbonyl clusters,¹⁵ have prepared a variety of transition metal complexes of ligands containing a quinone moiety, such as tetraphenylquinonylcyclopentadienide, 5-quinonylphenanthroline and diphenylquinonylphosphine.¹⁶ Unlike the redox-active chelating phosphines, or orthoquinones above, reduction and oxidation does not appreciably affect electron density of the metal center by inductive or resonance withdrawing or donating effects, but, in reverse of Mirkin's observations for the behavior of hemilabile ligands, the reduced quinone moiety may in some cases attack the metal center nucleophilically, thus directly

altering the coordination sphere. There are numerous other examples of the assembly of redox-active ligand/transition metal assemblies, the most notable of which include crystallographic characterization of the complex in two states of charge.¹⁷

The two organometallic systems we chose for the study of electrochemical control of reactivity are on opposite poles of transition metal reactivity, Scheme 2. In the first case we



Scheme 2. Redox-active ligand-transition metal assemblies for the study of redox induced change in reactivity.

study the state of charge dependent carbonyl carbon electrophilicity of $[\text{dppcRe}(\text{CO})_4]^{2+}$, a system that is as well defined and inert as any organometallic species, rhenium being perhaps the most inert transition metal. One goal of Chapter 2 is to develop a correlation between $\Delta\nu_{\text{CO}}$ and $\Delta\Delta H^\ddagger$ for the reaction with nucleophiles. The substitutional inertness of Re is important in this case because the interest is only in the rate of nucleophilic attack at carbon. The structure of the reacting species at the rate determining step is well defined. In contrast, in Chapter 3, we measure the changes in hydrogenation and hydrosilation catalyst properties of two states of charge of Rh(I) complexes of dppc and omdppf, rhodium perhaps being the most labile transition metal. The structure of the catalyst at the turnover limiting step of the process is much less defined and the lability is necessary for catalytic activity.¹⁸

In Chapter 4, the potential dependent reactivity of polyaniline with the electrophile trifluoroacetic anhydride is described. Unlike the Re and Rh cases studied above, which have only two states of charge and reactivity, ligand oxidized or ligand reduced, polyaniline

has access to a continuum of charge states corresponding to a continuum of reactivity states.

References.

1. (a) Rudie, A. W.; Lichtenberg, D. W.; Katcher, M. L.; Davison, A. *Inorg. Chem.* **1978**, *17*, 2859. (b) Dubois, D. L.; Eigenbrot, C. W., Jr.; Miedaner, A.; Smart, J. C.; *Organometallics* **1986**, *5*, 1405.
Trouve, G.; Broussier, R.; Gautheron, B.; Kubicki, M. M. *Acta Cryst.* **1991**, *C47*, 1966.
See, for example, *Acc. Chem. Res.* **1992**, *25*, 98-175. (the entire issue and references therein)
4. (a) Kealy, T. J.; Pauson, P. J. *Nature* **1951**, *168*, 1039. (b) Miller, S. A.; Tebboth, J. A.; Tremaine, J. F. *J. Chem. Soc.* **1952**, 632.
5. Wilkinson, G.; Rosenblum, M.; Whiting, M. C.; Woodward, R. B. *J. Am. Chem. Soc.*, **1952**, *74*, 2125.
6. Arnaud J. *Acc. Chem. Res.* **1979**, *12*, 401.
7. (a) Bishop, J. J.; Davison, A. *Inorg. Chem.* **1971**, *10*, 826. (b) (a) Bishop, J. J.; Davison, A. *Inorg. Chem.* **1971**, *10*, 832. (c) Bishop, J. J.; Davison, A.; Katcher, M. L.; Lichtenberg, D. W.; Merrill, R. E.; Smart, J. C. *J. Organomet. Chem.* **1971**, *27*, 241.
8. Miller, T. M.; Ahmed, K. J.; Wrighton, M. S. *Inorg. Chem.* **1989**, *28*, 2347.
9. Hush, N. S. *Adv. Inorg. Chem.* **1967**, 391.
10. (a) Hartl, F.; Vlcek, A., Jr.; deLearie, L. A.; Pierpont, C. G. *Inorg. Chem.* **1990**, *29*, 1073. (b) Hartl, F.; Vlcek, A., Jr. *Inorg. Chem.* **1991**, *30*, 3048. (c) Hartl, F.; Vlcek, A., Jr. *Inorg. Chem.* **1992**, *31*, 2869. (d) Hartl, F.; Vlcek, A., Jr. *Inorg. Chim. Acta* **1992**, *192*, 25.
11. (a) Carriedo, C.; Connelly, N. G. *J. Organomet. Chem.* **1991**, *403*, 359. (b) Atkinson, F. L.; Christofides, A.; Connelly, N. G.; Lawson, H. J.; Lowyns, A. C.; Orpen, A. G.; Rosair, G. M.; Worth, G. H. *J. Chem. Soc., Dalton Trans.* **1993**, 1441. (c) Carriedo, G. A.; Connelly, N. G.; Perez-Carreno, E.; Orpen, A. G.; Rieger, A. L.;

- Rieger, P. H.; Riera, V.; Rosair, G. M. *J. Chem. Soc., Dalton Trans.* **1993**, 3103. (d) Bardaji, M.; Brown, N. C.; Connelly, N. G.; Davies, R.; Orpen, A. G.; Rosair, G. M.; Seear, N. R. *J. Organomet. Chem.* **1994**, 474, C21.
12. Fenske, D. *Chem. Ber.* **1979**, 112, 363.
13. (a) Mao, F.; Tyler, D. R.; Keszler, D. *J. Am. Chem. Soc.* **1989**, 111, 130. (b) Mao, F.; Philbin, C. E.; Weakley, T. J. R.; Tyler, D. R. *Organometallics* **1990**, 9, 1510. (c) Mao, F.; Sur, S. K.; Tyler, D. R. *Organometallics* **1991**, 10, 419. (d) Mao, F.; Tyler, D.; Rieger, A. L.; Rieger, P. H. *J. Chem. Soc., Faraday Trans.* **1991**, 87, 3113. (e) Tyler, D. R. *Acc. Chem. Res.* **1991**, 24, 325. (f) Mao, F.; Tyler, D. R.; Bruce, M. R. M.; Bruce, A.; Rieger, A. L.; Rieger, P. L. *J. Am. Chem. Soc.* **1992**, 114, 6418. (f) Avey, A.; Schut, D. M.; Weakley, T. J. R.; Tyler, D. R. *Inorg. Chem.* **1993**, 32, 233.
14. (a) Allgeier, A. M.; Singewald, E. T.; Mirkin, C. A.; Stern, C. L. *Organometallics* **1994**, 13, 2928. (b) Singewald, E. T.; Mirkin, C. A.; Stern, C. L. Submitted.
15. (a) Colbran, S. B.; Robinson, B. H.; Simpson, J. *J. Chem. Soc., Chem. Commun.* **1982**, 1361. (b) Colbran, S. B.; Robinson, B. H.; Simpson, J. *Organometallics* **1983**, 2, 943. (c) Colbran, S. B.; Robinson, B. H.; Simpson, J. *Organometallics* **1983**, 2, 952. (d) Colbran, S. B.; Robinson, B. H.; Simpson, J. *Organometallics* **1984**, 3, 1344. (e) Colbran, S. B.; Robinson, B. H.; Simpson, J. *Organometallics* **1985**, 4, 1594. (f) Colbran, S. B.; Hanton, L. R.; Robinson, B. H.; Robinson, W. T.; Simpson, J. *J. Organomet. Chem.* **1987**, 330, 415.
16. (a) Colbran, S. B.; Craig, D. C.; Sembiring, S. B. *Inorg. Chim. Acta* **1990**, 176, 225. (b) Colbran, S. B.; Craig, C. C.; Harrison, W. M.; Grimley, A. M. *J. Organomet. Chem.* **1991**, 408, C33. (c) Berthon, R. A.; Colbran, S. B.; Craig, D. C. *Polyhedron* **1992**, 11, 243. (d) Sembiring, S. B.; Colbran, S. B.; Hanton, L. R. *Inorg. Chim. Acta* **1992**, 202, 67. (e) Berthon, R. A.; Colbran, S. B.; Moran, G. M. *Inorg. Chim. Acta* **1993**, 204, 3. (f) Saadeh, C.; Colbran, S. B.; Craig, D. C.; Rae, A. D. *Organometallics*, **1993**, 12, 133. (g) Colbran, S. B.; Harrison, W. M.; Saadeh, C.

Organometallics, **1994**, *13*, 1061. (h) Sembiring, S. B.; Colbran, S. B.; Craig, D. C.

Accepted for publication as a Communication in *Inorg. Chem.*

17. Sato, M.; Shintate, H.; Kawata, Y.; Sekino, M. *Organometallics* **1994**, *13*, 1956.

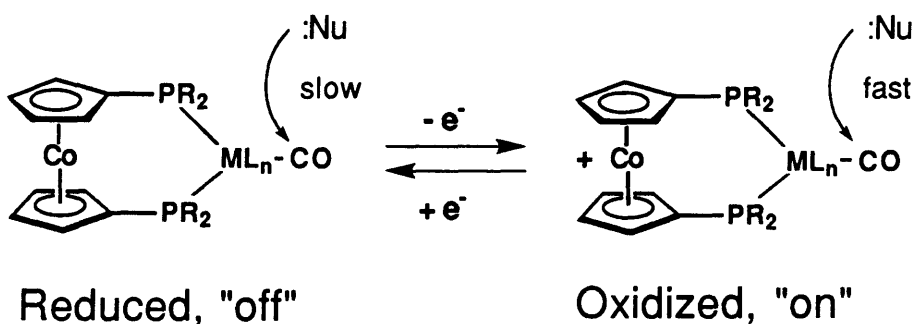
18. Collman, J. P.; Hegedus, L. S.; Norton, J. R.; Finke R. G. *Principles and Applications of Organotransition Metal Chemistry*. 1987, University Science Books, Mill Valley, CA.

Chapter 2

Use of a Redox-Active Ligand to Reversibly Alter Metal Carbonyl Electrophilicity

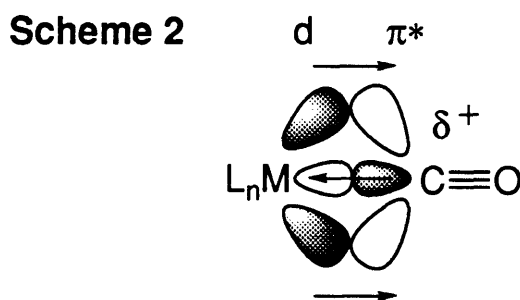
This chapter describes the synthesis, characterization, and reactivities of rhenium carbonyl derivatives of the reversibly redox-active chelating ligand 1,1'-*bis*(diphenylphosphino)cobaltocene (dppc). It is shown that the carbonyl carbon atoms are much more electrophilic when the ligand is oxidized. The results of this chapter illustrate the concept that electroactive ligands can be used to control reactivity of the moiety to which they are bound, Scheme 1.

Scheme 1



Reversibly redox-active centers in complex molecules have found use in a number of areas in chemistry, ranging from electrochemical sensing of small molecules¹ and ions,^{2,3} where the redox potential of the ligand changes upon binding of the analyte, to the development of molecular electrocatalysts for multielectron redox processes, such as the four electron reduction of oxygen to water,⁴ for which the electroactive ligands serve to store and deliver electrons to the catalytic site. More recently, use of electroactive ligands to alter binding properties has received attention. Association constants between cationic guests and ferrocene derived aza-crown ether hosts decrease several orders of magnitude upon oxidation of the host to ferrocenium.² Rate and product distribution of homogeneous Rh and Ir catalyzed reduction/isomerization of unsaturated functionality can be controlled by changing the state of charge of chelating metallocene-based phosphine ligands.⁵ For all these functions a high degree of communication between reactive and redox sites is important.

Carbon monoxide is remarkable as a ligand in its π acidity and capacity to act as an electronic "buffer" to stabilize metals in low oxidation states. The carbonyl stretching frequency (ν_{CO}) for terminally bound CO is observed anywhere from $\sim 2200 \text{ cm}^{-1}$ for electron-poor complexes to 1600 cm^{-1} for highly electron-rich ones, ranging over a full unit of apparent bond order. The carbon atom of CO bound to transition metals can be electrophilic,⁶⁻¹² more so for metal carbonyls with higher ν_{CO} .^{7,10} These trends are understood in terms of the degree of π back-donation from metal-d to CO- π^* orbitals. Increased d to π^* " π -backbonding" decreases carbon electrophilicity and ν_{CO} , Scheme 2.



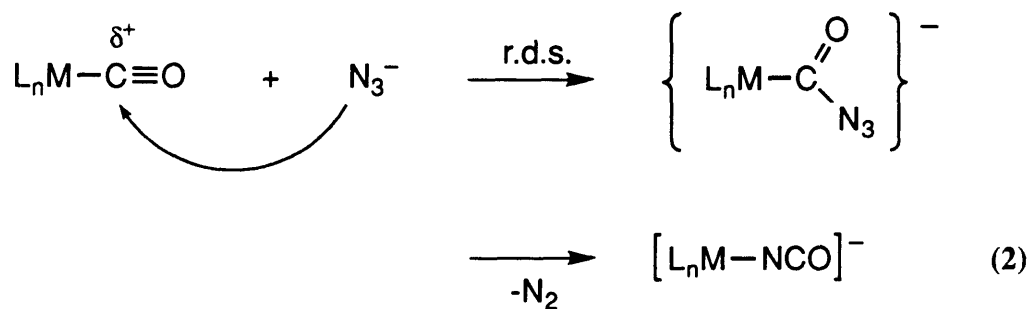
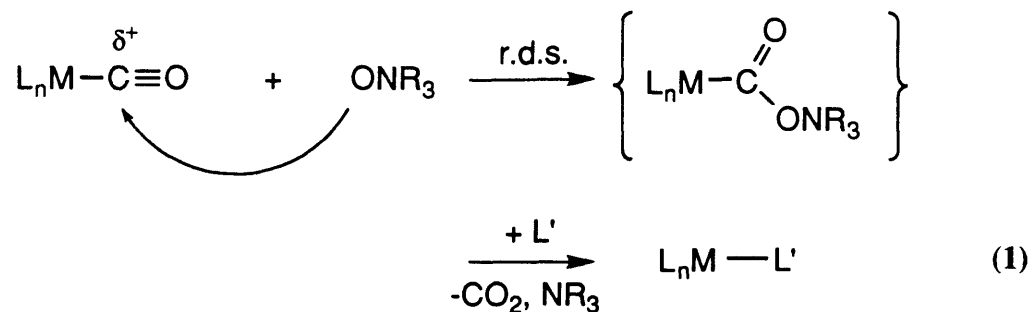
There is evidence that carbonyl carbon electrophilicity and ν_{CO} can be electrochemically tuned. Wrighton and Weaver have observed that in electrolyte solution, ν_{CO} for terminally bound CO on Pt electrodes increases in a linear fashion with the potential applied to the electrode.^{13a,b} Spectroelectrochemistry performed on high-nuclearity $Pt_n(\text{CO})_m$ clusters mirrors this behavior in a series of up to 10 discrete states of charge.^{13c} The electrophilicity of the carbonyl carbon in both of these cases changes accordingly with potential as shown by the fact that in aqueous media at high potentials and more positive states of charge electrode/cluster bound CO undergoes nucleophilic attack by water followed by electrooxidation to CO_2 .¹⁴

Previous workers in this group and others have shown that ν_{CO} of transition metal carbonyl complexes with ligands containing electroactive ferrocene moieties can be reversibly increased by up to 25 cm^{-1} in a one electron oxidation of ferrocene.¹⁵ As has been shown for CO bound to a Pt electrode, a potential dependent continuous range of CO

stretching frequencies has been demonstrated for metal carbonyl derivatives covalently bound to electrochemically polymerized thiophene derivatives incorporating a metal binding pyridine group, with ν_{CO} increasing with potential as charge is drawn out of the polymer.¹⁶

A quantitative correlation between ν_{CO} and reactivity with respect to nucleophilic attack at the CO carbon has been obtained for a series of tungsten carbonyl derivatives containing phosphines of varying basicity.^{10b} This type of correlation could also be established or tested by use of an electroactive ligand which provides an electrochemical means to a change in ligand donating ability and ν_{CO} . Cobaltocene derived phosphines¹⁷ are ideal electroactive ligands for such a study because cobaltocene derivatives can be durable in two states of charge in nucleophilic media. Thus, ligand decomposition should not interfere with measurements of CO reactivity. Furthermore, cobaltocene derivatives undergo minimal steric change upon oxidation, so that any change in reactivity observed will not likely be due to some change in the geometry of the complex leading a more or less sterically hindered transition state, but rather will only reflect changed orbital energetics or electrostatic effects.

Amine-N-oxides and N_3^- are good nucleophiles for performing reactivity studies with metal carbonyls because they react selectively and irreversibly with metal bound CO following a second order rate law consistent with a bimolecular mechanism, as shown in equations (1) and (2).^{9,11,12}



The rate determining step in both cases is thought to be nucleophilic attack at the carbonyl carbon atom. R_3NO yields an open coordination site, R_3N , and CO_2 while azide yields the metal isocyanate and N_2 . This chapter establishes that dppc can be used as an electrochemically tunable ligand to control electrophilicity (toward N_3^- and R_3NO) of the cationic Re(I) carbonyl moiety to which it is bound.

Experimental

Unless otherwise stated, all air sensitive procedures were carried out under an Ar atmosphere using standard Schlenk techniques or in a Vacuum Atmospheres drybox. CH₂Cl₂ and C₂H₅CN were distilled from P₂O₅. THF and Et₂O were heated under reflux over Na/benzophenone until purple and then distilled. Diglyme and CH₃CN were Aldrich Sureseal. [*n*-Bu₄N]PF₆ (Aldrich) was recrystallized twice from MeOH and dried *in vacuo* overnight at 120 °C. [*n*-Bu₄N]N₃ (American Tokyo Kasei), was dried in vacuo overnight at 80 °C. (CH₃)₃NO was purchased (Aldrich) as the dihydrate, dried by Dean Stark techniques and sublimed. N-methylmorpholine-N-oxide (Aldrich) was sublimed. N,N-dimethylaniline-N-oxide was prepared by literature techniques¹⁸ and purified by sublimation followed by recrystallization from dry CH₂Cl₂/Et₂O.

NMR spectra were recorded on either a Bruker 250MHz or Varian 300 MHz spectrometers using deuterated solvents at 25 ± 5 °C. All chemical shifts are given in ppm relative to TMS. Solution IR spectra were obtained in sealed CaF₂ or NaCl cells (0.2 or 0.1mm) on a Nicolet 60sx FTIR spectrometer with 2 cm⁻¹ resolution. Elemental analyses were performed by Galbraith Laboratories, Knoxville, TN and Schwartzkopf Laboratories, Woodside, NY. X-ray crystallography was performed on an Enraf-Nonius CAD-4 diffractometer at either ambient conditions (**2_{ox}**) or at 201 K under N₂ (**2_{red}**) and solved by direct methods. Electronic absorption spectra were recorded on a Hewlett-Packard 8452a diode array spectrophotometer. Electrochemical measurements were performed using a Pine Instruments model RDE-4 potentiostat with a Kipp and Zonen XY recorder, in a 0.1 M CH₃CN solution of [*n*-Bu₄N]PF₆ with Ag wire, Pt flag, and Pt gauze as quasi-reference, working, and counter electrodes, respectively. Ferrocene was added as an internal reference. Electrodes were cleaned by dipping in a freshly prepared solution of “piranha etch” (1 part 30% aqueous H₂O₂ and 3 parts concentrated H₂SO₄. **Caution**, strong oxidizer! Explosion hazard!), rinsing consecutively in H₂O and CH₃CN, and blowing dry.

Reaction rates of 2_{red} with N_3^- and 3 with amine-N-oxides were measured using an Applied Photophysics RX1000 Rapid Kinetics Accessory stopped flow apparatus interfaced to the spectrophotometer and a Lauda RC-6 constant temperature bath. The temperature was allowed to equilibrate for at least 15 min after the constant temperature bath had reached the desired temperature. For all reduced species, the drive syringes of the stopped flow apparatus were loaded in the dry box after having degassed the apparatus under active vacuum in the drybox antechamber for at least 12 h. The constant temperature bath was purged with Ar for at least 30 min prior to connection of the bath hoses to the stopped flow apparatus and for the duration of the experiment. Rates were measured at different temperatures in a random progression. The plots of $|A_t - A_\infty|$ versus time were fit for at least three half-lives ($R > 0.995$) using commercial spreadsheet exponential least-squares fitting software.

The reaction of 2_{ox} (typically 10-20 mM) with N_3^- (210-1000 mM) was followed using an Applied Photophysics DX-17 stopped flow apparatus which fit the absorbance rise curve for at least three half-lives ($R > 0.995$, except for the fastest rates measured (low ionic strength data at $T > 33$ °C or low dielectric strength data: $V(\text{C}_2\text{H}_5\text{CN}) \geq 20\%$), for which $R > 0.95$) at 254 nm upon acquisition. The reaction between 2_{red} (50-100 mM) and N_3^- (1000-3500 mM) was followed using the difference of average absorbances between 300 and 460 nm (rise) and between 500 and 650 nm (decay). The reaction between 3_{ox} (10-20 mM) and the aliphatic amine-N-oxides (500-2500 mM) was followed using the difference of the average absorbances between 234 and 246 nm (decay) and between 250 and 300 nm (rise), and for N,N-dimethylaniline-N-oxide, monitoring only the rise between 250 and 300 nm. The same reaction involving 3_{red} (100-150 mM, $[\text{R}_3\text{NO}] = 5\text{-}25$ mM) was followed, employing a 320 nm cutoff filter to protect the photosensitive solution, by monitoring the difference in the average absorbances between 390 and 460nm (rise) and between 480 and 600 nm (decay). For all reactions, the concentration of N_3^- or amine-N-oxide used was at least 20 times the concentration of 2 or 3 .

Syntheses.

1,1'-bis(diphenylmethylphosphonium)cobaltocenium triflate. To a solution of $\text{dppcCF}_3\text{SO}_3$ (200 mg, 0.28 mmol, prepared from the FcCF_3SO_3 oxidation of dppc), in CH_2Cl_2 (2 ml), was added $\text{CH}_3\text{OSO}_2\text{CF}_3$ (170 mg, 1.0 mmol). After allowing the solution to stir overnight, the solution was evacuated and recrystallized from $\text{CH}_2\text{Cl}_2/\text{diethyl ether}$. $^1\text{H-NMR}$, δ in acetone- d_6 : 8.00, m (12H); 7.80, m (8H); 6.62 q (4H, $J = 2.1$ hz); 6.42 q (4H, $J = 2.1$ hz); 3.31, d (6H, $J = 14.1$ hz).

[*fac*- $\text{Re}(\text{CO})_3(\text{dppc})\text{Br}$] PF_6 (1). Diglyme (15 ml) was added to a flask charged with $\text{Re}(\text{CO})_5\text{Br}$ (406 mg, 1.00 mmol) and 1,1'-bis(diphenylphosphino)cobaltocenium hexafluorophosphate ($[\text{dppc}]\text{PF}_6$)¹⁷ (702 mg, 1.00 mmol) and a magnetic stir bar. The contents were then heated at 105 °C while stirring until CO evolution stopped (~30 min). After cooling, the precipitated lighter yellow solid (940 mg, 90%) was collected by filtration in air and rinsed with Et_2O . $^1\text{H-NMR}$, δ in acetone- d_6 : 5.87 br (2H); 6.02 br (2H); 6.20 br (2H); 6.80 br (2H); 7.5-7.8 m (20H).

[*cis*- $\text{Re}(\text{CO})_4(\text{dppc})$] $[\text{PF}_6]_2$, 2_{ox} . Under a CO atmosphere, CH_2Cl_2 (20 ml) was added with stirring to a flask charged with **1** (500 mg, 0.47 mmol) and AgPF_6 (500 mg 2 mmol), forming a lemon yellow suspension. Stirring was continued under CO (1.2 atm) for 4 h. Solvent was removed *in vacuo*, CH_3CN added and the suspension filtered to remove AgBr . The CH_3CN was removed *in vacuo* and CH_2Cl_2 added to the yellow residue, inducing crystallization. The supernatant was decanted and the solid rinsed twice more with CH_2Cl_2 , the supernatant and rinsings saved. Analytically pure lemon yellow needles of 2_{ox} were obtained by dissolution in a minimum of CH_3CN , filtration through a pipette containing celite, addition of two volumes of CH_2Cl_2 , and slow diffusion of 10 volumes of Et_2O added carefully over the top. The solvent was removed from the previously saved supernatant and the residue recrystallized as described above. (overall yield ca. 50%). $^1\text{H-NMR}$, δ in acetone- d_6 . 6.33 br (4H), 6.40 br (4H), 7.75 m (20H). Elemental Analysis. Calculated C, 39.84; H, 2.46. Found C, 40.13; H, 2.59.

[*cis*-Re(CO)₄(dppc)]PF₆ (2_{red}**). In the drybox, a solution of cobaltocene (10 mg, 0.053 mmol) in CH₂Cl₂ (2 ml) was added dropwise to a stirred suspension of **2_{ox}** (63 mg, 0.055 mmol) in CH₂Cl₂ (2 ml). The resulting dark violet solution containing suspended insoluble cobaltocenium hexafluorophosphate was loaded onto a column of silica gel/CH₂Cl₂. The product was eluted with a 5:95 THF:CH₂Cl₂ mixture. The violet fraction was collected and solvent removed. Recrystallization from CH₂Cl₂/hexanes yielded black crystals containing 0.5 to 1 equivalents of CH₂Cl₂. (Yield >90%). Elemental analysis for a sample of **2_{red}** found by ¹H-NMR to contain 0.75 equivalents CH₂Cl₂: Calculated C, 43.72; H, 2.79; Cl, 5.00. Found C, 43.89; H, 2.73; Cl, 5.29.**

[*fac*-Re(CO)₃(CH₃CN)(dppc)][PF₆]₂ (3_{ox}**); Method A.** To a flask charged with **2_{ox}** (500 mg, 0.47 mM) and AgPF₆ (500 mg, 1.98 mmol) was added CH₂Cl₂ (10 ml), followed by CH₃CN (100 μL). The light yellow suspension was allowed to stir for 5 h and then filtered through a bed of celite. After removing the solvent *in vacuo*, the residue was chromatographed on a column of silica gel, eluting with a mixture of CH₂Cl₂, CH₃CN, and toluene (10:2:1). Yield: 80%. Attempted Recrystallization of **3_{ox}** from various solvent systems always resulted in the precipitation of amorphous, gooey solid which gave analytically pure **3_{ox}** after extensive evacuation. ¹H-NMR, δ in acetone-*d*₆: 2.33 s (3H); 6.2-6.4 m (8H); 7.6-7.8 m (20H). Elemental Analysis: Calculated C, 40.43; H, 2.69. Found C, 40.21; H, 2.78.

Method B. A solution of (CH₃)₃NO (10 mg, 0.13 mmol) in CH₃CN (5 ml) was added dropwise to a vigorously stirred solution of **2_{ox}** (153 mg 0.13 mmol) in CH₃CN (15 ml) cooled in an ice bath. After removing solvent *in vacuo*, the residue was chromatographed as above.

[*fac*-Re(CO)₃(CH₃CN)(dppc)]PF₆ (3_{red}**) Method A.** In the drybox, using only a red darkroom light for illumination, a solution of (CH₃)₃NO (5.0 mg, 0.067 mmol) in CH₃CN (2 ml) was added dropwise to a stirred solution of **2_{red}** (67 mg, 0.067 mmol). A color change to brick red was noted when the addition was complete. The solvent was

removed *in vacuo*, and the residue redissolved in a minimum of CH₂Cl₂, transferred to a vial, and three volumes of Et₂O layered on top. The vial was kept in the dark until crystallization was complete, giving brick red, analytically pure needles of **3_{red}** (60 mg, 90%), which incorporated approximately 1 equivalent of CH₂Cl₂ by ¹H-NMR. Elemental analysis: Calculated C, 43.73; H, 3.03; Cl, 6.45. Found C, 44.03; H, 2.85; Cl, 6.75. High resolution fast atom bombardment mass spectrometry: Calculated molecular ions (two major isotopes of Re); 867.06406, 869.06685. Found; 867.0646, 869.0673.

Method B. In the drybox, illuminated by only red light, a solution of cobaltocene (10 mg, 0.053 mmol) in CH₂Cl₂ (2 ml) was added dropwise to a stirred suspension of **3_{ox}** (60 mg, 0.052 mmol) in CH₂Cl₂ (2 ml). The resulting solution was loaded onto a column of silica gel, eluting first with CH₂Cl₂ to remove any excess cobaltocene, and thereafter with CH₂Cl₂:THF (10:1) to elute the dark red band. The recovered solution was purified as for Method A.

[*fac*-Re(CO)₃(NCO)(dppc)]PF₆ (4_{ox}**).** A solution of [(*n*-Bu)₄N]N₃ (20 mg, 0.070 mmol) in CH₃CN (1 ml) was added dropwise to a solution of **2_{ox}** (83 mg, 0.072 mmol) in CH₃CN (1 ml) accompanied by gas evolution and a color change to deeper yellow. After removing solvent *in vacuo*, the product was separated from the [(*n*-Bu)₄N]PF₆ impurity by loading a CH₂Cl₂ solution of the yellow residue onto a column of silica gel and eluting extensively with CH₂Cl₂, first pure and then with increasing percentages of added THF. Recrystallization from CH₂Cl₂/Et₂O gave analytically pure **4_{ox}**. ¹H-NMR, δ in acetone-*d*₆: 5.95 br (2H), 6.11 br (2H), 6.25 br (2H), 6.42 br (2H), 7.5-7.9 m (20H). Elemental analysis: Calculated C, 44.98; H, 2.78. Found C, 44.92; H, 2.72.

***fac*-Re(CO)₃(NCO)(dppc) (**4_{red}**).** In the drybox, solutions of [(*n*-Bu)₄N]N₃ (20 mg, 0.070 mmol) and cobaltocene (14 mg, 0.074 mmol), each in CH₂Cl₂ (1 ml), were sequentially added dropwise to a stirred solution of **2_{ox}** (80 mg, 0.070 mmol) in CH₃CN producing an amber solution. The solvent was removed *in vacuo* and the residue dissolved in CH₂Cl₂ and loaded onto a column of silica gel/CH₂Cl₂. Any excess cobaltocene was

eluted with CH₂Cl₂. A mixture of 95:5 CH₂Cl₂:THF was used to elute the deep amber product. The solids isolated by evaporation of the amber fraction were found to contain [(*n*-Bu)₄N]PF₆ impurity. The impure solid was dissolved in a mixture of CH₂Cl₂ and CH₃CN and the solvent volume reduced *in vacuo* until a red-brown solid precipitated. Decanting the solvent, rinsing the solid further with CH₃CN, and recrystallization from CH₂Cl₂/hexanes gave analytically pure **4_{red}** (50 mg, 82%). Elemental analysis: Calculated C, 52.48; H, 3.25. Found C, 52.30; H, 3.29. High resolution EIMS: Calculated molecular ions for the two major isotopes of Re, 868.03550, 870.03829. Found 868.0362, 870.0389.

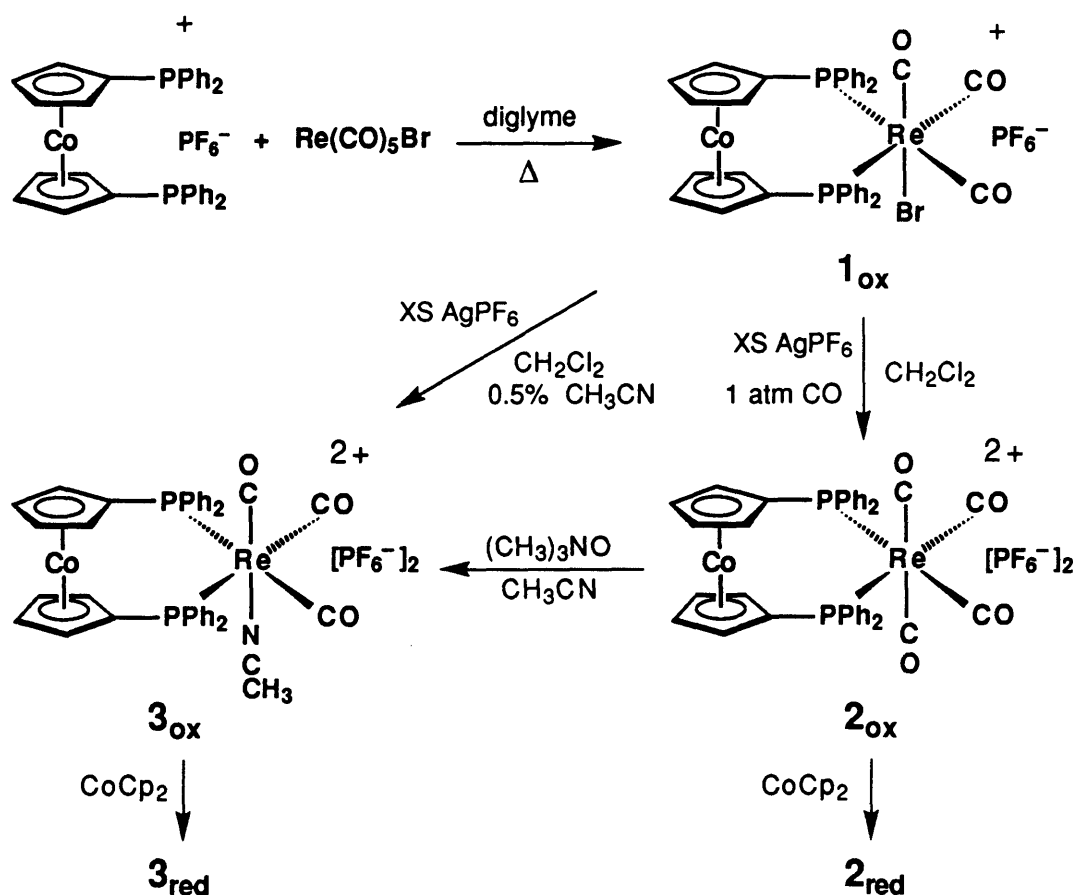
[*cis,cis*-Re(CO)₂(CH₃CN)₂(dppc)]PF₆ (5_{ox}**). A solution of (CH₃)₃NO (13.1 mg, 0.175 mmol) in CH₃CN (1 ml) was added dropwise, with a deepening of yellow color, to a stirred solution of **2_{ox}** (100 mg, 0.087 mmol) in CH₃CN (5 ml). The solvent was removed, and the residue redissolved in CH₂Cl₂ and loaded onto a column of silica gel/CH₂Cl₂, eluting with CH₂Cl₂:CH₃CN:toluene, 10:2:1. Attempts at crystallization were unsuccessful, yielding only an amorphous orange-yellow solid. Analytically pure **5_{ox}** was recovered by extensive evacuation of the chromatographed material. The assignment of the racemic *cis-cis* structure follows from its ¹H-NMR spectrum, which demonstrates that all 8 cyclopentadienyl protons and two sets of bound CH₃CN protons are inequivalent. ¹H-NMR, δ in acetone-*d*₆: 2.23, s (3H); 2.47, s (3H); 6.09-6.19, m (6H); 6.29, br (1H); 6.36, br (1H); 7.5-7.8, m (20H). Elemental analysis: Calculated C, 41.00; H, 2.92. Found C, 40.57; H, 2.89**

[*cis,cis*-Re(CO)₂(CH₃CN)₂(dppc)]PF₆ (5_{red}**). Synthetic procedures analogous to methods A and B for making **3_{red}** were performed, including the use of only a red darkroom lamp for illumination. The product was isolated as a brownish yellow amorphous solid, which when chemically oxidized with **2_{ox}**, displayed spectral properties identical to **5_{ox}**. High resolution FABMS: calculated molecular ions (two major isotopes of Re), 880.0957, 882.09849. Found, 880.0950, 882.0989.**

Results and Discussion

The synthesis of $[fac-Re(CO)_3(Br)dppc]^{+0}$ (**1**), $[cis-Re(CO)_4dppc]^{2+/+}$ (**2**), and $[fac-Re(CO)_3(CH_3CN)dppc]^{2+/+}$ (**3**) is represented in Scheme 3. To insure a good yield

Scheme 3



of 2_{ox} or 3_{ox} from the debromination of **1** in the presence of CO it is essential that a large excess of $AgPF_6$ be used and that the mixture be kept stirring under CO for at least 4 h. In a test of the durability of $dppc^+$ to the nucleophiles in this study, CD_3CN solutions of $[dppc]PF_6$ (0.1 M) with $[n-Bu_4N]N_3$ (0.13 M) or $(CH_3)_3NO$ (0.3 M) showed no reaction after 30 min at 25 °C. **2** reacts with either N_3^- or $(CH_3)_3NO$ (the latter at a rate too fast to measure ($k_2 > 5 \times 10^6 M^{-1}s^{-1}$)) in CH_3CN to form $[fac-Re(CO)_3(dppc)(NCO)]^{+0}$ (**4**), or **3**, respectively. **3** reacts further with $(CH_3)_3NO$ with replacement of a second CO to form racemic $[cis,cis-Re(CO)_2(CH_3CN)_2(dppc)]^{2+/+}$ (**5**). The important feature of the reactions

of **2** and **3** with N_3^- or $(\text{CH}_3)_3\text{NO}$ is that the same reaction occurs at the Re center regardless of the state of charge of the dppc ligand, allowing the comparison of relative reactivity of the two states of charge of complexes **2** and **3**.

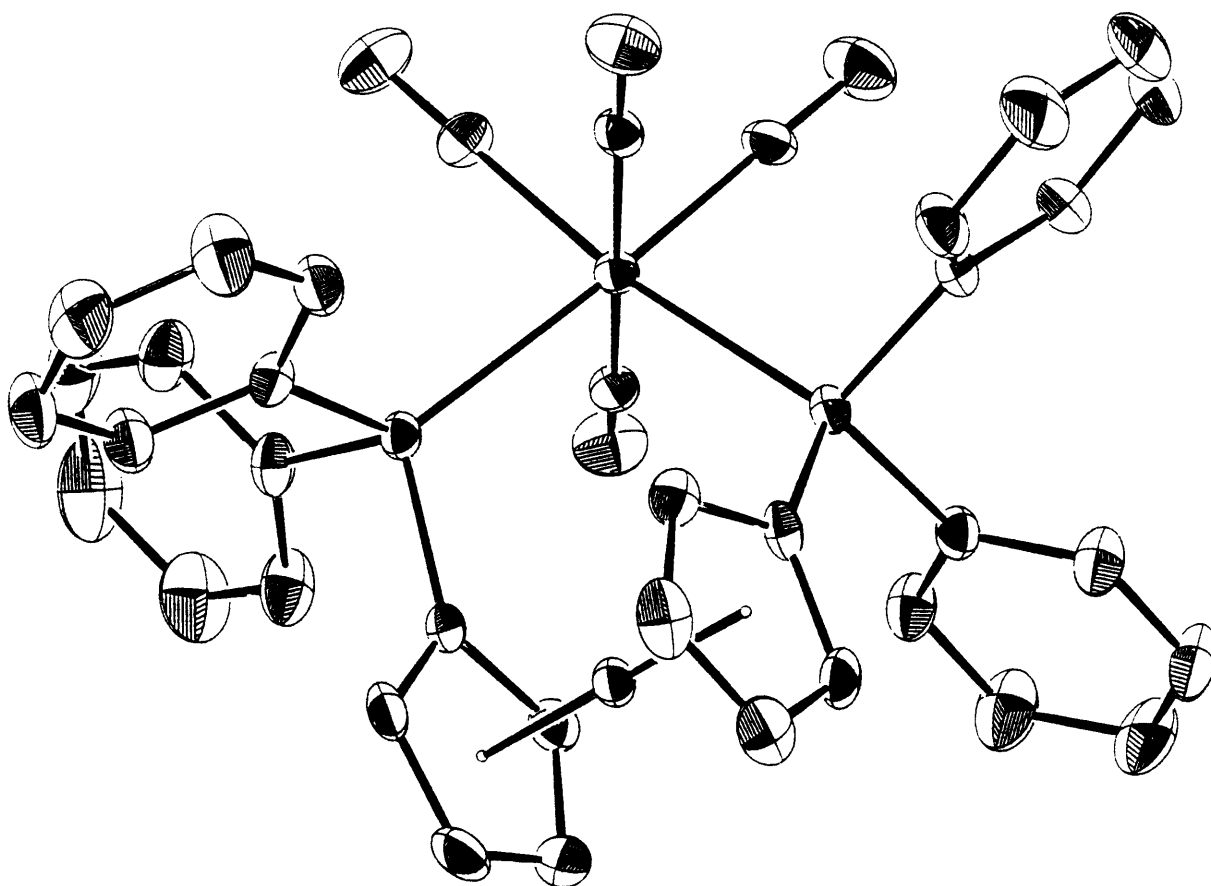
Crystal Data. Despite the large number of publications describing redox activity of metallocene-containing molecules, relatively few include crystal structures of the species in both states of charge.¹⁹ The crystallography of **2_{ox}** and **2_{red}** were undertaken to conclusively show that reduction of the ligand causes no major changes in the geometry of ligands about Re, and that the steric hindrance experienced by attacking nucleophiles is comparable for both states of charge of **2**.

Figure 1 shows the ORTEP diagrams of **2_{ox}** and **2_{red}**, with notable structural features shown in Table 1. Atom positional parameters and more extensive lists of bond lengths and angles are available as supplementary material. In both structures the Re and Co atoms are separated by 4.4 Å. For **2_{red}**, the average Cp-centroid to Co distance is 1.715 Å, in agreement with that calculated from the reported structure of dppc and $[\text{W}(\text{CO})_5]_2\text{dppc}$ (1.715 Å and 1.716 Å),^{17b} and 0.09 Å longer than for **2_{ox}**. This difference is longer than what has been observed for ferrocene/ferrocenium, for which the Fe to Cp-centroid distance typically increases by 0.06 Å upon oxidation to the 17-electron species,¹⁹⁻²² and cobaltocene/cobaltocenium for which Co-Cp distance typically increases by 0.07 Å upon reduction to the 19-electron cobaltocene.^{23,24} To summarize the structural comparison between **2_{ox}** and **2_{red}**, it is clear that the structures are nearly the same, but by no means superimposable. Besides the Co-Cp distance, other differences in solid state structure between **2_{ox}** and **2_{red}** are likely removed by interconversion between ligand conformations, as born out by the high symmetry ¹H-NMR spectra (*vide supra*) and striking similarity in the solution IR spectra in the CO region (*vide infra*) of **2_{ox}** and **2_{red}**.

Electrochemistry. While most of this paper concerns changes in a metal carbonyl center induced by gain or loss of an electron at Co, shifts in the redox potential of the ligand

Figure 1. Ortep diagram of **2_{ox}** (a) and **2_{red}** (b) with ellipsoids drawn at the 35% probability level. In (b) ellipsoids without octant shading represent carbon atoms, all of which were refined only isotropically.

A.



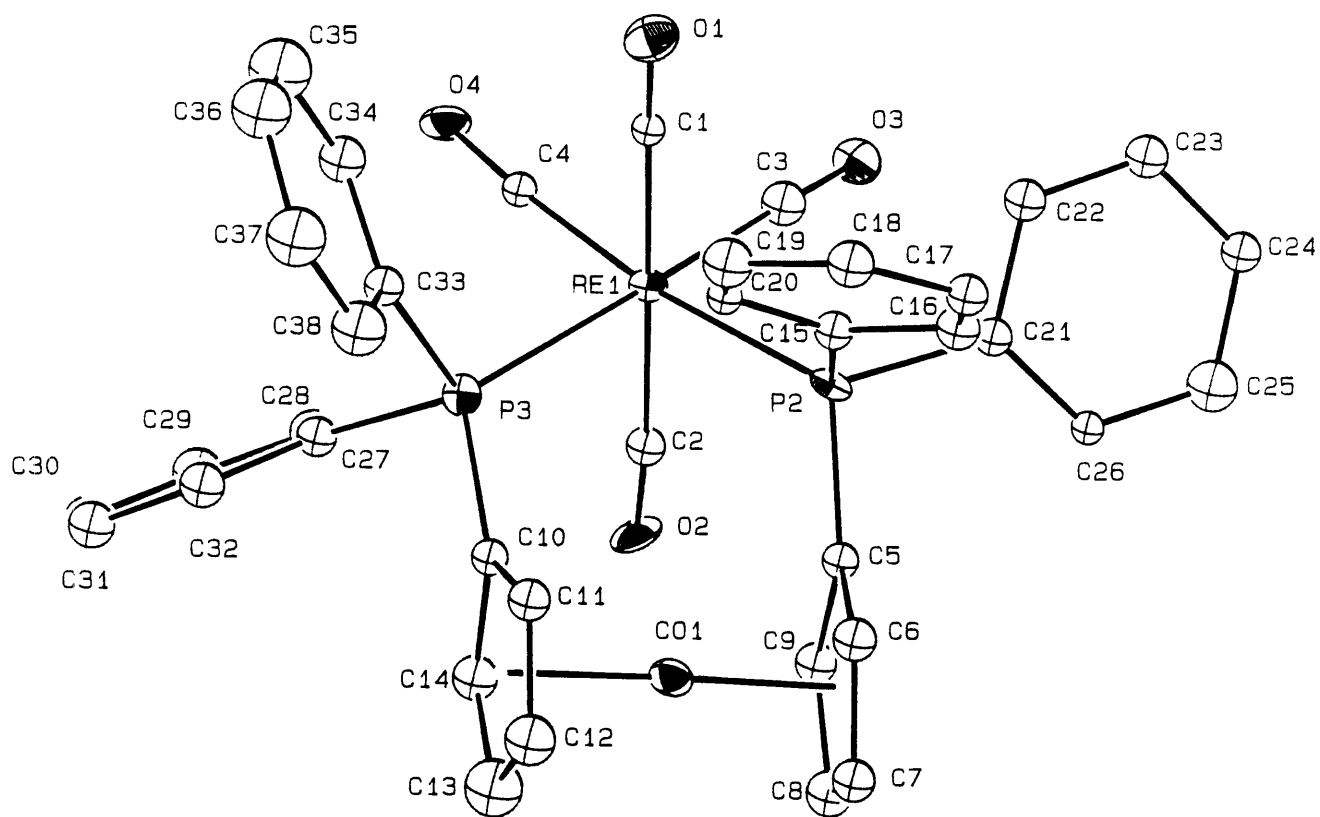
B.

Table 1. Key bond distances and angles in the crystal structures of **2_{ox}** and **2_{red}**.

	2_{ox}	2_{red}
Re-Co	4.402(1) Å	4.394(3) Å
Co-Cp(centroid)	1.628(3) Å	1.72(1), 1.71(1) Å
Re-P	2.502(1) Å	2.501(6), 2.496(6) Å
Re-C1, Re-C2	1.996(6) Å	1.96(2), 2.03(2) Å
Re-C3, Re-C4	1.953(6) Å	2.00(3), 1.91(2) Å
C1-Re-C2	172.6(3)°	179.1(9)°
C3-Re-C4	87.5(3)°	85.6(9)°
P-Re-P	99.70(6)°	95.7(2)°
Cp stagger	44°	21.8°

induced by changes in the coordination sphere of the Re center are also of great interest and demonstrate in a complementary fashion electronic and/or electrostatic communication between reactive and redox sites. The free dppc ligand has a reduction potential about 200 mV more positive than that of cobaltocene while the potential of the ligand when bound to the Re complexes studied here results in a further anodic shift of 230 mV for **5** up to 450 mV for **2**. The $E_{1/2}$ for the Co(III)/Co(II) couple are included in Table 2. Replacement of one CO ligand on Re with NCO^- or Br^- results in a negative shift in the redox potential of 180 and 200 mV, respectively, while substitution by CH_3CN leads to a negative shift of 100 mV for each CO substituted. Thus, the ligand reduction potential is sensitive to the coordination environment of the Re. For comparison with coordinated dppc, the electrochemistry of methylated dppc (phosphonium) was assayed. The reduction potential of $\text{Me}_2\text{dppc}^{3+}$ is shifted positive of the free ligand by a whopping 860 mV.

Although under the right conditions cobaltocene can be stable in up to 4 states of charge, dication (d^5) to anion (d^8),²⁵ in CH_3CN at 23 °C only the middle two are durable. Under these conditions, a second wave associated with the Co(II)/Co(I) couple is observed at potentials ~900 mV more negative than the Co(III)/Co(II) wave, consistent with established trends.²⁵ This second reduction process is reversible at scan rates down to at least 10 mV/S for complexes **3**, **4**, and **5**, but quasi-reversible for the free ligand and irreversible for **1** and **2**. The electrochemical reversibility of the Co(II)/Co(I) couple for complexes in which dppc binds as a chelate has been explained in terms of a template effect which holds the otherwise dissociation prone cobaltocene anion intact.^{9b} Attempted preparation of the doubly reduced form of **3** by chemical reduction using decamethylcobaltocene in THF led to decomposition. Attempts to prepare $\text{Me}_2\text{dppc}^{2+}$ by chemical reduction resulted detection of a paramagnetic species with similar $^1\text{H-NMR}$ spectroscopic properties to dppc which decomposed ($t_{1/2} = 1 \text{ h}$, 23° C) likely caused by the electrostatic strain on the weakened (relative to the cobaltocenium species) Cp-Co bond.

Table 2. Spectroscopic and electrochemical data in CH₃CN at 23±3 °C.

compound ($E_{1/2}$, V) ^a		IR	UV/VIS
		ν_{CO} , cm ⁻¹	λ , nm
		(ϵ , M ⁻¹ cm ⁻¹)	(ϵ , M ⁻¹ cm ⁻¹) ^b
CoCp ₂ ⁺	(-1.34)		404 (208, p)
			362 (110, v)
			300 (1060, p)
			292 (1020, v)
			262 (33000, p)
			228 (777, v)
CoCp ₂			480 (110, s)
			400 (430, s)
			326 (6700, p)
			286 (1800, v)
			260 (6100, p)
			244 (5800, v)
dppc ⁺	(-1.14, -2.02 (q))		378 (4030, p)
			332 (2490, v)
			268 (23200, s)
			248 (27000, p)
			232 (23300, v)

dppc			450 (1200, s)
			344 (4300, p)
			332 (3900, v)
			250 (24000, p)
			238 (22000, v)
[Me ₂ dppc] ³⁺	(-0.28,		420 (390, p)
	-1.24 (i))		392 (340, v)
			346 (1500, s)
			274 (24000, p)
			246 (6300, v)
			224 (47000, p)
			216 (42000, v)
			198 (100000, p)
1	(-0.91)		
2_{ox}	(-0.71,	2121 (1940)	412 (408, s)
	-1.58 (i),	2049 (1750)	274 (17000, p)
	-1.86 (i, 2e ⁻))	2022 (4140)	254 (13000, v)
			222 (67000, s)
2_{red}		2110 (1960)	566 (1200, p)
		2032 (1870)	468 (820, v)
		2006 (4010)	420 (980, s)
			326 (4800, p)
			312 (4600, v)
			274 (10800, s)

3_{ox}	(-0.80, -1.70)	2062 (3040)	274 (21500, p)
		1991 (1800)	260 (19200, v)
		1953 (1500)	236 (40500, s)
3_{red}		2048 (3540)	478 (1140, p)
		1970 (2040)	400 (760, v)
		1940 (1700)	316 (4130, s)
4_{ox^c}	(-0.89, -1.82)	2237 (1500, v _{NCO})	420 (510, s)
		2046 (3900)	274 (18800, p)
		1973 (2250)	252 (19800, s)
		1925 (2300)	234 (36900, s)
4_{red^c}		2245 (1900, v _{NCO})	460 (1300, p)
		2032 (3800)	400 (1000, v)
		1950 (2100)	328 (5600, s)
		1906 (2000)	302 (7350, s)
5_{ox}	(-0.91, -1.83)	1982 (2370)	526 (150, s)
		1903 (2060)	408 (540, s)
			258 (27000, p)
			246 (24000, v)
			228 (49000, s)

$\tilde{\nu}_{\text{red}}$	1963 (2480)	440 (1280, p)
	1887 (2100)	398 (1090, v)
		324 (5700, s)

^a Potentials vs. Fc/Fc⁺ using 0.1M [*n*-Bu₄N]PF₆. "i" and "q" denote irreversible and quasireversible, respectively.

^b "p", "v", and "s" denote peak, valley, and shoulder, respectively.

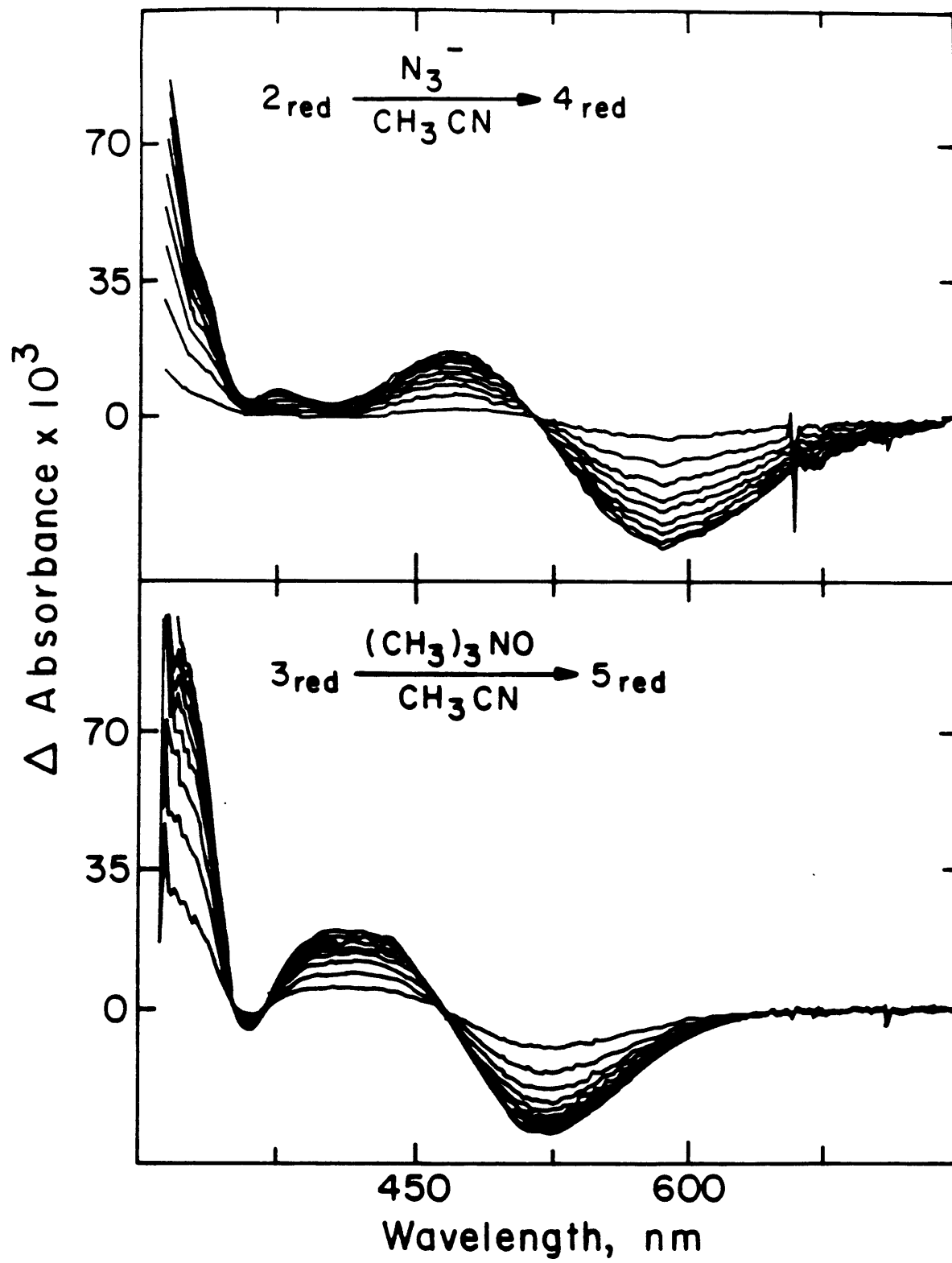
^c IR data obtained from a CH₂Cl₂ solution.

For **2**, the Co(I)/Co(II) wave is followed by an irreversible two electron reduction assignable to the Re(I)/Re(-I) couple.

UV/Vis Absorption Spectroscopy: The oxidized state of free dppc and Re(dppc) carbonyl complexes all show tail absorption, to varying extents, into the visible region of the spectrum. Since the analogous Re(dppe) (dppe = 1,2-*bis*(diphenylphosphino)ethane) complexes are all colorless,²⁶ the visible absorption of the dppc complexes must be attributed to the colored cobaltocenium moiety. The onset of visible absorption is ordered energetically according to the following: **2** > **3** > **4** > **5**. The studies (*vide infra*) of reactivity toward nucleophiles (N₃⁻ or amine-N-oxide) show that their electrophilicity shows the same order. Taking electrophilicity to reflect the extent to which the Re center is electron-poor, the visible absorption of the oxidized complexes may have a component of Re(I) → Co(III) charge transfer character. The first absorption of cobaltocenium which gives rise to its yellow color is a ligand field band and should not be affected significantly by variations in the ligands surrounding the Re center. Thus, while the lowest ligand field absorption of cobaltocenium is likely a component of the visible absorption of the oxidized complexes **2**, **3**, **4**, and **5**, the absorption also likely includes some Re(I) → Co(III) character.

For the reduced species **2**, **3**, **4**, and **5**, the absorptions dominating the visible region are lower in energy than for their oxidized analogues. This, too, follows the behavior of the absorption of cobaltocene vs cobaltocenium; the reduced species absorbs at longer wavelength. However, the nature of the Re fragment in the dppc complexes alters the position of the first absorption. The first absorption energy is in the following order for the reduced complexes. **5** > **4** > **3** > **2**. Figure 2 shows UV/vis spectral changes upon reaction of **2**_{red} (60 mM in CH₃CN) with N₃⁻ and **3**_{red} (60 mM in CH₃CN) with (CH₃)₃NO. As the more π-acidic CO is substituted by more basic NCO⁻ or CH₃CN the visible absorption band shifts to higher energy. From these observations it is reasonable to suggest that the visible absorption of the reduced Re(dppc) complexes possesses some

Figure 2. UV/Visible spectral changes, acquired using stopped flow techniques showing the reaction of **2_{red}** (0.08 mM) with N_3^- (2 mM) to form **4_{red}** (top) and reaction of **3_{red}** (0.08 mM) with $(\text{CH}_3)_3\text{NO}$ (5 mM) to form **5_{red}** (bottom) in CH_3CN at 25.0 °C showing that upon substitution of CO for less p-acidic ligands such as CH_3CN or NCO^- , the cobaltocene-based absorbance undergoes a hypsochromic shift. Presence of isosbestic points demonstrates absence of secondary reactions.



Co(II) \rightarrow Re(I) charge transfer character, the excited state for which becomes higher in energy as the Re center is made more electron-rich.

Solution FTIR. FTIR spectra of two states of charge of **2**, **3**, **4**, and **5** are shown in Figure 3 and tabulated in Table 2 and the data are characteristic of octahedral *cis*-tetracarbonyl (**2**), *fac*-tricarbonyl (**3** and **4**), and *cis*-dicarbonyl (**5**). Oxidizing the dppc ligand causes an increase in ν_{CO} of $\sim 15 \text{ cm}^{-1}$ with no change in the number or relative intensities of the absorptions. Thus, in solution, the steric properties of the two states of charge of **2** and **3** are, on average, effectively equivalent.

Kinetics, Part A: Reaction of 3 with amine-N-oxides. Tertiary amine-N-oxides have long been known as good oxygen atom transfer reagents, being more reactive than phosphine, arsine, or stibine oxides as a consequence of the absence of a low lying π -accepting empty d orbital on N, lending zwitterionic character to the N-O bond. Amine-N-oxides are particularly reactive in the oxidation of transition metal bound CO to CO_2 . More basic amine-N-oxides are more reactive, and it is believed that nucleophilic attack of oxide at the CO carbon is the rate limiting step.¹²

The kinetics results from studies of the reaction between **3** and amine-N-oxides ($\text{CH}_3)_3\text{NO}$ (TMANO), N-methylmorpholine-N-oxide (NMMNO), and N,N-dimethylaniline-N-oxide (DMANO) in CH_3CN to form **5** are summarized in Table 3. The reaction was determined to be first-order in **3** by virtue of the exponential absorbance rise and decay curves obtained under the pseudo-first-order conditions employed in this study. In addition, the pseudo-first-order rate constants observed for **3_{ox}** using $[\text{TMANO}] = 0.504, 1.008 \text{ and } 2.52 \text{ mM}$ were $0.378, 0.771, \text{ and } 2.00 \text{ s}^{-1}$, respectively, while those for **3_{red}** using $[\text{TMANO}] = 13.9 \text{ and } 21.8 \text{ mM}$ were $0.059 \text{ and } 0.083 \text{ s}^{-1}$, demonstrating that the reaction was also first-order in TMANO. The reaction of **3_{ox}** with both NMMNO and DMANO was likewise found to be first order in both N-oxides. The reduction of the dppc ligand causes approximately a 200-fold decrease in the rate constant for reaction between **3** and all three amine-N-oxides, Table 3 and Scheme 4. Figure 4 shows the Eyring plots

Figure 3. Solution IR spectra in the carbonyl region for **2**, **3**, **4** and **5**, showing that the spectrum of the reduced form of all species is identical to the oxidized form except that all absorptions for the reduced species are $\sim 15\text{ cm}^{-1}$ lower in energy.

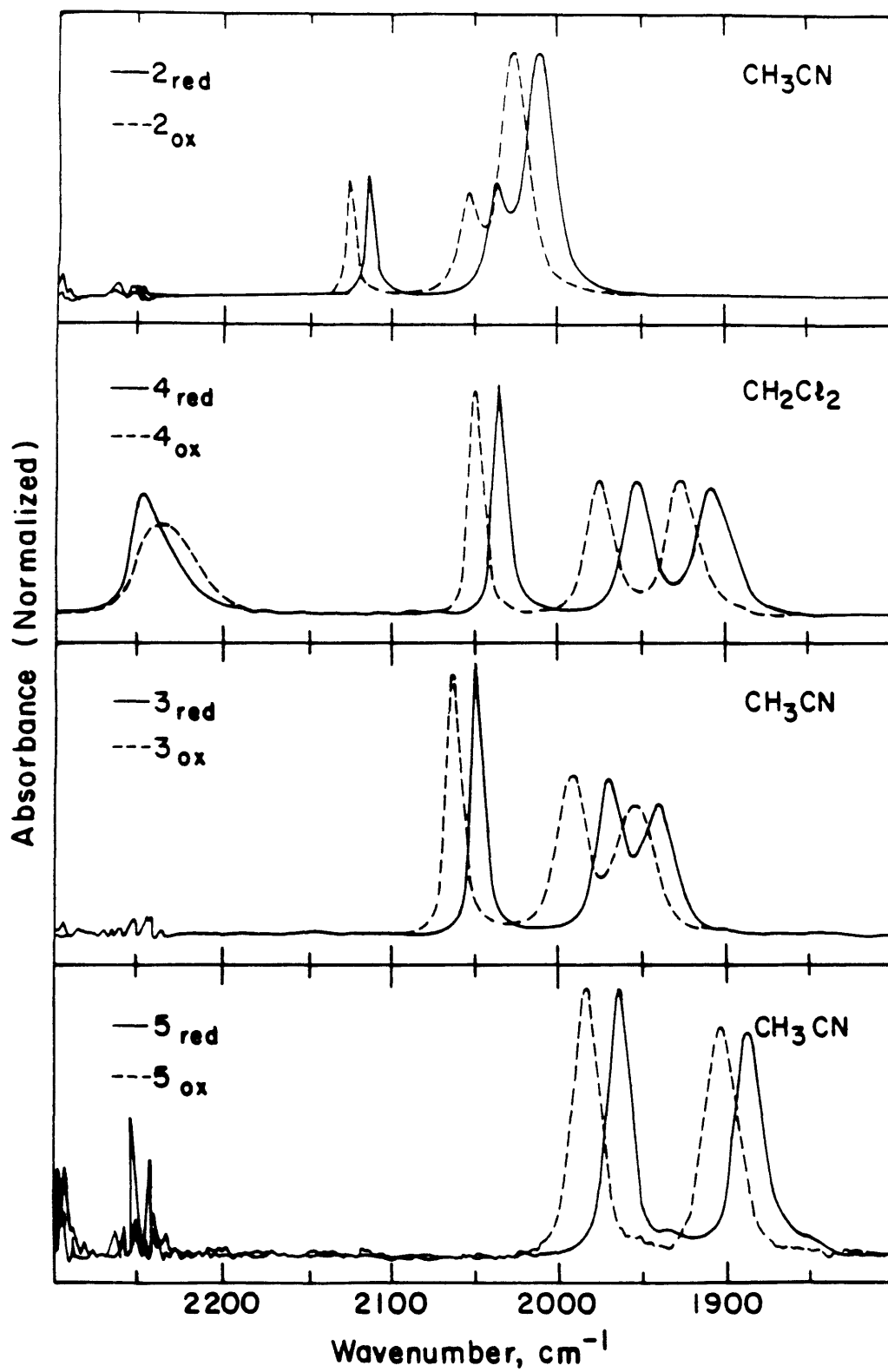


Table 3. Rate constants and activation parameters for the reaction between **3** and amine-N-oxides^a in CH₃CN (T = 25-39 °C).

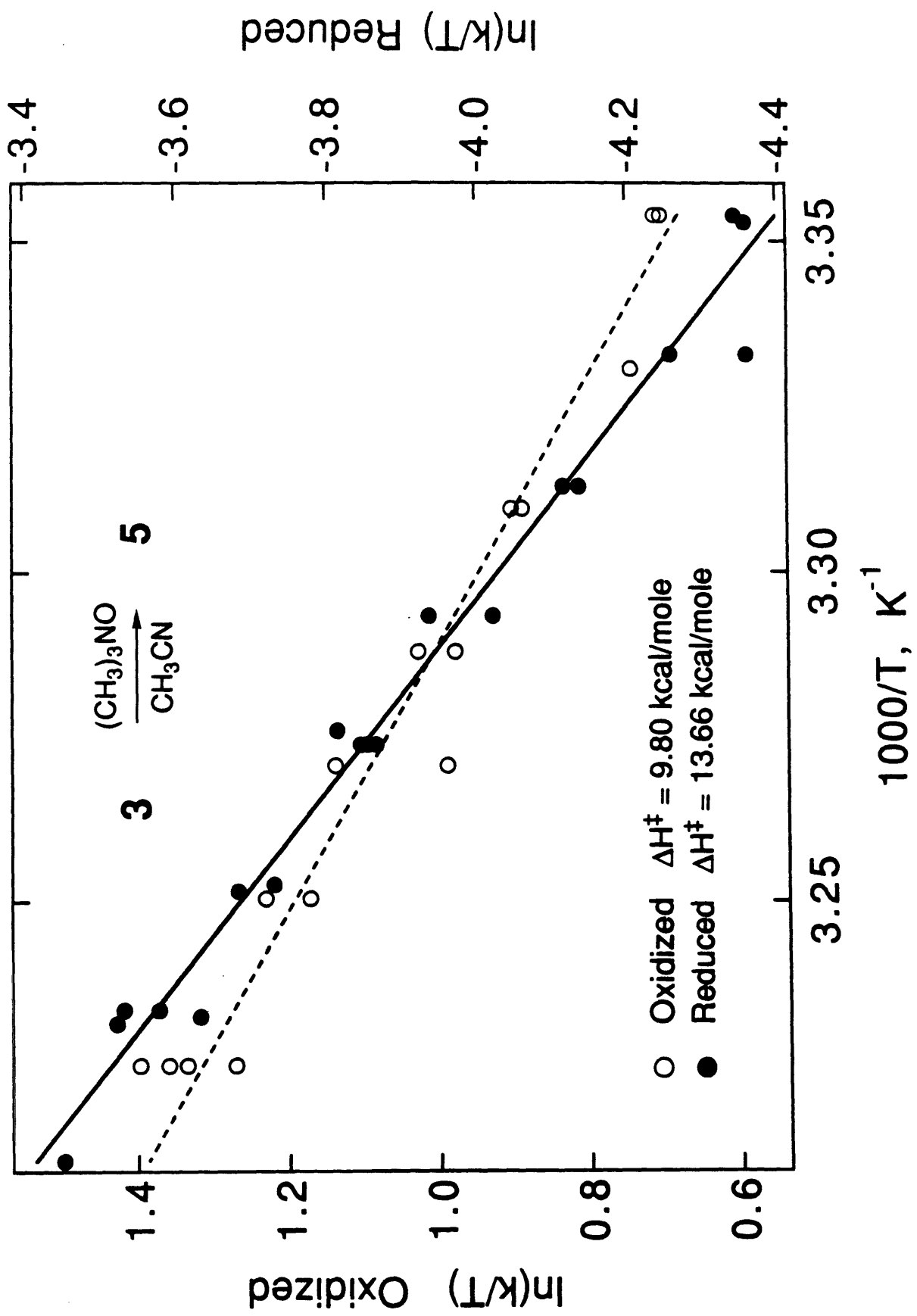
	I (mM) ^b	k ₂ , 25.0 °C M ⁻¹ s ⁻¹	k _{ox} /k _{red}	ΔH [‡] (s) Kcal/mole	ΔS [‡] (s) e.u.
TMANO					
3 _{ox}	0.03	741	193	9.80(47)	-12.7(1.6)
3 _{ox}	100 ^c	621	156		
3 _{red}	0.10	3.84		13.66(44)	-10.1(1.4)
3 _{red}	100 ^c	3.97			
NMMNO					
3 _{ox}	0.03	77.6	179	10.26(49)	-15.5(1.6)
3 _{red}	0.10	0.433		13.34(77)	-15.4(2.5)
DMANO					
3 _{ox}	0.03	2700	226	8.15(47)	-15.5(1.6)
3 _{red}	0.10	11.9		9.31(26)	-22.33(86)

^a TMANO, NMMNO, and DMANO are trimethylamine-N-oxide, N-methylmorpholine-N-oxide, and dimethylaniline-N-oxide, respectively.

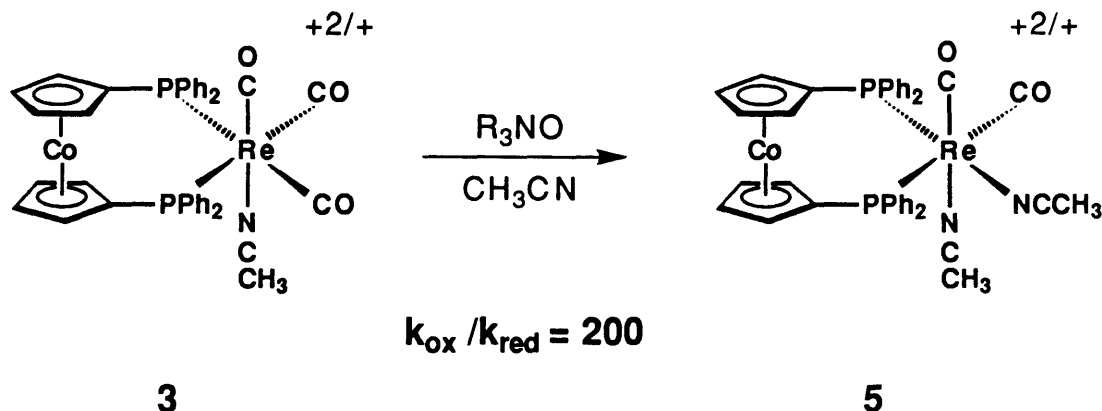
^b I is ionic strength.

^c [*n*-Bu₄N]PF₆ was used as supporting electrolyte.

Figure 4. Eyring plot for the temperature-dependent rate of reaction between TMANO and **3_{ox}** (open circles, left y-axis) and between TMANO and **3_{red}** (filled circles, right y-axis) showing that reduction of the redox-active ligand induces an increase in the activation enthalpy of nucleophilic attack at the carbonyl carbon atom of **3**.



Scheme 4



for the reaction between TMANO and both 3_{ox} and 3_{red} . The marked increase in the activation enthalpy (3.9 ± 0.9 kcal/mole) for the reaction upon reduction is evident. With NMMNO, for both states of charge of **3** the reaction is 10 times slower and ΔS^\ddagger about 4 e.u. more negative than with TMANO, reflecting similar basicity for the two amine-N-oxides and bulkier nature of NMMNO. DMANO, despite its lower basicity, was the most reactive of the three amine-N-oxides studied, as has previously been observed,^{12b} reacting 4 times faster with **3** than TMANO. Imposing the condition that ΔS^\ddagger for both states of charge be identical in the reaction of **3** with the amine-N-oxides studied, the reactivity differences observed correspond to a $\Delta\Delta H^\ddagger$ of 3.1-3.2 Kcal/mole.

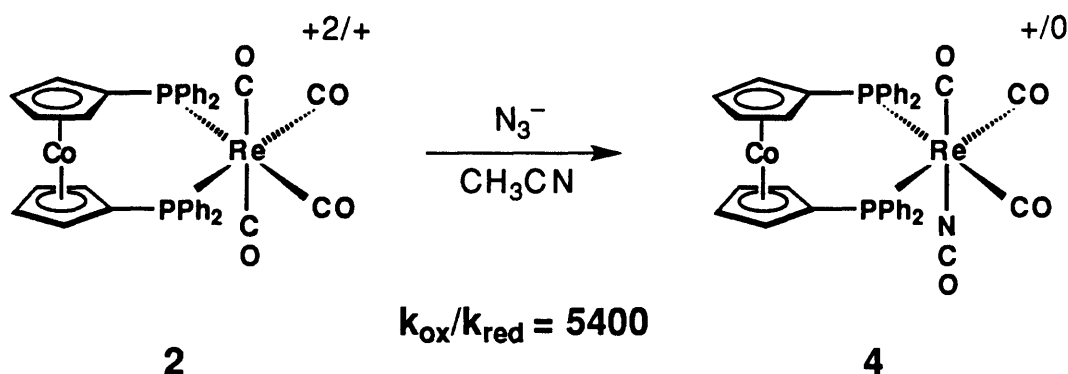
The reaction between 3_{ox} and TMANO proceeded at a $14 \pm 5\%$ slower rate in CH_3CN containing 0.1 M $[\text{n-Bu}_4\text{N}]\text{PF}_6$ at 25 °C, while the same reaction with 3_{red} was unaffected by the presence of electrolyte. These results, compared to the strong ionic strength dependence of the reactions between **2** and N_3^- (*vide infra*) are consistent with the activated complex bearing the same overall charge as the dicationic reactant.

An interesting property of the reaction of 3_{ox} with TMANO is that at $T < 20$ °C or higher concentrations of TMANO, with no change in the yield of 5_{ox} , the absorbance change with time exhibits biexponential behavior. Accumulation of a significant concentration of the putative intermediate rhenium(O-trimethylamino)-carboxylate, equation (2), which to my knowledge has never been directly observed, is consistent with these

observations. Another possibility is that the intermediate is the $N(\text{CH}_3)_3$ complex. A low temperature spectral study of this reaction would be instructive in this regard.

Kinetics, Part B: Reaction of 2 with the Anionic Nucleophile N_3^- . Azide anion reacts with metal carbonyls in a fashion similar to amine-N-oxides in that the rate limiting step is thought to be nucleophilic attack at the CO carbon.⁹ A rapid Curtius type rearrangement is postulated to follow, giving the metal isocyanate and free N_2 . At 25 °C in CH_3CN the reaction between 2 and N_3^- to form 4 was found to be first-order in 2 by virtue of the exponential absorbance rise and decay curves observed under pseudo-first-order conditions. In addition, the pseudo-first-order rate constants, corrected for ionic strength differences (*vide infra*), observed for 2_{ox} using $[\text{N}_3^-] = 0.21, 0.42$ and 0.82 mM were 150, 270, and 560 s^{-1} , respectively, while those for 2_{red} using $[\text{N}_3^-] = 1.00$ and 3.27 mM were 0.106 and 0.324 s^{-1} , respectively, demonstrating that the reaction was also first-order in N_3^- . 2_{ox} reacts with N_3^- 5400 times faster than 2_{red} , Table 4 and Scheme 5.

Scheme 5



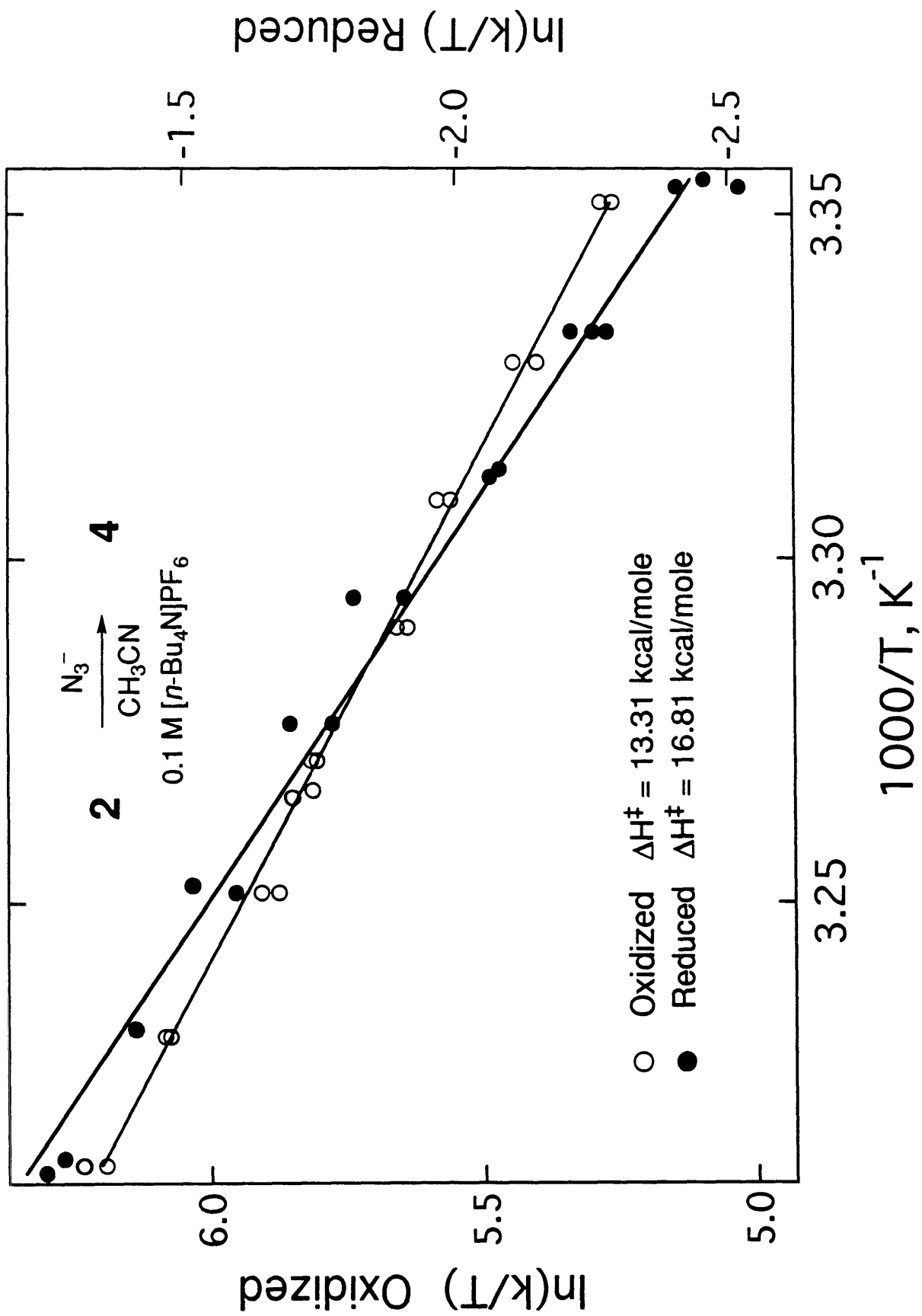
In a $0.1 \text{ M } [n\text{-Bu}_4\text{N}]\text{PF}_6/\text{CH}_3\text{CN}$ solution, however, 2_{ox} and 2_{red} react 8 and 3 times slower, respectively, with N_3^- than with no supporting electrolyte, and the redox-induced rate constant change is only a factor of 2200. The Eyring plots for the reaction between both states of charge of 2 and N_3^- in $\text{CH}_3\text{CN}/0.1 \text{ M } [n\text{-Bu}_4\text{N}]\text{PF}_6$ are shown in Figure 5 and the activation parameters for both media are summarized in Table 4. Similar to what was observed for the reaction between 3 and TMANO, ΔH^\ddagger is 3.5 ± 0.7 kcal/mole higher

Table 4. Rate constants and activation parameters for the reaction between **2** and N_3^- in CH_3CN ($T = 25\text{-}39\text{ }^\circ\text{C}$).

	I (mM)	k_2 , 25.0° C $\text{M}^{-1}\text{s}^{-1}$	$k_{\text{ox}}/k_{\text{red}}$	ΔH^\ddagger (s) Kcal/mole	ΔS^\ddagger (s) e. u.
2_{ox}	0.3	567,000	5400	12.64(23)	10.22(75)
2_{red}	1.1	106		14.21(47)	-1.6(1.5)
2_{ox}	100 ^a	72,000	2200	13.31(26)	7.86(84)
2_{red}	100 ^a	33		16.81(47)	4.3(1.6)

^a [*n*-Bu₄N]PF₆ was used as supporting electrolyte.

Figure 5. Eyring plot for the temperature dependent rate of reaction between N_3^- and $\mathbf{2}_{\text{ox}}$ (open circles, left y-axis) and between N_3^- and $\mathbf{2}_{\text{red}}$ (filled circles, right y-axis) showing that reduction of the redox-active ligand induces an increase in the activation enthalpy of nucleophilic attack at the carbonyl carbon atom of **2**.



for the reaction of the reduced form of the species. Considering the relative rates of reaction of the oxidized and reduced Re species with the neutral amine-N-oxides (*vide supra*), the enhancement in reaction rate of 2_{ox} with N_3^- over 2_{red} is greater than one might expect solely on the basis of $\Delta v_{\text{CO}} = 15 \text{ cm}^{-1}$. The additional enhancement is attributed to the fact that N_3^- is negatively charged. It is important to realize that the electrostatic effect is at least partly derived from changes in positive charge localized in the dppc ligand, the center (Co atom) of which is 4.4 \AA from the Re atom. In order to better understand the enhanced reactivity due to the electrostatic attraction between dppc^+ in 2_{ox} and N_3^- , the ionic strength (I) and dielectric strength (ϵ) dependence of the rate of reaction between 2 and N_3^- were investigated.

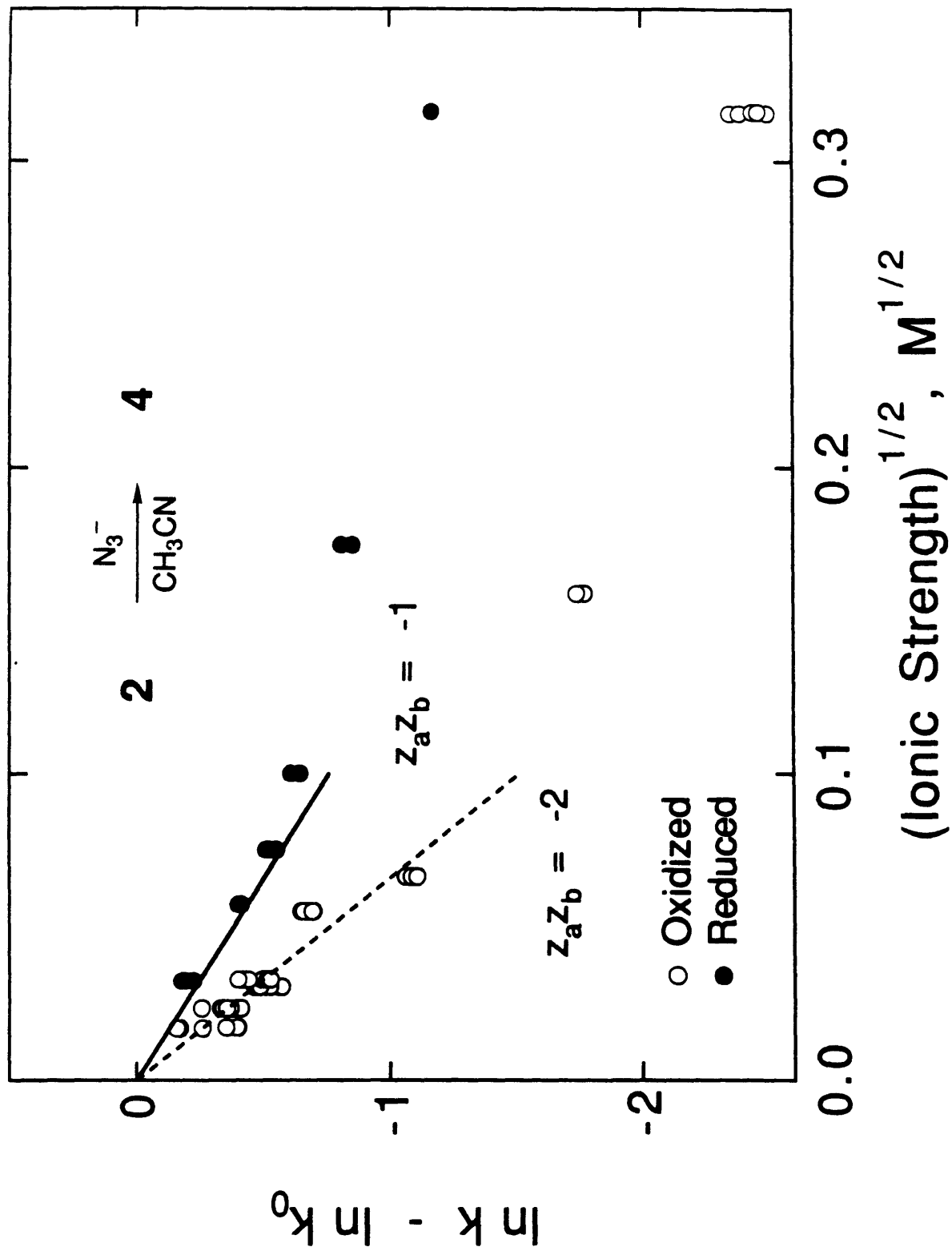
The Brønsted primary salt effect,^{27,28} described by equation (3) for a solution in

$$\ln k = \ln k_{I=0} - 2Az_a z_b I^{1/2} \quad (3)$$

$$A = 0.05628 F^3 N_A^{-1} (\epsilon \epsilon_0 R T)^{-3/2}$$

which all ions are dissociated, dictates that, as I (defined here as having units moles/dm³) approaches 0, $\ln k$ should change linearly with $I^{1/2}$, where F is $96,485 \text{ C mole}^{-1}$, N_A is $6.022 \times 10^{23} \text{ mole}^{-1}$, and ϵ_0 is $8.854 \times 10^{-12} \text{ C}^2 \text{ J}^{-1} \text{ m}^{-1}$. For CH_3CN at $25.0 \text{ }^\circ\text{C}$ ($\epsilon = 36.7$)²⁹, A is 3.67. Figure 6 shows theoretical and experimental plots for the reaction between N_3^- and both states of charge of 2 as a function of the concentration of [*n*-Bu₄N]PF₆ supporting electrolyte. The observed $I^{1/2}$ dependence of $\ln k$, at $I < 20 \text{ mM}$, agrees well with the predicted slopes of -7.34 for 2_{red} and -14.68 for 2_{ox} . These results are consistent with all ions in solution being dissociated and the activity of 2_{ox} being that of a dication. The ionic strength dependence of the reactivity of 2_{ox} is expected to be typical of a dication, because the Debye length is at least 10 \AA for the conditions used in this study,²⁸ significantly longer than the Co to CO carbon distance (4.8 \AA). The Debye

Figure 6. Ionic strength dependence of the reaction between N_3^- and 2_{ox} (open circles) and N_3^- and 2_{red} (filled circles). Shown as solid line segments are ionic strength dependences for a bimolecular reaction between a cation and an anion and between a dication and an anion predicted by the Debye-Hückel Limiting Law in a medium having ϵ of 36.7 at 25.0 °C.



length characterizes distances over which the ionic atmosphere stabilizes the charged reactant and activated complexes.

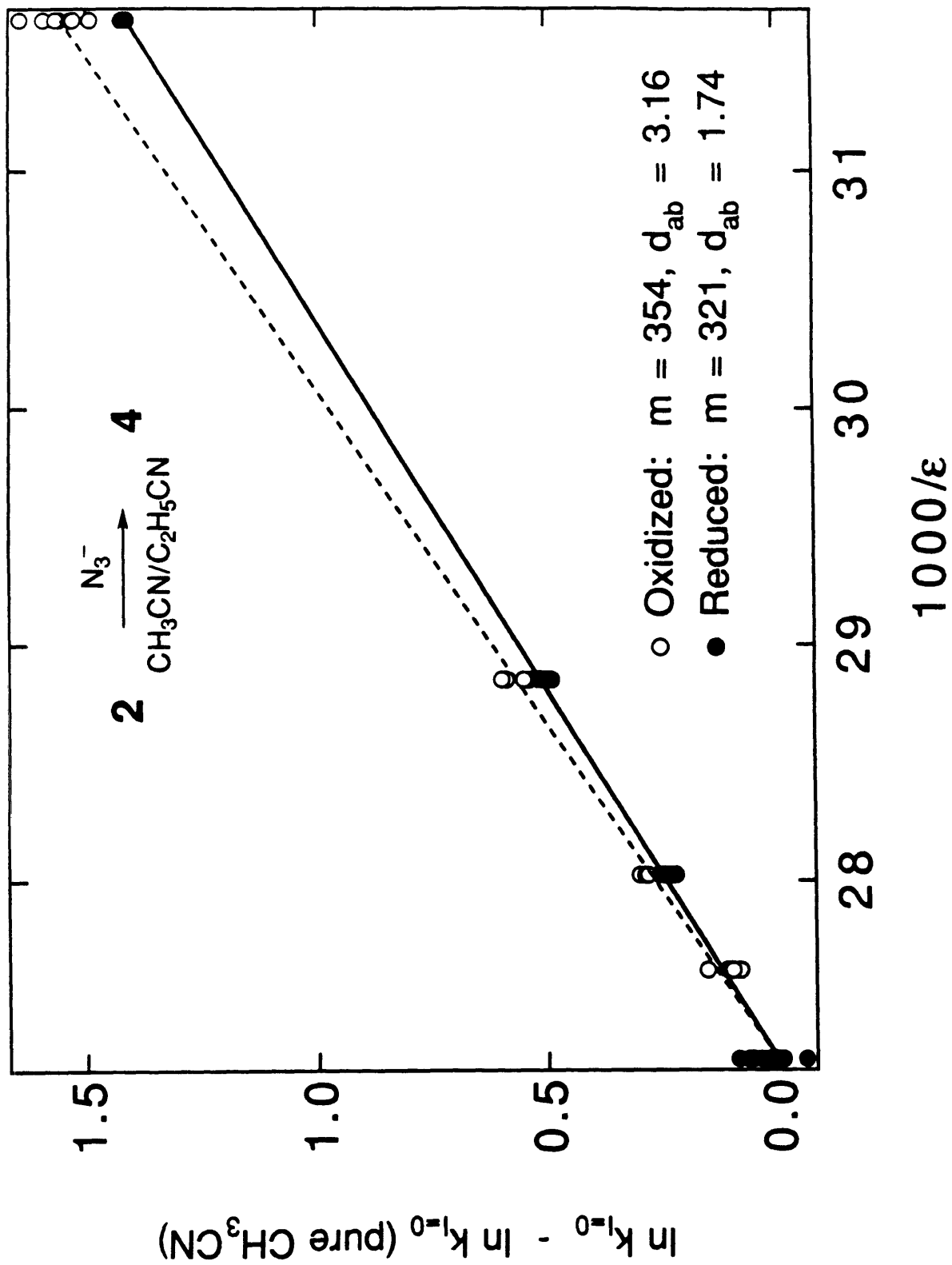
The dielectric strength dependence of the reactivity between ions has been approximated by the "double sphere"²⁷ model, equation (4), which predicts a linear relationship between $\ln k$ and ϵ^{-1} , where k_{∞} is the rate constant in a medium of infinite dielectric strength. The apparent center-to-center distance between the ions in the activated

$$\ln k = \ln k_{\infty} - 1/\epsilon(z_a z_b e^2 / 4\pi\epsilon_0 d_{ab} kT) \quad (4)$$

complex, d_{ab} , can be calculated from the slope of the line obtained by plotting $\ln k_{I=0}$ (obtained by extrapolating the observed rate constants at non-zero ionic strength to $I = 0$ using equation (3)) vs ϵ^{-1} . Figure 7 shows a plot of $\ln k_{I=0}$ vs ϵ^{-1} for the reaction between **2** and N_3^- . In this experiment, ϵ was varied by preparation of CH_3CN solutions containing different volume percentages of C_2H_5CN ($\epsilon = 26.5$ at 25.0 °C) and assuming that ϵ is a linear function of the volume (or mass, since $\rho(CH_3CN) = 0.786$ g/ml \approx $\rho(C_2H_5CN) = 0.782$ g/ml) percent composition of the binary mixture. In this case, oxidizing dppc increases the slope by only $10 \pm 2\%$ (321 to 354), giving an apparent d_{ab} of 1.74 and 3.16 Å for **2_{red}** and **2_{ox}**, respectively. A possible explanation for the fact that the ϵ dependence of the reaction of **2** with N_3^- is relatively insensitive to the state of charge of the dppc ligand is that the distances characterizing the relative dielectric stabilization of the electrostatic potential energies of the reactants and activated complex are on the order of d_{ab} (~ 2 Å), which is considerably shorter than the Co to CO carbon distance (~ 4.8 Å). Thus, **2_{ox}** behaves as a molecule containing two separate monocationic centers in the ϵ dependence of its reactivity with N_3^- , in contrast to the behavior upon variation in ionic strength, where **2_{ox}** behaves as a simple dication.

The activation parameters measured at low ionic strength ($\Delta H_{obs}^{\ddagger}$ and $\Delta S_{obs}^{\ddagger}$) for the reaction between **2** and N_3^- shown in Table 4 may be separated into electrostatic (e.s.)

Figure 7. Dielectric strength dependence of the reaction between N_3^- and $\mathbf{2}_{\text{ox}}$ (open circles) and N_3^- and $\mathbf{2}_{\text{red}}$ (filled circles) at 25.0 °C. For this figure the dielectric strength is decreased by addition of $\text{C}_2\text{H}_5\text{CN}$, and it is assumed that the dielectric strength of the mixture is linearly dependent on the volume percent of $\text{C}_2\text{H}_5\text{CN}$. The best fit slopes for $\mathbf{2}_{\text{ox}}$ and $\mathbf{2}_{\text{red}}$ are 354 and 321, corresponding to $d_{\text{ab}} = 3.16 \text{ \AA}$ and 1.74 \AA respectively.



and nonelectrostatic (n.e.s.) contributions, equations (5) and (6). Since the reaction of

$$\Delta H^\ddagger_{\text{obs}} = \Delta H^\ddagger_{\text{e.s.}} + \Delta H^\ddagger_{\text{n.e.s.}} \quad (5)$$

$$\Delta S^\ddagger_{\text{obs}} = \Delta S^\ddagger_{\text{e.s.}} + \Delta S^\ddagger_{\text{n.e.s.}} \quad (6)$$

$$\Delta\Delta H^\ddagger_{\text{e.s.}} = \Delta H^\ddagger_{\text{e.s.}}(\mathbf{2}_{\text{ox}}) - \Delta H^\ddagger_{\text{e.s.}}(\mathbf{2}_{\text{red}}) \quad (7)$$

$$\Delta\Delta S^\ddagger_{\text{e.s.}} = \Delta S^\ddagger_{\text{e.s.}}(\mathbf{2}_{\text{ox}}) - \Delta S^\ddagger_{\text{e.s.}}(\mathbf{2}_{\text{red}}) \quad (8)$$

$\mathbf{2}_{\text{ox}}$ and $\mathbf{2}_{\text{red}}$ with N_3^- is between ions, both reactions have significant $\Delta H^\ddagger_{\text{e.s.}}$ and $\Delta S^\ddagger_{\text{e.s.}}$. The difference in these parameters between the states of charge of $\mathbf{2}$ ($\Delta\Delta H^\ddagger_{\text{e.s.}}$ and $\Delta\Delta S^\ddagger_{\text{e.s.}}$), equations (7) and (8), is the additional electrostatic contribution caused by changing the charge on the dppc ligand.

The rate constant for reaction between ions as a function of temperature, but at constant ϵ (by using different solvent mixtures), gives the non-electrostatic activation parameters.²⁹ Unfortunately, data are not available regarding the temperature dependence of ϵ for the binary mixtures of CH_3CN and $\text{C}_2\text{H}_5\text{CN}$ used. The essential information can, however, be obtained from the data, because the temperature dependence of ϵ for CH_3CN is known³⁰ and the ϵ dependence of the rate of reaction between $\mathbf{2}$ and N_3^- at a fixed temperature has been measured, Figure 7. Thus, according to the literature,²⁹ $\Delta H^\ddagger_{\text{n.e.s.}} = 10.22 \pm 0.23$ and 12.02 ± 0.47 kcal/mole and $\Delta S^\ddagger_{\text{n.e.s.}} = -15.83 \pm 0.75$ and -25.2 ± 1.5 e.u. for $\mathbf{2}_{\text{ox}}$ and $\mathbf{2}_{\text{red}}$, respectively. Furthermore, using equations (5)-(8) $\Delta\Delta H^\ddagger_{\text{e.s.}} = 0.23$ kcal/mole and $\Delta\Delta S^\ddagger_{\text{e.s.}} = 2.45$ e.u., leading to the conclusion that there is a five-fold overall electrostatic rate enhancement in the relative reactivity of $\mathbf{2}_{\text{ox}}$ to $\mathbf{2}_{\text{red}}$ with N_3^- . Hence, the non-electrostatic rate constant ratio between $\mathbf{2}_{\text{ox}}$ and $\mathbf{2}_{\text{red}}$ in the reaction with N_3^- is approximately 1100 ($\Delta\Delta H^\ddagger_{\text{n.e.s.}} = 4.1$ kcal/mole, assuming $\Delta\Delta S^\ddagger = 0$) at 25 °C.

To summarize, using the reversibly redox-active chelating cobaltocene ligand dppc, electrochemical control of the reactivity of a Re carbonyl moiety towards nucleophilic attack at a carbonyl carbon atom has been demonstrated. Ligand (dppc) oxidation by one electron results in a $\Delta\nu_{\text{CO}}$ of $\sim 15\text{ cm}^{-1}$, a ~ 200 -fold increase in reactivity of **3** with tertiary amine-N-oxides, a 5400 fold increase in reactivity of **2** with N_3^- , and, for both reactions, a 3-4 kcal/mole decrease in ΔH^\ddagger . The reactivity of **2** with N_3^- displays a classic Brønsted primary salt effect, with **2_{ox}** subject to twice the ionic strength dependence of **2_{red}**, but minimal change in dielectric strength dependence upon ligand oxidation.

References

1. (a) Mirkin, C. A.; Wrighton, M. S. *J. Am. Chem. Soc.* **1990**, *112*, 8596. (b) Singewald, E. T.; Mirkin, C. A. *Abstracts of Papers*, 206th National Meeting of the American Chemical Society, Chicago, IL; American Chemical Society: Washington, DC, 1993; INOR 405.
2. (a) Medina, J. C.; Goodnow, T. T.; Rojas, M. T.; Atwood, J. L.; Lynn, B. C.; Kaifer, A. E.; Gokel, G. W. *J. Am. Chem. Soc.* **1992**, *114*, 10583, and references therein. (b) Allgeier, A. M.; Singewald, E. T.; Mirkin, C. A. *Abstracts of Papers*, 206th National Meeting of the American Chemical Society, Chicago, IL; American Chemical Society: Washington, DC, 1993; INOR 404.
3. (a) Beer, P. D.; Crowe, D. B.; Main, B. *J. Organomet Chem.* **1989**, *375*, C35. (b) Beer, P. D.; Keefe, A. D. *J. Organomet Chem.* **1989**, *375*, C40. (c) Beer, P. D.; Blackburn, C.; McAleer, J. F.; Sikanyika, H. *Inorg. Chem.* **1990**, *29* 378. (d) Beer, P. D.; Keefe, A. D.; Sikanyika, H.; Blackburn, C.; McAleer, J. F.; *J. Chem. Soc., Dalton Trans.* **1990**, 3289. (e) Beer, P. D.; Nation, J. E.; McWhinnie, S. L. W.; Harman, M. E.; Hursthouse, M. B.; Ogden, M. I.; White, A. H. *J. Chem. Soc., Dalton Trans.* **1991**, 2485. (f) AlObaidi, N. J.; Salam, S. S.; Beer, P. D.; Bush, C. D.; Hamor, T. A.; McQuillan, F. S.; Jones, C. J.; McLeverly, J. A. *Inorg. Chem.* **1992**, *31*, 263. (g) Beer, P. D.; Heseck, D.; Hodacova, J.; Stokes, S. E. *J. Chem. Soc., Chem. Commun.* **1992**, 270. (h) Beer, P. D.; Drew, M. G. B.; Hazlewood, C.; Heseck, D.; Hodacova, J.; Stokes, S. E. *J. Chem. Soc., Chem. Commun.* **1993**, 229.
4. (a) Shi, C.; Anson, F. C. *J. Am. Chem. Soc.* **1991**, *113*, 9564. (b) Shi, C.; Anson, F. C. *Inorg. Chem.* **1992**, *31*, 5078.
5. Lorkovic, I. M.; Duff, R. R.; Wrighton, M. S. Manuscript in preparation.
6. Mutterties, E. L. *Inorg. Chem.* **1965**, *4* 1841. Darensbourg, D. J.; Drew, D. *J. Am. Chem. Soc.* **1976**, *98*, 275.

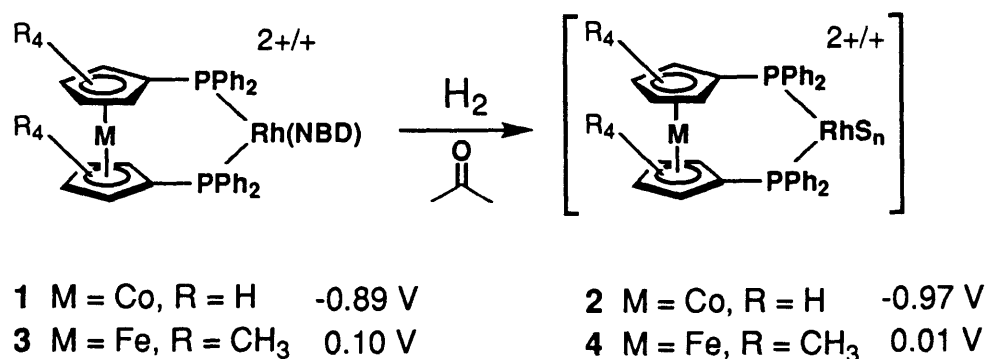
7. Angelici, R. J. *Acc. Chem. Res.* **1972**, *5*, 335. Angelici, R. J.; Brink, R. W. *Inorg. Chem.* **1973**, *12*, 1067. Angelici, R.J.; Blacik, L. J. *Inorg. Chem.* **1972**, *11*, 1754.
8. Kruck, T.; Noack, M. *Chem. Ber.* **1964**, *97*, 1693.
9. (a) Beck, W.; Smedal, H. S. *Angew. Chem.* **1966**, *78*, 267. (b) Beck, W.; Smedal, H. S. *Angew. Chem., Int. Ed. Engl.* **1966**, 5253 (c) Werner, H.; Beck, W.; Engelmann, H. *Inorg, Chim. Acta* **1969**, *3*, 331. (d) Graziani, M.; Busetto, L.; Palazzi, A. *J. Organomet. Chem.* **1971**, *26*, 261.
10. (a) Darensbourg, D. J.; Darensbourg, M. Y. *Inorg. Chem.* **1970**, *9*, 1691. (b) Darensbourg, M. Y.; Conder, H. L.; Darensbourg, D. J.; Hasday, C. *J. Am. Chem. Soc.* **1973**, *95*, 5919. (c) Dobson, G. R.; Paxson, J. R. *J. Am. Chem. Soc.* **1973**, *95* 5925.
11. (a) Hieber, W.; Lipp, A. *Chem. Ber.* **1959**, *92*, 2085. (b) Alper, H.; Edward, J. T. *Can. J. Chem.* **1970**, *48*, 1543.
12. (a) Shi, Y.-L.; Gao, Y.-C.; Shi, Q.-Z.; Kershner, D. L.; Basolo, F. J. *Organometallics* **1987**, *6*, 1528. (b) Shen, J.-K.; Gao, Y.-C.; Shi, Q.-Z.; Basolo, F. J. *J. Organomet. Chem.* **1991**, *401*, 295. (c) Shi, Y.-L.; Gao, Y.-C.; Shi, Q.-Z.; Rheingold, A. R.; Basolo, F. J. *Inorg. Chem.* **1991**, *30*, 1868.
13. (a) Andre, J.-F.; Wrighton, M. S. *Inorg. Chem.*, **1986**, *25*, 532. (b) Lewis, G. J.; Roth, J. D.; Montag, R. A.; Safford, L. K.; Gao, X.; Chang, S. C.; Dahl, L. F.; Weaver, M. J. *J. Am. Chem. Soc.* **1990**, *112*, 2831. (c) Roth J. D.; Lewis, G. D.; Safford, L. K.; Jiang, X.; Dahl, L. F.; Weaver, M. J. *J. Am. Chem. Soc.* **1992**, *114*, 6159.
14. For example, (a) Leung, L.-W. H.; Wieckowski, A.; Weaver, M. J. *J. Phys. Chem.* **1988**, *92*,6985. (b) Chang, S.-C.; Leung, L.-W. H.; Weaver, M. J. *J. Phys. Chem.* **1989**, *93*, 5341.
15. (a) Elschenbroich, C.; Stohler, F. *Angew. Chem., Int. Ed. Engl.* **1975**, *14*, 174. (b) Kotz, J. C.; Nivert, C. L.; Lieber, J. M.; Reed, R. C. *J. Organomet. Chem.* **1975**, *91*, 87. (c) Colbron, S. B.; Robinson, B. H.; Simpson, J. *Organometallics* **1983**, *2*, 943. (d) Miller, T. M.; Ahmed, K. J.; Wrighton, M. S. *Inorg. Chem.* **1989**, *28*, 2347.

16. Wolf, M. O.; Wrighton, M. S. *Chem. Mat.* **1994**, *6*, 1526.
17. (a) Rudie, A. W.; Lichtenberg, D. W.; Katcher, M. L.; Davison, A. *Inorg. Chem.* **1978**, *17*, 2859. (b) Dubois, D. L.; Eigenbrot, C. W. Jr.; Miedaner, A.; Smart, J. C. *Organometallics* **1986**, *5*, 1405.
18. Craig, J. C.; Purushothaman, K. K. *J. Org. Chem.* **1970**, *35*, 1721.
19. Gallucci, J. C.; Opromolla, G; Paquette, L. A.; Pardi, L.; Schirch, P. F. T.; Sivik, M. R.; Zanello, P. *Inorg. Chem.* **1993**, *32*, 2292, and references therein.
20. Cullen, W. R.; Kim, T. J.; Einstein, F. W. B.; Jones, T. *Organometallics* **1985**, *4*, 346.
21. Seiler, P.; Dunitz, J. D. *Acta Cryst.* **1979**, *B35*, 1068.
22. (a) Webb, R. J.; Lowery, M. D.; Shiomi, Y; Sorai, M.; Wittebort, R. J.; Hendrickson, D. N. *Inorg. Chem.* **1992**, *31*, 5211. (b) Mammano, N. J.; Zalkin, A.; Landers, A. Rheingold, A. L. *Inorg. Chem.* **1977**, *16*, 297.
23. Bündler, W.; Weiss, E. *J. Organomet. Chem.* **1975**, *92*, 65.
24. Churchill, M. R.; DeBoer, B. G. *J. Am. Chem. Soc.* **1974**, *96*, 6310.
25. Bard, A. J.; Garcia, E.; Kukharenko, S.; Strelets, V. V. *Inorg. Chem.* **1993**, *32*, 3528.
26. Lorkovic, I. M.; Christ, C. S.; Wrighton, M. S. Unpublished Results.
27. Laidler, K. J. *Chemical Kinetics*; McGraw Hill: New York, 1965; Chapter 5.
28. Atkins, P. W. *Physical Chemistry*; W. H. Freeman: New York, 1986; Chapter 11.
29. Amis, E. S.; La Mer, V. K. *J. Am. Chem. Soc.* **1939**, *61*, 905.
30. Maryott, A. A.; Smith, E. R. *Table of Dielectric Constants of Pure Liquids*. NBS Circular #514, U.S. Government Printing Office: Washington, D. C., 1951.

Chapter 3

Use of Redox-active 1,1'-*Bis*(diphenylphosphino)metallocene Ligands to Reversibly
Control the Rate of the Rhodium(I) Catalyzed Hydrogenation, Hydrosilation and
Isomerization of Ketones and Alkenes

One of the goals of this research group is to characterize well-defined catalysts having multiple redox states. Reported in this chapter is the synthesis and characterization of a set of reversibly redox-active hydrogenation catalyst precursors $[\text{Rh}(\text{dppc})\text{NBD}]^{2+/+}$ (NBD = bicyclo[2.2.1]-2,5 heptadiene, $\text{dppc} = 1,1'$ -bis(diphenylphosphinocobaltocene), **1**, and $[\text{Rh}(\text{omdppf})\text{NBD}]^{2+/+}$ $\text{omdppf} = \text{octamethyl-}1,1'$ -bis(diphenylphosphinoferrrocene), **3**, $[\text{Ir}(\text{dppc})\text{COD}]^{2+/+}$, COD = 1,5-cyclooctadiene, **5**, and $[\text{Ir}(\text{omdppf})\text{COD}]^{2+/+}$, **6**. **1** and **3** react in both states of charge with H_2 in acetone to give $[\text{Rh}(\text{dppc})(\text{acetone})_n]^{2+/+}$, **2** and $[\text{Rh}(\text{omdppf})(\text{acetone})_n]^{2+/+}$, **4**, respectively, Scheme 1.



Scheme 1. Activation of Rh(I) reduction catalysts having dppc and omdppf ligands. Redox potentials are relative to $E^0(\text{Fc}^+/\text{Fc}) = 0.39 \text{ V vs SCE}$.

We show here that variation in the state of charge of the redox-active ligand in **1-6** can dramatically alter the catalytic properties of the Rh or Ir center. Overall, the oxidized catalysts are generally more durable than the reduced catalysts. Particularly interesting are the findings that **2_{red}** is a faster hydrogenation catalyst than **2_{ox}**, while **2_{ox}** is a faster hydrosilation catalyst, and that **3** shows activity as an electrocatalyst for H_2 oxidation.

There have been many studies on ligand electronic and steric effects on the reactivity and selectivity of transition metal catalysts.¹ A redox-active ligand provides a

way to probe electronic effects on reactivity without significantly altering the steric factors, since the immediate coordination sphere is fixed. Reactivity with neutral substrates should not be affected by the electrostatic factors associated with changing the state of charge.² Thus, rate variations for catalytic reactions involving neutral substrates such as H₂, alkenes and ketones should be due to variation in electronic factors at the catalytic center to which the redox-active ligand is bound

As demonstrated in the previous chapter, chelating redox-active phosphine ligands based on ferrocene and cobaltocene can be used to alter electron density of a transition metal to which it is bound such that its stoichiometric reactivity changes by up to four orders of magnitude. We thus felt that use of such a ligand would be warranted in the study of redox-induced homogeneous *catalytic* reactivity changes, the next step of this project.

The Schrock-Osborn cationic Rh(I)³ and Crabtree cationic Ir(I)⁴ olefin reduction catalysts are a well studied classes of homogeneous catalysts. We chose to make redox-active metallocene bisphosphine derivatives of these catalysts, since catalytic activity does not appear to involve dissociation of the chelating phosphine. Electronic influence over the reactivity depends on the fact that both phosphines of the chelating redox ligand are bound to Rh throughout the catalytic cycle. Other Rh(I) catalysts such as Vaska's type halocarbonyl bisphosphines were not as desirable because the *cis* isomer, which is the only possible isomer for chelating metallocene *bis*phosphines is prone to rearrangement to form dimers with bridging bisphosphines, thus complicating the reactivity.⁵

While cationic Rh reduction catalysts containing both achiral⁶ and chiral⁷ ferrocene-based phosphines are well studied, there have been no reports describing the use of changes in the state of charge of the metallocene-based ligand to reversibly alter the properties of the catalysts. A point that bears repeating is that the first choice of a redox-active chelating ligand which comes to mind for this type of work, dppf, or 1,1'-*bis*(diphenylphosphino)ferrocene, is not durable when oxidized. For the work in Chapter

2, a ligand was required which was not only durable when oxidized but also durable in the presence of nucleophiles, a role which dppc filled well. For the work in this chapter, namely the catalytic hydrogenation and hydrosilation of olefins and ketones, the ligand need not be so inert to nucleophiles in its oxidized form. Therefore, another ligand based on permethylated ferrocene, octamethyl-1,1'-*bis*(diphenylphosphino)ferrocene (omdppf),⁸ was prepared. When complexed to Rh(I) or Ir(I), omdppf has a redox potential similar to ferrocene, and is durable in its oxidized form. One problem encountered with the Rh(omdppf) (but not for Ir) complexes in comparative catalytic reactivity studies was that the oxidized form was reduced in the presence of substrates such as H₂ or silane, precluding comparison of catalytic reactivity between the two states of charge but suggesting the use of the Rh(omdppf) species as an electrocatalyst for the oxidation of H₂ or silane. Thus, complexes of dppc remained the ones of choice for the study of catalytic reactivity differences between the two catalyst states of charge. It is shown in this chapter that simple reversible electrochemical control over the rate of a catalytic reaction is achievable by altering the state of charge of a redox-active ligand bound to a catalytic center.

Experimental

All solvents and electrolytes used were purified by standard techniques. Acetone (Omnisolv) was dried over B₂O₃ and distilled through three bump traps. All reactions and manipulations were performed under an Ar atmosphere in a drybox or using standard Schlenk techniques unless otherwise noted. NMR spectra were acquired on a Bruker AC-250, Varian 300-XL or Unity 300 MHz instruments. UV-Vis spectra were recorded on an HP-8452a diode-array spectrophotometer. Electrochemical measurements were performed in a 0.1 M [*n*-Bu₄N]PF₆ acetone or CH₂Cl₂ solution with glassy carbon working, Pt counter, Ag wire quasireference electrodes with a Pine Instruments RDE4 potentiostat, using either ferrocene (Fc) or [Co(η⁵-C₅H₅)₂]PF₆ ([CoCp₂]PF₆) as internal reference. Hexaethyldisiloxane and triethylsilanol were obtained from Aldrich.

Syntheses.

Ferrocenium salts (FcPF₆, ClO₄⁻, CF₃SO₃⁻) were prepared either by metathesis of ferrocenium hydrogensulfate produced from sulfuric acid oxidation of ferrocene, or by oxidation using the appropriate silver salt (acetylferrocenium (AcFc)⁺ PF₆⁻, CF₃SO₃⁻) in CH₂Cl₂, followed by filtration and precipitation with diethyl ether. [Fe(C₅Me₅)₂]PF₆ (Fc*PF₆) was prepared by metathesis of Fc*Cl (Fc* + HCl, O₂). Pentyltriethylsilane and isopropoxytriethylsilane were prepared by preparative gas chromatography purification of reaction products of triethylchlorosilane with pentylmagnesium bromide (Aldrich 2.0 M in diethyl ether, 24 h reflux) and isopropanol (neat), respectively.

omdppf.⁸ NMR, CD₂Cl₂, ¹H, δ: 7.34, m, 8H; 7.20, m, 12H; 1.74, s, 12H; 1.29, s, 12H. C₆D₆, ³¹P, δ (rel. to H₃PO₄ ext. ref.): 20.95. UV-Vis, λ in acetone (values are for peaks unless labeled v or s, for valley or shoulder, respectively), nm (ε, M⁻¹cm⁻¹): 396 (150) v, 448 (310) p. E_{1/2} = -0.35 vs Fc⁺/Fc (CH₂Cl₂).

[omdppf]PF₆. CH₂Cl₂ (2 ml) was added to a 10 ml flask charged with FcPF₆ (332 mg, 1mmol), omdppf (667 mg, 1mmol), and a magnetic stir bar. The solution was stirred for 10 min and diethyl ether (8 ml) added. The precipitated [omdppf]PF₆ was collected and

recrystallized from CH₂Cl₂/diethyl ether, giving green needles. NMR, acetone-*d*₆, ¹H, δ: 15.12, b, 8H; 9.00, b, 8H; 7.92, b, 4H; -40.0, vb, 24H. UV-Vis λ in acetone, nm (ε, M⁻¹cm⁻¹): 434 (2600), 560 (100) v, 820 (510). Anal.: Calcd. for FeP₃F₆C₄₂H₄₄ • 0.5(C₄H₁₀O): C, 62.00; H, 5.45. Found C, 61.38; H, 5.54.

[(dppc)Rh(NBD)](PF₆)₂ (1_{ox}**). A modification of the procedure reported by Schrock and Osborn^{3a} was employed. THF (1 ml) was added to a 10 ml flask charged with a magnetic stir bar, [(NBD)RhCl]₂ (233 mg, 1.00 mmol), dppcPF₆⁹ (702 mg, 1.00 mmol), and NaPF₆ (168 mg) and the mixture stirred magnetically at room temperature until the initial black suspension became yellow (0.5-4 h). For some batches addition of diethyl ether (1-2 ml) was required before the color changed. After addition of 5 ml of diethyl ether, the suspension was vacuum filtered through a fine porosity frit. The collected solid was further washed with ether and benzene, and then dissolved from the frit with CH₂Cl₂. Addition of diethyl ether gave crystalline plates of **1_{ox}**, which upon collection and drying became opaque and easily crumbled. NMR, acetone-*d*₆, ¹H, δ: 7.95, m, 8H; 7.25, m, 12H; 6.10, b, 4H; 6.08, b, 4H; 4.75, m, 4H; 4.10, m, 2H; 1.58, m, 2H. ³¹P, δ (rel. to H₃PO₄ ext. ref.): 28.0, d, (J_{Rh-P} = 159 Hz). UV/Vis, λ in acetone, nm (ε, M⁻¹cm⁻¹): 410 (950) v, 460 (2400). E_{1/2} = -0.89 V vs Fc⁺/Fc (acetone). Anal.: Calcd. for RhCoP₄F₁₂C₄₁H₃₆ C, 47.25; H, 3.48. Found C, 47.18; H, 3.37.**

[(dppc)Rh(NBD)]PF₆ (1_{red}**). **1_{red}** was prepared as for **1_{ox}**, using dppc¹⁰ (557 mg, 1.00 mmol). Although an X-Ray quality crystal of **1_{red}** was obtained by recrystallization from CH₂Cl₂/diethyl ether, to obtain analytically pure **1_{red}** on a larger scale, a final recrystallization from minimal CH₂Cl₂/MeOH was required. **1_{red}** was also prepared as the ClO₄⁻ and CF₃SO₃⁻ salts by substitution of NaPF₆ with the appropriate Na salt. NMR, acetone-*d*₆, ¹H, δ: 8.30, b, 8H; 7.56, t (J = 7.3 Hz), 4H; 7.00, b, 8H; 4.06, b, 2H; 3.15, b, 2H; 2.92, b, 4H; -12.2, b, 4H; -52.0, b, 4H. UV/Vis, λ in acetone, nm (ε, M⁻¹cm⁻¹): 424 (1400) v, 470 (2800), 510 (1100) v, 544 (1300). Anal.: Calcd. for RhCoP₃F₆C₄₁H₃₆ C, 54.88; H, 4.04. Found C, 54.52; H, 4.16.**

[(dppc)RhS_n](PF₆)₂ (2_{ox}**). A solution of **1_{ox}** in acetone, or alternatively, solid **1_{ox}** was treated with H₂ for 15 min. NMR, acetone-*d*₆, ¹H, δ: 8.00, q(J = 6 Hz), 8H, 7.67, t(J=7 Hz), 4H; 7.58, t(J = 7 Hz), 8H; 6.09, b, 4H; 6.06, b, 4H. ³¹P, δ (rel. to H₃PO₄ ext. ref.): 51.3, d (J_{Rh-P} = 209 Hz). E_{1/2} = -0.97 V vs Fc⁺/Fc (acetone).**

[(dppc)RhS_n]PF₆ (2_{red}**). Prepared as for **2_{ox}**, or by chemical reduction of **2_{ox}** with cobaltocene. NMR, acetone-*d*₆, ¹H, δ: 8.00, b, 8H; 7.37, t (J = 7.3 Hz), 4H; 6.82, b, 8H; -9.5, b, 4H; -50, b, 4H. Chemically oxidizing (reducing) a solution of **2_{red}** (**2_{ox}**) in acetone-*d*₆ prepared from **1_{red}** (**1_{ox}**) with Fc⁺PF₆ (cobaltocene) yields a solution having an NMR spectrum identical to **2_{ox}** (**2_{red}**) prepared from **1_{ox}** (**1_{red}**).**

[(omdppf)Rh(NBD)]PF₆ (3_{red}**). **3_{red}** was prepared as for **1** using omdppf (668 mg 1 mmol). **3_{red}** was also prepared as the CF₃SO₃⁻ salt using the same procedure but with NaCF₃SO₃. A final recrystallization from 1,2-dichloroethane/heptane gave solid **3_{red}** which entrained 1 equivalent of 1,2-dichloroethane (DCE). NMR, acetone-*d*₆, ¹H, δ: 7.84, tm, 8H; 7.57, m, 12H; 4.69, m, 4H; 4.09, m, 2H; 1.70, s, 12H; 1.64, s, 12H; 1.57, b, 2H. ³¹P, δ(rel. to H₃PO₄ ext. ref.): 27.8, d, (J_{Rh-P} = 157 Hz). UV/Vis, λ in acetone, nm (ε, M⁻¹cm⁻¹): 414 (1020) v, 462 (1900). E_{1/2} = 0.10 V vs Fc⁺/Fc (acetone). Anal.: Calcd. for RhFeP₃F₆C₄₉H₅₂ • CH₂ClCH₂Cl C, 55.41; H, 5.11. Found C, 55.48; H, 5.08.**

[(omdppf)Rh(NBD)](PF₆)₂ or (CF₃SO₃⁻)₂ (3_{ox}**). yellowish green **3_{ox}** was prepared by treatment of **3_{red}** with AgPF₆, followed by filtration through celite, or AcFcPF₆ in CH₂Cl₂, followed by addition of diethyl ether to precipitate solid **3_{ox}**, and filtration, with subsequent recrystallization from CH₂Cl₂/ether. Attempted recrystallization of **3_{ox}** from any solvent combination which included MeOH resulted in formation of **3_{red}**. **3_{red}** was also prepared as the CF₃SO₃⁻ salt using NaCF₃SO₃ in the prep above as for **1_{ox}** or **1_{red}**. **3_{ox}** was prepared as the CF₃SO₃⁻ salt by treating **3_{red}** in CH₂Cl₂ with AcFcCF₃SO₃. Unlike for the PF₆⁻ salt, using AgCF₃SO₃ as oxidant for the CF₃SO₃⁻ salt of **3_{red}** gave a mixture of products containing Ag(omdppf)²⁺, Ag(omdppf)⁺, and **3_{ox}** and**

3_{red}. The CF₃SO₃⁻ salt was more stable to hydrolysis than the PF₆⁻ salt. NMR, acetone-*d*₆, ¹H, δ: 13.4, b, 8H; 8.81, b, 8H; 7.95, b, 4H; -0.93, b, 2H; -2.1, b, 6H; -26.6, b, 12H; -34.2, b, 12H. UV/Vis λ in acetone, nm (ε, M⁻¹cm⁻¹): 418 (1600) v, 452 (2100), 600 (100) v, 820 (360). Anal. (CF₃SO₃⁻ salt): Calcd. for RhFeP₂S₂F₆O₆C₅₁H₅₂ C, 52.80; H, 4.52. Found C, 51.99; H, 4.55.

[(omdppf)RhS_n]PF₆ (4_{red}). A solution of **3_{red}** in acetone was treated with H₂ giving a dark orange solution. **4_{red}** decomposes in CH₂Cl₂. NMR, acetone-*d*₆, ¹H, δ: 8.28, m, 8H, 7.47, m, 12H; , 8H; 1.62, s, 12H; 1.52, s, 12H. ³¹P, δ(rel. to H₃PO₄ ext. ref.): 54.3, d (J_{Rh-P} = 219 Hz). E_{1/2} = 0.01 V vs Fc⁺/Fc (acetone).

[(omdppf)RhS_n](PF₆)₂ (4_{ox}). Treatment of **3_{ox}** with H₂ initially gives **4_{ox}**, which is then reduced by H₂ in acetone, giving **4_{red}**. **4_{ox}** was not isolated in a pure state. The reduction of **4_{ox}** to **4_{red}** by H₂ is slowed in acetone and completely stopped in CH₂Cl₂ by excess olefin (cyclohexene or, more effectively, norbornadiene) or HSO₃CF₃ (>0.5 M, in acetone)

[(dppc)Ir(COD)](PF₆)₂ (5_{ox}). Acetone (5 ml) was added to a flask charged with [dppc]PF₆ (700 mg, 1.0 mmol) and [Ir(pyridine)₂(COD)]PF₆^{4b} (600 mg, 1.0 mmol). After stirring for 30 min the solvent was removed *in vacuo*, the residue recrystallized from CH₂Cl₂/diethyl ether. A final recrystallization from CH₂Cl₂/heptane gave flaky opaque crystals which entrained 0.50 and 0.15 equivalents of CH₂Cl₂ and heptane, respectively. NMR, acetone-*d*₆, ¹H, δ: 7.6-7.8, m, 20H; 5.89, b, 4H; 5.77, b, 4H; 4.30, b, 4H; 2.32, dm(J = 9 Hz), 4H; 2.06, q(J = 9 Hz), 4H. ³¹P, δ(rel. to H₃PO₄ ext. ref.): 14.46. UV/Vis λ in acetone, nm (ε, M⁻¹cm⁻¹): 364 (1600) v, 390 (2800), 440 (600) v, 496 (2300), 534 (230) v, 578 (460). E_{1/2} = -0.86 V vs Fc⁺/Fc (CH₂Cl₂). Anal.: Calcd. for IrCoP₄F₁₂C₄₂H₄₀ • 0.5(CH₂Cl₂) • 0.15 (C₇H₁₆) C, 43.75; H, 3.64, P, 10.40 Found C, 42.86; H, 3.47; P, 8.82.

[(dppc)Ir(COD)]PF₆ (5_{red}). Cobaltocene (37 mg, 0.20 mmol) dissolved in CH₂Cl₂ (1 ml) was added dropwise to a rapidly stirred solution of **5_{ox}** (200 mg 0.20 mmol) in

CH₂Cl₂ (2 ml). The deep red solution, containing suspended CoCp₂PF₆, was filtered through celite and solvent removed. The residue was recrystallized from minimal CH₂Cl₂/MeOH. Attempts to prepare **5_{red}** from dppc and [Ir(COD)(pyridine)₂]PF₆ gave uncharacterizable products. NMR, acetone-*d*₆, ¹H, δ: 8.24, b, 8H; 7.39, b, 4H; 6.84, b, 8H; 3.41, b, 4H; 2.32, b, 8H; -21.3, b, 4H; -50.7, b, 4H. UV/Vis λ in acetone, nm (ε, M⁻¹cm⁻¹): 372 (2600) v, 392 (3100), 436 (1270) v, 496 (3000), 580 (520) s. Anal.: Calcd. for IrCoP₃F₆C₄₂H₄₀ C, 50.30; H, 4.01. Found C, 50.02; H, 4.03.

[(omdppf)Ir(COD)]PF₆ (6_{red}**)**. The procedure used to prepare **5_{ox}** was followed, using omdppf (666 mg) instead of dppcPF₆. NMR, acetone-*d*₆, ¹H, δ: 7.90, b, 8H; 7.58, b, 12H; 4.32, b, 4H; 2.33, dm(J = 9 Hz), 4H; 1.84, q(J = 9 Hz), 4H; 1.70, s, 12H; 1.59, s, 12H. ³¹P, δ(rel. to H₃PO₄ ext. ref.): 18.19. UV/Vis λ in acetone, nm (ε, M⁻¹cm⁻¹): 368 (1600) v, 384 (1900) p, 426 (810) v, 470 (1700) s, 486 (2100) p, 566 (390) s, 630 (40) s. E_{1/2} = 0.13 V vs Fc⁺/Fc (CH₂Cl₂). Anal: Calcd. for IrFeP₃F₆C₅₀H₅₆ C, 54.00; H, 5.08. Found C, 53.97; H, 5.04.

[(omdppf)Ir(COD)](PF₆)₂ (6_{ox}**)**. A solution of AgPF₆ (68 mg 0.27 mmol) in CH₂Cl₂ (1 ml) was added dropwise to a stirred solution of **6_{red}** (300 mg, 0.27 mmol) in CH₂Cl₂ (5 ml). After removal of the Ag suspension by filtration through celite, diethyl ether was carefully added to the flask to precipitate **6_{ox}** as a mauve powder. Once precipitated, **6_{ox}** was difficult to redissolve in CH₂Cl₂, but was soluble in acetone or nitromethane. NMR, CD₃NO₂ (acetone-*d*₆), ¹H, δ: 11.80 (12.07), b, 8H; 9.36 (9.32), b, 8H; 8.67 (8.61), b, 4H; -2.16 (-2.16), b, 8H; -2.79 (-2.75), b, 4H; -22.0 (-22.1), b, 12H; -34.7 (-34.7), b, 12H. UV/Vis λ in acetone, nm (ε, M⁻¹cm⁻¹): 382 (3700) s, 442 (1300) v, 486 (1800), 514 (1096) v, 520 (1102), 600 (290) v, 618 (200) v, 820 (470). Anal: Calcd. for IrFeP₄F₁₂C₅₀H₅₆ C, 47.80; H, 4.49. Found C, 47.47; H, 4.21.

Catalysis. To change the state of charge of the catalyst *in situ*, an appropriate amount of a concentrated deoxygenated solution of either cobaltocene or Fc*PF₆ in acetone, or

CH_2Cl_2 for reactions run in THF, was added to the stirred solution via syringe. For the hydrogenations and hydrosilations of olefins in acetone or THF, catalyzed by **2** or **4**, typical experiments were performed as follows: Precatalyst solutions (0.2-5 mM) of **1_{ox}** (yellow), **1_{red}** (burgundy), or **3_{red}** (yellow) in acetone or THF were prepared in an inert atmosphere glovebox in Schlenk flasks equipped with stir bars. The flasks were sealed with wired-down rubber septa, removed from the drybox, evacuated and purged twice with H_2 ($P_{\text{total}} = 870 \pm 20$ torr), forming solutions of **2_{ox}** (paler yellow), **2_{red}** (pine green), **4_{red}** (dark orange). For olefin hydrogenations, after allowing the solutions to stir under H_2 for at least 15 min while immersed in a $20.0 \pm 0.5^\circ \text{C}$ bath, deoxygenated cyclohexene or 1-pentene was added via syringe. Aliquots (50-200 μL) were removed via cannula and quenched with CH_3CN (ca. 4 mL), and the resulting solutions were analyzed by GC/MS. For acetone hydrogenation, solutions of **1_{ox/red}** were prepared with methylcyclohexane (ca. 15 mM) as internal standard. For catalytic hydrosilation, solutions of **1_{ox/red}** were prepared with decane (ca. 0.12 M) internal standard. After formation of **2_{ox/red}** with H_2 the solutions were evacuated and purged with Ar twice before addition of Et_3SiH (to make a 0.6 M solution) or $\text{Et}_3\text{SiH}/2\text{-pentene}$ (1:1, 0.4 M). Analyte concentrations were determined by comparison with standard solutions analyzed by GC at the same time as the reaction aliquots.

Catalytic hydrogenation of cyclohexene in CH_2Cl_2 using **1_{ox/red}**, **3_{ox/red}**, **5_{ox/red}** and **6_{ox/red}** was performed as above by preparation in the drybox of CH_2Cl_2 solutions containing the catalyst precursor and cyclohexene. H_2 was admitted last, by evacuating and purging twice after temperature equilibration ($20.0 \pm 0.5^\circ \text{C}$), since activation of the catalyst (hydrogenation of cyclooctadiene or norbornadiene) in the absence of substrate results in decomposition of the catalyst. Aliquots were taken by syringe or cannula and quenched with CH_3CN .

The hydrosilation of 1-hexene catalyzed by **1** and **3** was followed by $^1\text{H-NMR}$ in CD_2Cl_2 and acetone- d_6 . Solutions consisting of catalyst (5-20 mM), $\text{Et}_3\text{SiH}/1\text{-hexene}$, 1/1

(0.5 M) were prepared in the drybox and quickly transferred to air tight NMR tubes and a series of spectra taken with the samples held at 23 ± 2 ° C. Percent yield of hydrosilation versus isomerization was determined by integration of the non-olefinic protons, using a delay time of 10 s between pulses.

Results and Discussion

X-Ray Crystallography. Changing the state of charge of a reversibly redox-active ligand bound to a reactive metal complex allows one to alter the electronic properties of the complex in a well-defined way. Until very recently, there have been very few reports of transition metal complexes with redox-active ligands crystallographically characterized in two states of charge.¹¹ The crystallographic analysis of **1** was undertaken to find out what structural changes in the rhodium center accompany the oxidation or reduction of the dppc ligand, and thus to determine whether the reactivity differences may be ascribed to electronic or structural effects. X-ray quality crystals of **1_{red}** were obtained by recrystallization from CH₂Cl₂/Et₂O, but suitable crystals of **1_{ox}** could not be obtained. Repeated attempts to recrystallize **1_{ox}** in its BF₄⁻, ClO₄⁻ and PF₆⁻ salts from various solvents for comparison with **1_{red}** always resulted in formation of crystals which would rapidly desolvate upon isolation. The CF₃SO₃⁻ salt did not form crystals.

The ORTEP diagram for the solid state structure of **1_{red}** is shown in Figure 1. Experimental Details of the crystallography of **1_{red}** are presented in Table 1, with key structural features in Table 2. As might be expected, the structure of **1_{red}** is very similar to that of [(NBD)Rh(dppf)]ClO₄ reported by Cullen and coworkers.^{6d} Consistent with the other two crystal structures of metal bound reduced dppc (Chapter 2 and ref. 10), the average Co-Cp distance is about 1.715 Å, about 0.08 Å longer than for the oxidized form, and about 0.07 Å longer than the Fe-Cp distance in dppf complexes. Correspondingly, the bite angle, at 98.1° is also wider by 3°. The Rh-Co distance, at 4.17 Å, is closer than Rh-Fe distance in [(NBD)Rh(dppf)]⁺ 4.263 Å and the Re-Co distance (4.4 Å) in [Re(CO)₄dppc]⁺. As noted in Chapter 2, the high symmetry of the NMR spectra of **1_{ox}** in solution demonstrates that most of features relating to dppc ligand conformation around Rh disappear or become averaged at room temperature. The bite angle, which is partially determined by the Co-Cp distance, likely remains wider on average than for **1_{ox}**.

Figure 1. Ortep Diagram of **1_{red}** shown with 35% probability ellipsoids. The carbon atoms, showing only principle ellipses, were refined only isotropically.

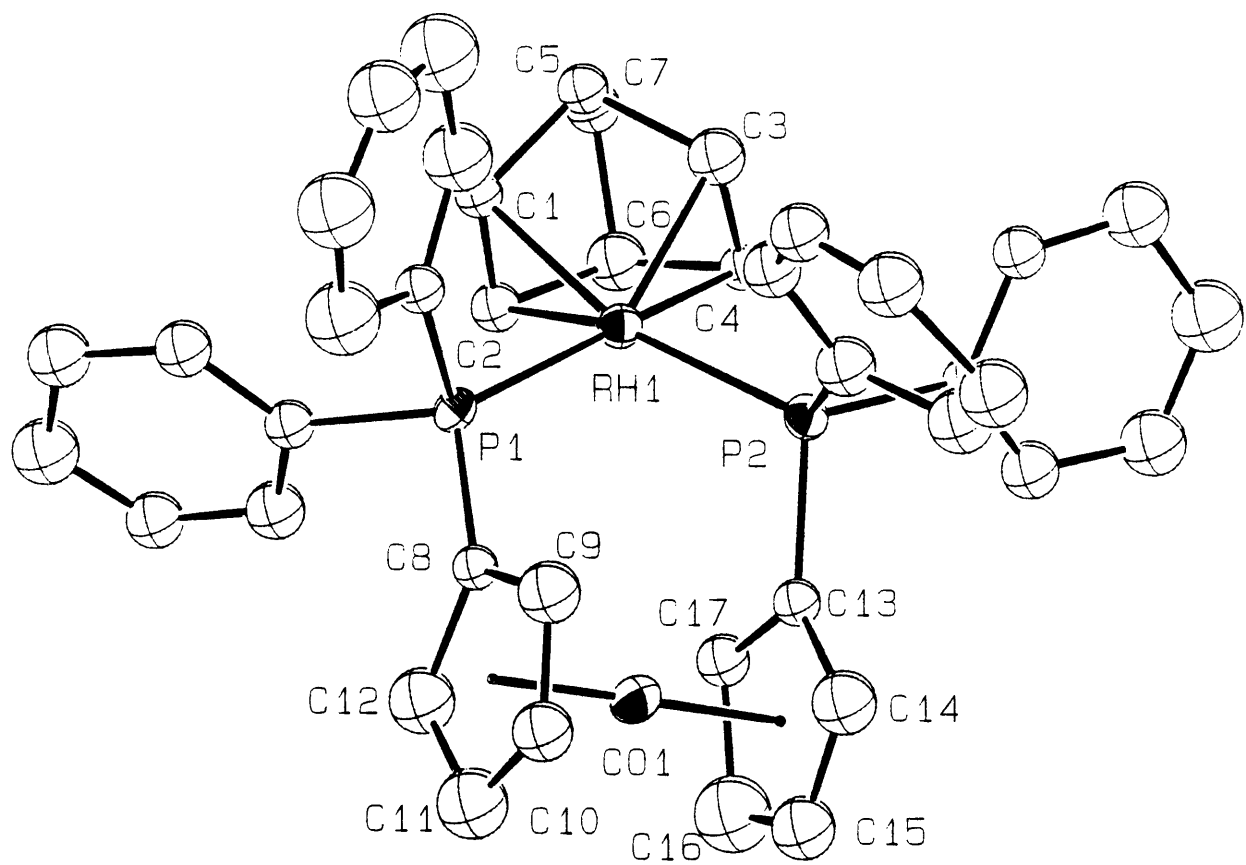


Table 1. Experimental details of X-ray crystallography of [(dppc)Rh(NBD)]⁺[PF₆]
(**1_{red}**).

formula	RhCoP ₃ F ₆ C ₄₁ H ₃₆
fw	897.49
Crystal Color, Habit	black, needle
Crystal Dim. (mm)	0.12 X 0.12 X 0.38
No. refl (unit c. det)	13 (12.04 - 24.00°)
Omega Scan Peak FWHM	0.43
crystal system	<i>orthorhombic</i>
space group	<i>P212121</i> (#19)
<i>a</i> , Å	16.938
<i>b</i> , Å	17.082
<i>c</i> , Å	12.863
<i>V</i> , Å ³	3722
<i>Z</i>	4
ρ_{calcd} , g/cm ³	1.602
<i>T</i> , K	296
<i>F</i> ₀₀₀	1812
μ (Mo K α)	10.67
Diffractometer	Rigaku AFC6R
Radiation	Mo K α (λ = 0.71069 Å)
Take-off Angle	6.0°
Detector aperture	6 mm x 6 mm
Crystal-Detector Dist.	40 cm
Scan Type	ω -2 θ
Scan Rate	8.0°/min (in ω) (8 rescans)

Scan Width	$(1.37 + 0.35 \tan\theta)^\circ$
$2\theta_{\max}$	55.0°
Reflections	4751
Corrections	Lorentz-polarization
Structure solution	Direct Methods
Refinement	Full-matrix least-squares
Function Minimized	$\sum w (F_o - F_c)^2$
Least-squares Weights	$4F_o^2/\sigma^2(F_o^2)$
<i>p</i> -factor	0.03
Anomalous Dispersion	All non-H atoms
No. Observations ($I > 3.00\sigma(I)$)	1616
no. of parameters	264
Residuals: R^a (R_w^b)	0.062 (0.077)
Goodness of fit ind.	1.95
Max shift/esd, final cycle	0.09
min, max peak, $e/\text{\AA}^3$	-0.57, 0.61

$$^a \sum ||F_o| - |F_c|| / \sum |F_o|$$

$$^b [(\sum w (|F_o| - |F_c|)^2 / \sum w F_o^2)]^{1/2}$$

Table 2. Key features of the solid state structure of **1_{red}**.**Distances**

Rh-Co	4.176(4) Å
Co-Cp(centroid)	1.73(1), 1.70(1) Å
Rh-P1, Rh-P2	2.346(7), 2.315(7) Å
Rh-C1, Rh-C2	2.20(2), 2.20(2) Å
Rh-C3, Rh-C4	2.18(3), 2.24(2) Å
Rh-midpoint(C1-C2,C3-C4), av	2.09 Å
C1-C2, C3-C4	1.36(3), 1.39(3) Å
Co-plane(P1-Rh-P2)	1.92 Å

Angles

P1-Rh-P2	98.1(2)°
midpoint(C1-C2)-Rh-midpoint(C3-C4)	71.3°
NBD "twist" ^a	13°
Cp stagger	30.3°

^aAngle between midpoint(C1-C2)-midpoint(C3-C4)-Rh and P1-Rh-P2 planes.

Catalysis. The norbornadiene complex of Rh(I) bisphosphines is a convenient, easily purified catalyst precursor. Treatment with H₂ releases norbornene and generates the active catalyst. The rate of this initial activation for **1_{ox}** and **1_{red}** was investigated in acetone at 20° C. Excess NBD was used so that the reaction could be followed conveniently and quantitatively by GC. Some results are shown in Figure 2, and more data are tabulated in Table 3, including results for other substrates. The reaction is found to be zeroth order in NBD for the concentration regime studied here ([NBD] > 0.2 M), but at lower [NBD] (less than 0.03M), changes to first order. When the hydrogenation of NBD in acetone catalyzed by **1_{ox}** and **1_{red}** is carried out in a cuvette ([NBD] > 0.1 M), UV-Vis spectra of **1_{ox}** and **1_{red}** during the hydrogenation of NBD, the most prominent feature of which is the the Rh-diolefin absorbance near 450 nm, remain identical to the spectra measured before admission of H₂. This is also true for NBD hydrogenation catalyzed by both states of charge of **1** and **3** in CH₂Cl₂ or 1,2-dichloroethane (DCE). Thus, in this NBD concentration range, NBD association is considerably faster than hydrogenation and dissociation. For **3_{ox}** and **3_{red}** in acetone, however, less than half the absorbance observed in the 450-470 nm range before hydrogenation is observed during NBD hydrogenation, along with a superimposed spectral change caused by ligand reduction in the case of **3_{ox}**. The primary products formed, norbornene and nortricyclene, are those corresponding to reaction of NBD with one equivalent of H₂. For **1_{ox}** and **1_{red}** the conversion of NBD to nortricyclene, identified by its mass spectrum,¹² is about 20% and 7% (using relative total ion count), respectively, the remaining detected products being norbornene and norbornane. Nortricyclene formation may result from a homoallylic rearrangement¹³ of a (5-norbornenyl)RhH species formed after insertion of NBD into the other Rh-H bond. Norbornane is a secondary product and is only observed as a product after most of the NBD has been consumed.

Ir(bisphosphine)-diolefin catalyst precursors **5** and **6** have UV-Vis absorptions analogous to those for the Rh species **1** and **3**. In the Ir(COD) case, the hydrogenation of

Figure 2. Hydrogenation of norbornadiene in acetone at 20.0 °C at a total pressure (H₂ + acetone) of 870 torr, catalyzed by **1_{ox}** (3.6 mM, [NBD] = 0.23 M) and **1_{red}** (4.5 mM, [NBD] = 0.58 M), followed by GC/MS.

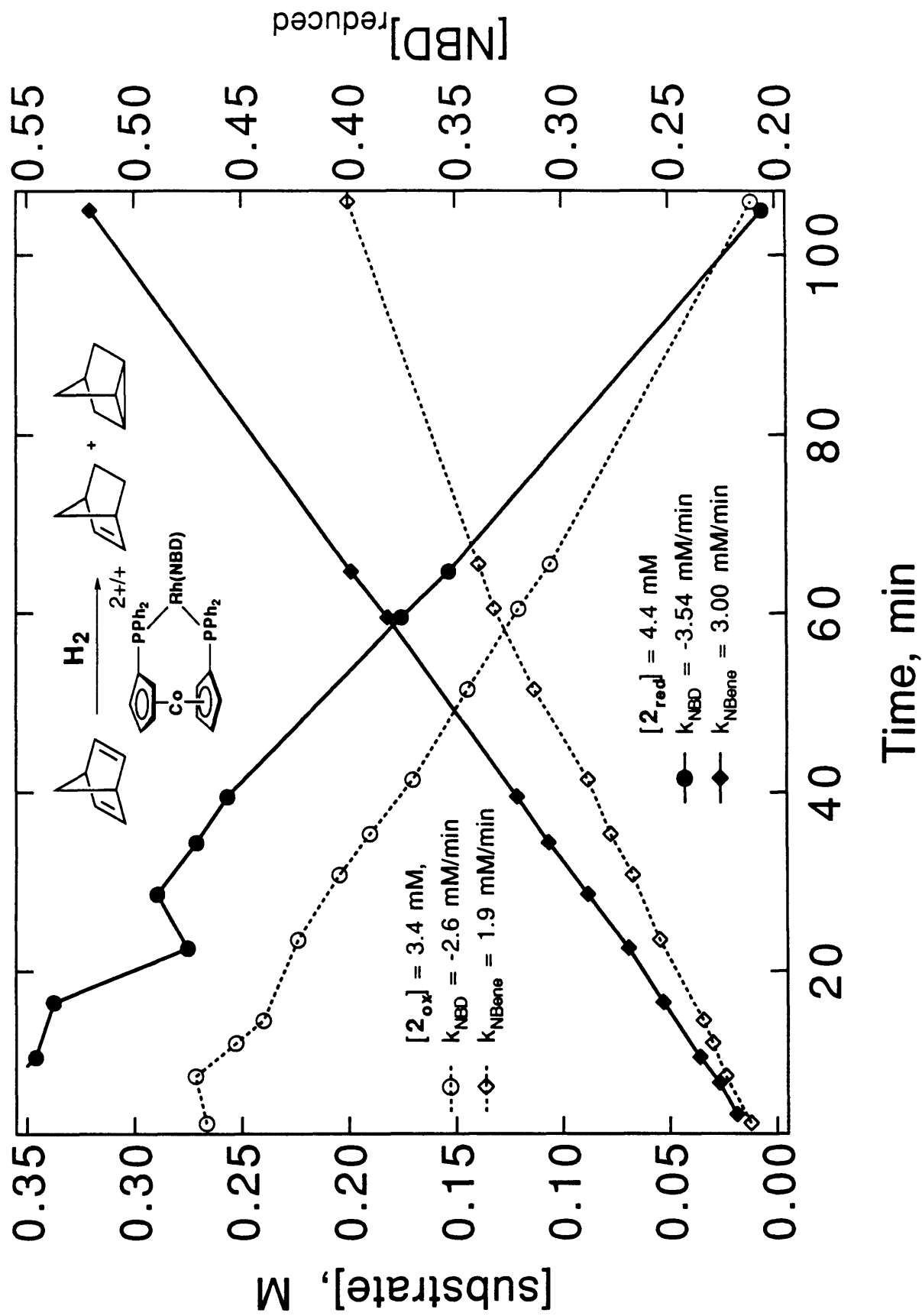


Table 3. Rate data for hydrogenation ($P_{\text{total}} = 870$ torr) catalyzed by \mathbf{I}_{ox} and \mathbf{I}_{red} at 20 °C in acetone.

Substrate (c, M)	cat oxidation st	[Rh], mM	init rate, mM/min
norbornadiene ^a			
(0.27)	oxidized	0.50	0.291
(0.026)		1.06	0.288
(0.23)		3.55	1.89
(0.25)	reduced	0.54	0.47
(0.026)		1.04	1.0
(0.58)		4.28	3.0
cyclohexene ^b			
(0.90)	oxidized	4.03	0.14
(0.90)		2.2	0.21
(0.90)		1.8	0.14
(0.90)		0.44	0.043
(0.90)	reduced	4.0	3.5
(0.90)		2.4	1.6
(1.05)		2.7	4.0
(0.82)		0.49	1.42
1-pentene			
(0.83)	oxidized	1.04	0.02 (isom) 0.06 (hydrog)
(0.83)	reduced	1.17	5.6 (isom) 2.0 (hydrog)
acetone, solvent			
	oxidized	1.69	0.0032
	reduced	0.52	0.042
		1.11	0.061
		4.4	0.11

^arates of norbornene formation

^baverage of cyclohexene consumption and cyclohexane production rates.

excess COD in DCE results in loss of about 60% of the UV-Vis absorptions at 390, 496, and 580 nm, with no change in their relative absorbances, consistent with the buildup of a large concentration of nonabsorbing Ir(I) or Ir(III) complexes. In contrast to NBD hydrogenation catalyzed by **1** and **3**, hydrogenation of COD by **5** and **6** at room temperature in DCE or CH₂Cl₂ gives cyclooctane directly, without significant buildup of free cyclooctene.

The general trend observed in the hydrogenations of other unsaturated substrates is that **2_{red}** is a more effective hydrogenation catalyst than **2_{ox}**. The only products detected by GC/MS or NMR are cyclohexane (hydrogenation of cyclohexene) and pentane and 2-pentene (1-pentene hydrogenation/isomerization). Figure 3 shows the effect of changing the catalyst concentration on the rate of cyclohexane hydrogenation. Although there is much scatter in the data, the reaction looks to be 1/2 order in **2_{ox}** and even lower order in **2_{red}**. The same features are observed when **4_{red}** is used as catalyst, Figure 4. The differences in rates observed between **2_{ox}** and **2_{red}** are also observable by chemical reduction or oxidation of the catalysts *insitu* and this is shown in Figures 5 and 6. In Figure 5, after 65 min of cyclohexene hydrogenation catalyzed by **2_{red}**, Fc*PF₆ is added to change the catalyst to **2_{ox}**. The rate of cyclohexane formation drops dramatically, and after another 125 min cobaltocene is added to reform **2_{red}**, and the cyclohexane formation rate rises again. Figure 6 shows the hydrogenation/isomerization of 1-pentene to pentane and 2-pentene catalyzed by both **2_{ox}** and **2_{red}**. **2_{ox}** again is the much less effective catalyst for these transformations. Chemical reduction of the solution containing **2_{ox}** results in catalytic activity which is nearly the same as that of **2_{red}**, consistent with the **2_{red}** formed from **1_{red}** being the same species as that formed from reduction of **2_{ox}**. Chemical reoxidation of **2_{red}** with Fc*PF₆ does somewhat slow 1-pentene hydrogenation but not to the dormancy observed before the reduction, and does not slow the isomerization, indicating that **2_{red}** partially decomposed to some catalytically active species not affected by the addition of Fc*+. **2_{red}** is initially much more reactive than **2_{ox}** for the hydrogenation

Figure 3. Plot of the log of cyclohexene hydrogenation rate versus log of catalyst concentration in acetone at 20.0 °C catalyzed by **1_{ox}** and **1_{red}**.

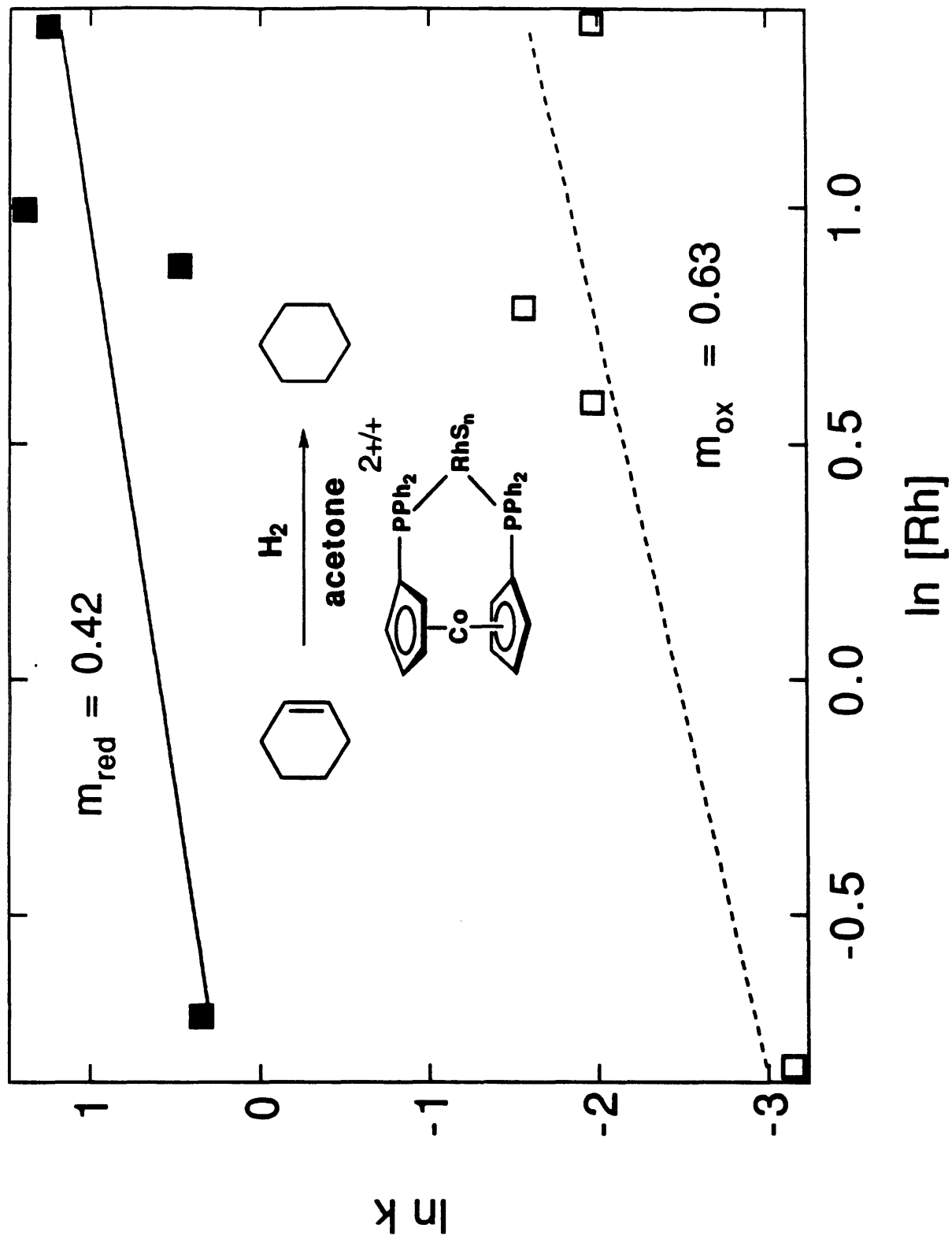


Figure 4. Hydrogenation of cyclohexane in acetone at 20.0 °C catalyzed by **4_{red}**.

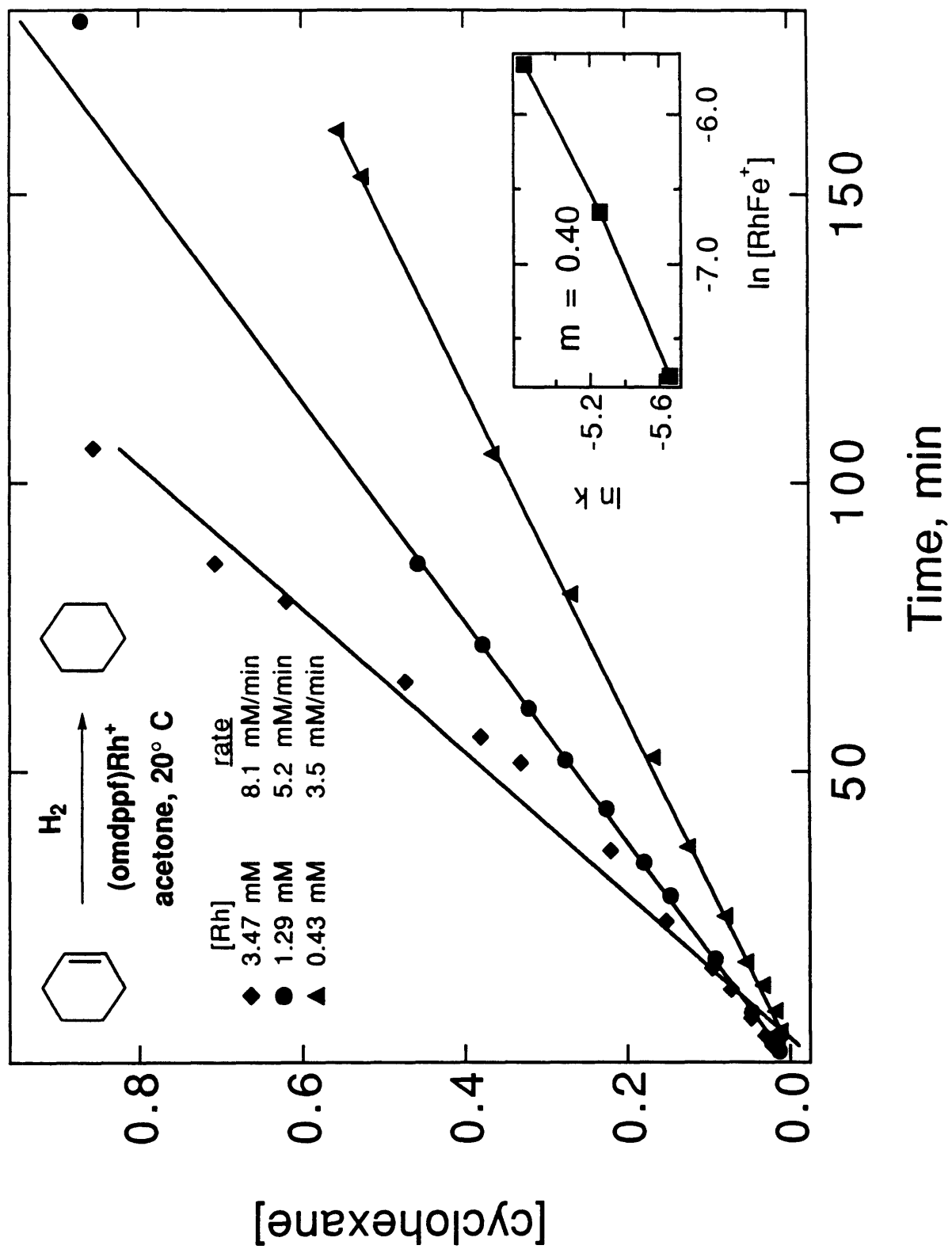


Figure 5. Progress of the hydrogenation of cyclohexene in acetone at 20.0 °C catalyzed by a solution of **2** prepared from 0.044 mmol of **1_{red}**. At 65 min and 125 min, 0.044 mmol of Fc*PF₆ and cobaltocene are added, respectively.

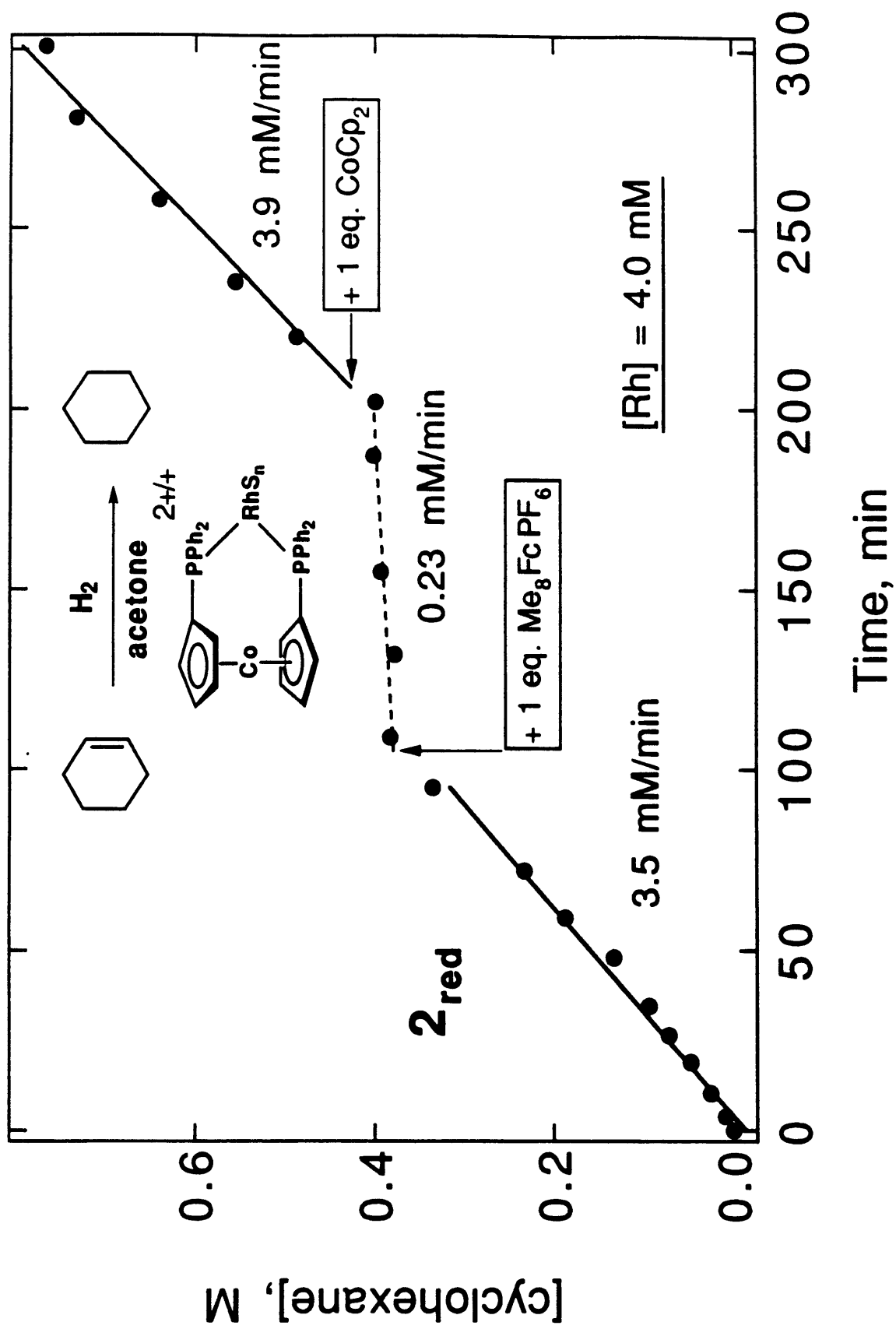
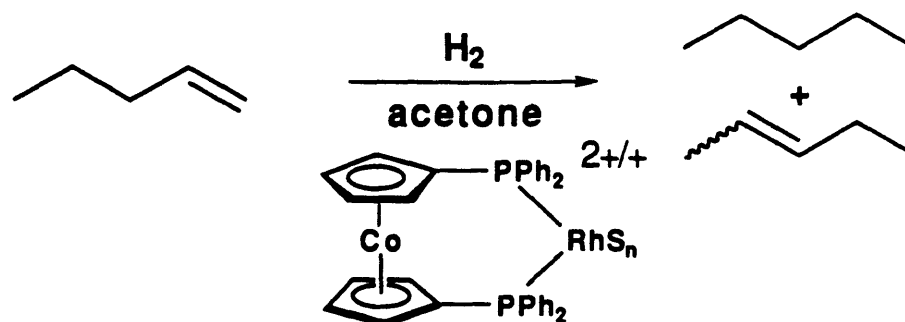


Figure 6. Progress of the hydrogenation/isomerization of 1-pentene to pentane and cis and trans 2-pentene in acetone at 20.0 °C catalyzed by a solutions of **2_{red}** prepared from 0.013 mmol of **1_{red}** (top) and **2_{ox}** prepared from 0.0095 mmol of **1_{ox}** (bottom). After 146 min, 0.013 mmol of cobaltocene is added to the solution containing **2_{ox}** and after 201 min 0.013 mmol of Fc*PF₆ is added to the same solution.



of acetone to isopropanol, but the reaction is slow compared to olefin hydrogenation, and the catalytic activity decreases over time ($t_{1/2} = 1$ h). It should be noted that addition of excess Fc^+PF_6^- to solutions containing $\mathbf{2}_{\text{ox}}$ does not change the rate of catalysis, while adding excess cobaltocene suppresses the catalytic activity completely. Since the reducing power of $\mathbf{2}_{\text{red}}$ is only 350 mV lower than that of cobaltocene, the relative instability of $\mathbf{2}_{\text{red}}$ is possibly a consequence of a disproportionation-like decomposition.

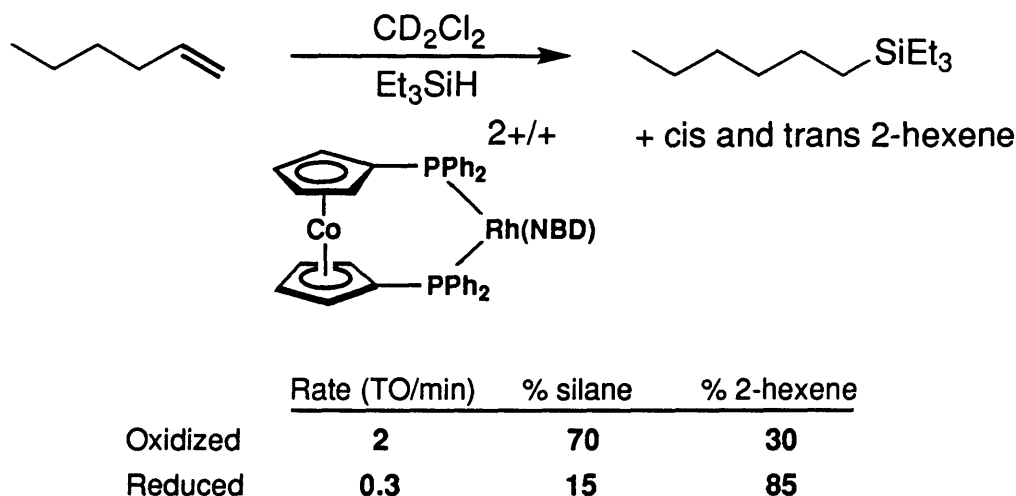
The iridium analogues to the chelating bis(phosphine) cationic Rh hydrogenation catalysts have been studied by Crabtree and coworkers,⁴ and these are found to be most effective as catalysts in non-coordinating solvents such as CH_2Cl_2 . The iridium is found to bind too strongly to solvents such as acetone. We synthesized cationic Ir(COD) complexes of dppc and omdppf to assay how the state of charge of the ligand affects catalytic reactivity. The catalytic hydrogenation of cyclohexene using **1**, **3**, **5**, and **6** was investigated in CH_2Cl_2 . The results are summarized in Table 4. The rhodium catalysts **1** and **3** are also very effective in CH_2Cl_2 . The largest differences in reactivity between the two states of charge are observed for $\mathbf{5}_{\text{ox}}$ and $\mathbf{5}_{\text{red}}$, where $\mathbf{5}_{\text{red}}$ is about twice as fast as $\mathbf{5}_{\text{ox}}$. A more striking feature of the charge dependent reactivities of the Rh and Ir redox-active catalysts in CH_2Cl_2 is that the oxidized catalysts are much more durable than the reduced, a trend also seen in the reactivities in acetone, but more obvious here. Since oligomerization of catalyst monomers is the main cause of catalyst deactivation for Crabtree type catalysts,^{4b-d} it is possible that the stability of the oxidized catalysts is due to electrostatic repulsion between the dicationic monomers of the oxidized catalyst being much greater than that between the monocationic monomers of the reduced forms. Collision frequencies between free ions in solution are known to increase/decrease 1-3 orders of magnitude per unit decrement/increment in the product of charges between the two reacting ions, depending on the dielectric strength of the solution.² Another possibility is that the effects are due to lower overall basicity of the catalyst leading to lower oligomerization rate. This is consistent with the fact that dicationic $\mathbf{6}_{\text{ox}}$, for which the chelating omdppf⁺ ligand

Table 4. Rate data for cyclohexene hydrogenation catalyzed by **1**, **3**, **5**, and **6** at 20 °C.
in CH₂Cl₂.

[cyclohexene], M	Catalyst	[cat], mM	k _{init} , mM/min	% completion
0.022	1_{ox}	0.046	0.99	100
1.00		2.1	1.8	100
0.022	1_{red}	0.69	0.72	40
1.00		2.2	1.9	<100
0.022	3_{ox}	0.51	1.7	100
1.00		1.01	2.9	100
0.022	3_{red}	0.63	1.7	100
1.00		1.23	2.8	30
0.020	5_{ox}	0.41	1.1	100
0.044		0.53	1.5	100
1.00		1.70	2.9	100
0.05	5_{red}	0.59	3.0	95
1.00		1.8	6.5	20
0.038	6_{ox}	0.46	1.4	95
1.00		0.79	3.6	72
0.034	6_{red}	0.50	0.71	85
0.022		0.46	0.95	92
1.00		0.97	2.7	50

is more basic than dppc^+ , is not as rugged as $\mathbf{5}_{\text{ox}}$.

Hydrosilation. The Schrock-Osborn and Crabtree catalysts are not as well studied in their activity as catalysts for hydrosilation of olefins and ketones as for hydrogenation of these substrates. When a 1:1 mixture of 1-hexene and triethylsilane was added to a CD_2Cl_2 solution containing $\mathbf{1}_{\text{ox}}$ or $\mathbf{1}_{\text{red}}$, production of hexyltriethylsilane and internal hexenes was observed, Scheme 2. Moreover, the reaction occurred after a short induction



Scheme 2. Difference between $\mathbf{1}_{\text{ox}}$ and $\mathbf{1}_{\text{red}}$ in catalysis of 1-hexene hydrosilation / isomerization.

period without catalyst activation with H_2 . Reproducibly, $\mathbf{2}_{\text{ox}}$ had a much shorter induction period (10 min) than $\mathbf{2}_{\text{red}}$ (30-60 min) and catalyzed the disappearance of 1-hexene about an order of magnitude faster than $\mathbf{1}_{\text{red}}$. In addition, the relative ratio of hexyltriethylsilane to internal hexene, which did not react further, was much higher for the oxidized form (70:30) than for the reduced (15:85), as shown in Scheme 2. During the entire course of the reaction, the NMR peaks of the catalyst remained those of $\mathbf{1}_{\text{ox}}$ or $\mathbf{1}_{\text{red}}$. No reaction was observed in the presence of 100 mM NBD, or if triethylsilane was excluded. The results are consistent with the active catalyst being formed by a small

amount of NBD hydrosilation and dissociation giving a small concentration of "naked" bisphosphine rhodium catalyst, which is quenched by free NBD, if present. The existence of an induction period argues against mere thermal dissociation of NBD. A rate study of NBD exchange with 7-*tert*-butoxynorbornadiene in acetone- d_6 on **1_{ox}** and **1_{red}** shows that $t_{1/2}$ for the exchange at room temperature is about 3 days and is not noticeably affected by the presence of 0.1 M triethylsilane or olefin.

Performing the hydrosilation of 1-pentene in acetone- d_6 gives roughly the same initial results as the hydrosilation of 1-hexene in CD_2Cl_2 , except that at longer times, isopropoxytriethylsilane- d_6 , hexaethyldisiloxane and triethylsilanol are produced, all identified by ^{13}C -NMR, and GC/MS. Unlike in CD_2Cl_2 , **1_{ox}** shows significant conversion to **2_{ox}** after 3 h. It is possible that NBD is hydrogenated by the H_2 formed in the hexaethyldisiloxane and triethylsilanol production. Use of **3_{red}** for the hydrosilation of 1-pentene in both CD_2Cl_2 and acetone- d_6 gave about 30% pentyltriethylsilane and 70% 2-pentenes. Attempted hydrotriethylsilation of cyclohexene in acetone- d_6 , catalyzed by **4_{red}** resulted in the formation of isopropoxytriethylsilane- d_6 in high yield. When use of **3_{ox}** as a catalyst for hydrosilation of pentene was attempted, however, the greenish yellow solution turned orange seconds after the introduction of triethylsilane, signaling the formation of **3_{red}** and precluding its comparison to the reduced form as a catalyst but stimulating the study of the use of **3** as an electrocatalyst.

Since there is an induction period for hydrosilation catalyzed by **1**, hydrosilation catalyzed by **2_{ox}** and **2_{red}** in acetone or THF was studied. The results are summarized in Table 5. The most obvious feature of the results is that, in contrast to the hydrogenation results, **2_{ox}** is a more active catalyst than **2_{red}** for hydrosilation. For acetone hydrosilation, besides the expected product isopropoxytriethylsilane, hexaethyldisiloxane and a trace of triethylsilanol were also observed as products, in increasing amounts in acetone with higher $[H_2O]$. Figure 7 shows the dependence of the reaction rate on the catalyst concentration between 0.2 and 5 mM. Excluding the rate observed for the lowest

Table 5. Rate data for hydrosilation catalyzed by **2_{ox}** and **2_{red}** at 20° C.

[Substrate], M	[Et ₃ SiH], M	catalyst	[Rh], mM	k _{init} , mM/min	k no induc ^a
acetone, solvent	0.57	2_{ox}	0.16	0.19	
	0.57		0.70	0.89	
	0.57		1.55	1.27	
	0.57		1.68	1.47	
	0.57		3.40	2.03	
	0.57		4.26	2.01	
	0.57		4.48	2.42	
	0.52	2_{red}	0.19	0.16	
	0.57		0.75	0.29	
	0.57		1.53	0.34	
	0.57		4.89	0.61	0.42
	0.57		5.04	0.45	0.27
2-pentene ^b					
0.39	0.39	2_{ox}	0.93	1.1	
0.59	0.59		1.1	1.4	
0.39	0.39	2_{red}	0.95	0.45	0.0

^a Obtained by excluding the t=0 point in the regression.

^b In THF at 20° C

catalyst concentration, the reaction order in 2_{ox} is again about 0.5 and less than 0.5 order in 2_{red} . One consequence of the difference in reaction order is that greater differences between 2_{ox} and 2_{red} in catalytic acetone hydrosilation rate are observed for solutions with higher catalyst concentrations. As for the hydrogenation reaction in Figures 5 and 6, changes in reactivity may be induced by ligand reduction or oxidation *in situ*. Figure 8 shows the results of acetone hydrotriethylsililation catalyzed by 2_{ox} which is reduced after 65 min by the addition of 1 equivalent of cobaltocene, slowing the reaction down by an order of magnitude. Reoxidation by addition of Fc^*PF_6 results in recovery of some, but not all catalytic activity. The same phenomenon is observed if 2_{red} is the initial form of the catalyst. Oxidation of 2_{red} after 60 min in the catalytic solution increases the catalytic activity, but not to the rate reached if starting with 2_{ox} . As was observed in hydrogenation reactions, addition of excess cobaltocene results in catalyst deactivation, while excess Fc^*PF_6 does not effect the reactivity.

For completeness, the hydrosilation/isomerization of 1-pentene catalyzed by 2_{ox} and 2_{red} was studied in acetone. Unlike the unactivated catalysts in CD_2Cl_2 , however, there was no clear difference in reactivity between the two states. Both reacted extremely rapidly (more than 30 turnovers/min) to give pentyltriethylsilane and 2-pentenes. Thereafter the main reaction observed was acetone hydrosilation. It also appeared that 2_{ox} was isomerizing/hydrosilating 2-pentene to pentyltriethylsilane along with some pentenyltriethylsilanes (3%). To study the isomerization/hydrosilation of 2-pentene in a solvent with no competing reaction but which was coordinating enough to stabilize both states of charge of **2**, THF was used as the solvent with the same protocol for catalyst preparation used in acetone. 2_{ox} was stable in this medium and was indeed an efficient catalyst for the isomerization/hydrosilation. 2_{red} could be prepared in this medium but was not durable. Solutions of 2_{ox} and 2_{red} (both 0.9 mM) catalyze the formation of 1-pentyltriethylsilane at initial rates of 1.1 and 0.4 mM/min, respectively, with 2_{red} quickly losing activity ($t_{1/2} = 30$ min). In summary then, for 2-pentene

Figure 7. Plot of the the log of isopropoxytriethylsilane formation rate on the concentration of 2_{ox} and 2_{red} at 20° C. with $[\text{Et}_3\text{SiH}] = 0.57 \text{ M}$, showing 1/2 order dependence on $[2_{\text{ox}}]$.

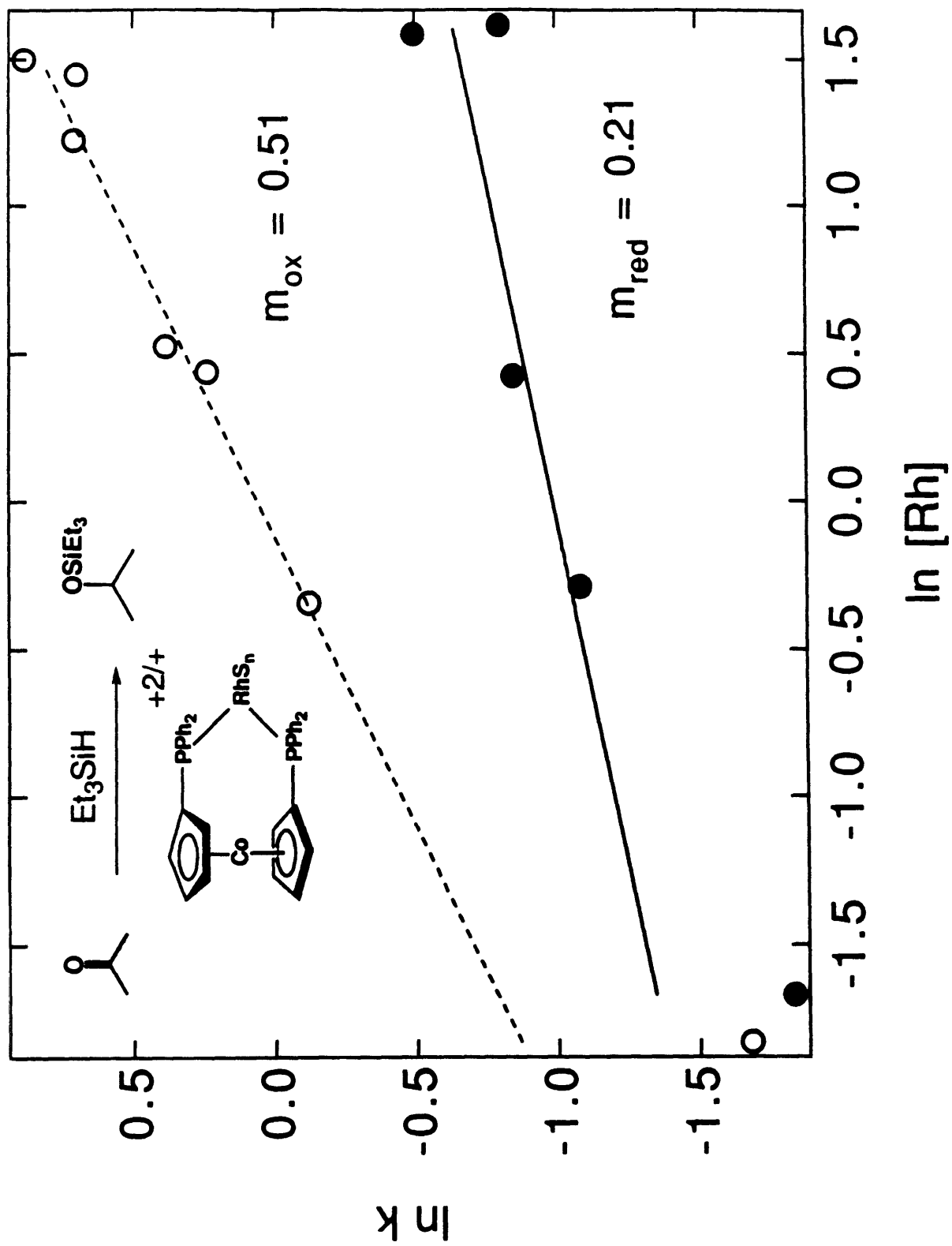
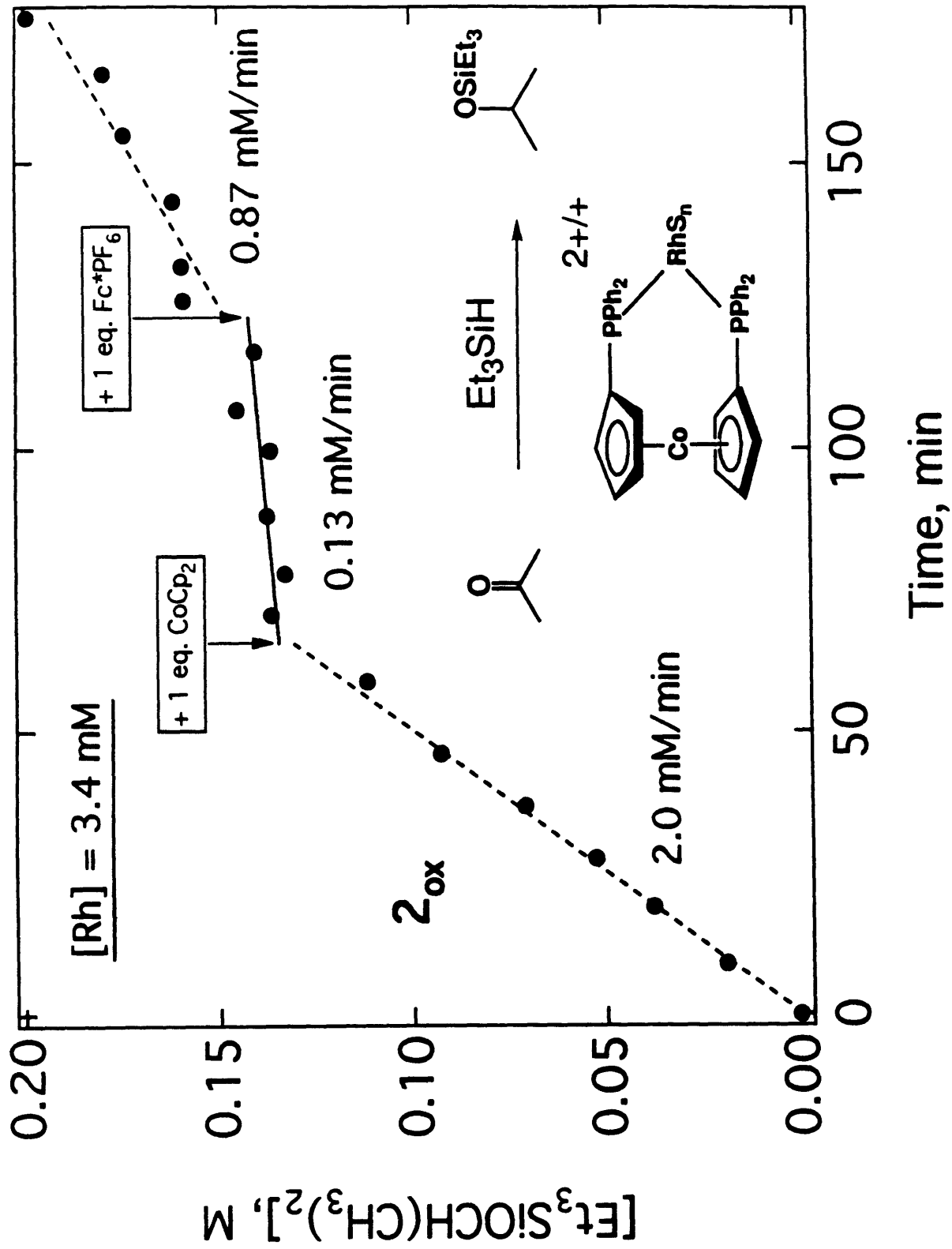
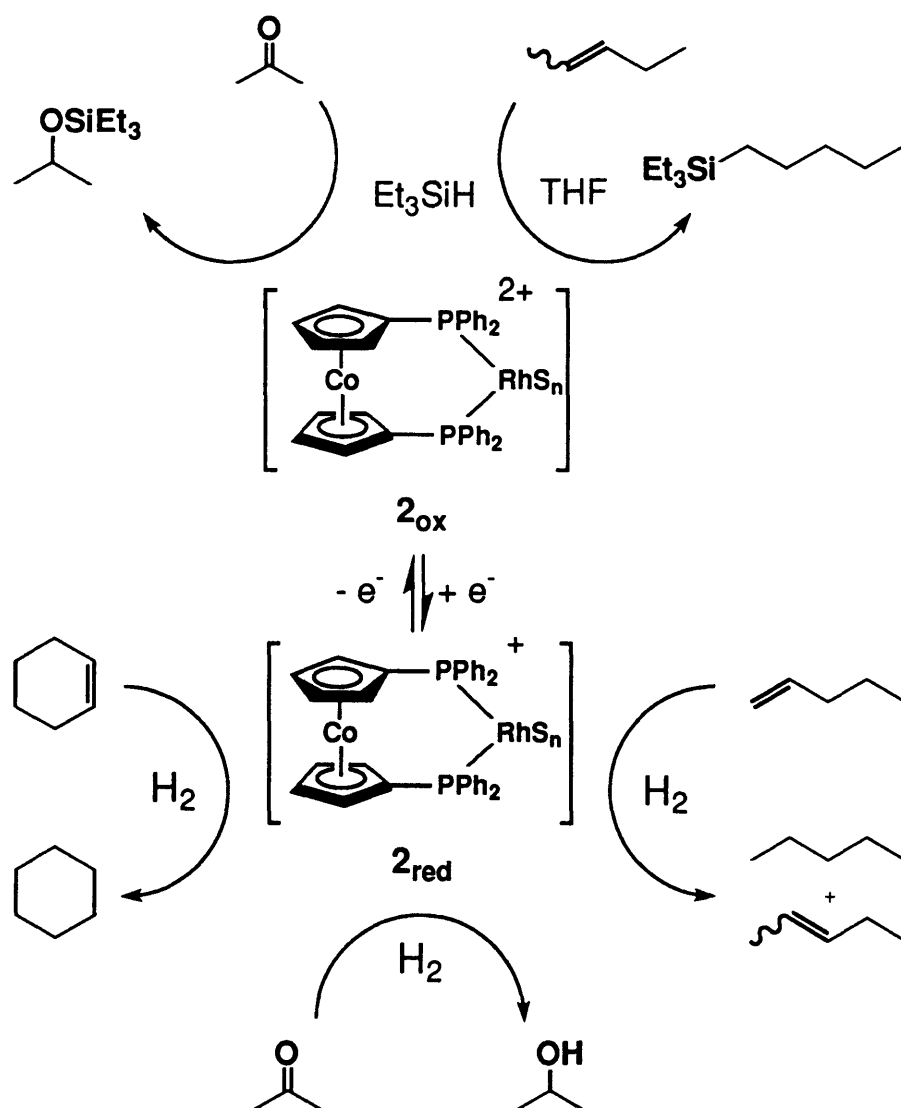


Figure 8. Progress of the hydrosilation of neat acetone at 20.0° C catalyzed by **2**, prepared from 0.038 mmol of **1_{ox}**. At 65 and 125 min, 0.038 mmol of cobaltocene and Fc^*PF_6 are added, respectively.



isomerization/hydrosilation, initially, 2_{ox} is the faster catalyst and is also more durable. Overall, 2_{ox} and 2_{red} , the best studied catalyst in this chapter, exhibits the general reactivity traits shown in Scheme 3, where, for olefin and ketonic substrates the reduced



Scheme 3. Catalytic properties of 2_{ox} versus 2_{red} .

catalyst 2_{red} is the better hydrogenation catalyst and 2_{ox} is more durable under all conditions and is also the better hydrosilation catalyst.

Reduction of dppc^+ or dppf^+ in Re(I) carbonyl complexes causes the CO absorbances to shift 15 cm^{-1} to lower frequency, which, as discussed in Chapter 2, indicates the difference in phosphine basicity between the two states of charge of the ligands is roughly equivalent to that between diphos and 1,2-bis(dicyclohexylphosphino)ethane.¹⁴ The three types of reactions catalyzed by **2** in this chapter, the hydrogenation of a chelating diolefin, the hydrogenation of olefins and ketones, and the hydrosilation of olefins and ketones, show different sensitivity to the oxidation state of the dppc ligand and the consequent change in electron density at Rh. The hydrogenation of norbornadiene, perhaps the best defined reaction in terms of knowledge of the structure of the catalyst resting state, shows virtually no sensitivity to the dppc oxidation state, Figure 2. For the hydrogenation of simple olefins and acetone, **2_{red}** is the faster catalyst, by at least an order of magnitude, Figures 5 and 6 and Table 2. The hydrogenation rate, however, is 0.5 order or less in catalyst concentration. Finally, for hydrosilation reactions catalyzed by **2_{red}** or **2_{ox}**, **2_{ox}** is the faster catalyst, by up to an order of magnitude, and, for the hydrosilation of acetone, the reaction order was again about 0.5 in **2_{ox}** and less than 0.5 in **2_{red}**. It has been proposed that more basic phosphines on RhL_2S_2^+ complexes facilitate the oxidative addition of H_2 and thus speed up the catalysis.^{15, 3b} Based on the lack of charge dependent reactivity differences for **2** in NBD hydrogenation, where this effect should be the most noticeable, the mechanistic consequences of changing the state of charge of dppc seem to be more complicated than simply a ligand basicity effect.

The apparent low molecularity of the reaction rate deserves comment. The reaction order of 0.5 in **2_{ox}** for hydrogenation and hydrosilation indicates that the principle species is a catalytically inactive dimer, which dissociates to give a small concentration of catalytically active monomer. There are two documented types of polynuclear bonding arrangements for Rh(I) chelating *bis*(diarylphosphine) species in the presence of H_2 : those involving hydride bridges^{16, 17a} or those involving η^6 -arene bridges.^{6f, 17} Hydrides have

characteristically high field $^1\text{H-NMR}$ resonances while the protons of Rh(I)-coordinated arenes appear 1 to 2 ppm upfield of uncoordinated arenes. Neither of these features are observed in the $^1\text{H-NMR}$ spectra of $\mathbf{2_{ox}}$ or $\mathbf{4_{red}}$ in acetone- d_6 , although a rapid exchange between the four phenyl groups available for bridging cannot be ruled out. Other workers have shown that formation and dissociation of arene-Rh dimers is a facile process, easily influenced by solvent, phase, or ligand electronic properties.¹⁷ Evidence for oligomer formation in $\mathbf{2_{red}}$ lies in its green color. For all other monomeric complexes of dppc in this thesis, there is a correlation between the position of the lowest energy absorbance maximum and the electrophilicity of the transition metal fragment to which it is bound, as judged by how far positive coordination to the metal center shifts the redox potential of the dppc moiety. as discussed in chapter 2 (pp. 42-50). Upon hydrogenation of a burgundy ($\lambda_{\text{max}} = 542 \text{ nm}$) solution of $\mathbf{1_{red}}$ the dppc redox potential shifts 90 mV *negative*, indicating that the Rh center has become more electron rich and that the absorbance maximum should move to higher energy. The green color of $\mathbf{2_{red}}$ indicates a lower energy absorption. Crabtree type catalysts analogous to $\mathbf{5_{red}}$ form catalytically inactive dimeric or trimeric clusters having bridging hydrides under H_2 in the absence of substrate. The hydrogenation of the initially deep red $\mathbf{5_{red}}$ gives a catalytically inactive deep green solution (showing bridging-type hydrides by $^1\text{H-NMR}$), also formed when the deactivated hydride-bridged cluster derived from $\mathbf{5_{ox}}$ is reduced with cobaltocene. Moreover, when a reaction aliquot containing the green $\mathbf{2_{red}}$ is quenched with CH_3CN , a deep red color reappears, consistent with CH_3CN binding to Rh, reforming monomeric species with typical metal-dppc visible absorption. In any case it is clear that variable temperature NMR experiments, and further attempts to isolate and structurally characterize $\mathbf{2_{ox}}$ and $\mathbf{2_{red}}$ are necessary if the catalysis results are to be better explained. Also, confinement of analogues of $\mathbf{1}$ and $\mathbf{2}$ to electrode surfaces may be useful in better understanding the consequences of changes in the state of charge of the pendant group, since catalyst oligomerization may be hindered by site isolation. These experiments and detailed kinetic studies are in progress.

A topic briefly touched upon in this chapter is that **4** shows promise as an electrocatalyst for the oxidation of H₂ and triethylsilane. In addition to the preliminary observations of changes in the optical properties of **3**_{ox} in the presence of H₂ and triethylsilane, some cyclic voltammetry experiments have been performed on acetone solutions of **4**. We find that at a scan rate of 50 mV/sec the reversible ferrocene-based oxidation of **4** becomes sigmoidal in the presence of 100 mM Et₃SiH, with roughly 50% higher peak anodic current. Under the same conditions, cyclic voltammetry of BrRe(CO)₃(omdppf), which has a redox potential within 50 mV of **4**, remains reversible and non-electrocatalytic. Cyclic voltammetry of Rh(diphos)⁺ shows an irreversible oxidation wave 300 mV positive of **4** and displays electrocatalytic anodic current upon addition of 100 mM Et₃SiH. Thus it appears that RhP₂S₂⁺ species themselves are electrocatalysts for silane oxidation, but that the presence of the reversible redox center on omdppf in **4** facilitates by 300 mV the electron transfer to the electrode. Another worker in this group (Ron Duff) has synthesized analogues of **3** which contain electropolymerizable 3-alkylthiophene groups tethered to phosphorus. XPS analysis, electrochemistry, and catalytic reactivity of electropolymerized films of these species are consistent with the presence of surface confined Rh(I)octamethylferrocenyl-*bis*phosphine species. Further catalytic and electrocatalytic studies of these films are in progress.

References

- 1.(a) For Example: Tolman, C. A. *Chem. Rev.* **1977**, *77*, 313. (b) Rajanbabu, T. V.; Ayers, T. A.; Casalnuovo, A. L. *J. Am. Chem. Soc.* **1994**, *116*, 4101, and references therein.
- 2.(a) Laidler, K. J. *Chemical Kinetics*; McGraw Hill: New York, 1965; Chapter 5. (b) Atkins, P. W. *Physical Chemistry*; W. H. Freeman: New York, 1986; Chapter 11.
3. For example: (a) Schrock, R. R.; Osborn, J. A. *J. Am. Chem. Soc.* **1971**, *93*, 2397. (b) Schrock, R. R.; Osborn, J. A. *J. Am. Chem. Soc.* **1976**, *98*, 2134. (c) Halpern, J. *Inorg. Chim. Acta* **1981**, *50*, 11. (d) Halpern, J. *Science* **1982**, *217*, 401.
4. (a) Crabtree, R. H.; Felkin, H.; Morris G. E. *J. Chem. Soc., Chem. Commun.* **1976**, 716. (b) Crabtree, R. H.; Felkin, H.; Morris G. E. *J. Organomet. Chem.* **1977**, *141*, 205. (c) Crabtree, R. H.; Morris, G. E. *J. Organomet. Chem.* **1977**, *135*, 395. (d) Crabtree, R. *Acc. Chem. Res.* **1979**, *12*, 331.
5. Sanger, A. R. *J. Chem. Soc., Dalton Trans.* **1977**, 120.
6. (a) Unruh, J. D.; Christenson, J. R. *J. Mol. Cat.* **1982**, *14*, 19. (b) Cullen, W. R.; Kim, T.-J.; Einstein, F. W. B.; Jones, T. *Organometallics* **1983**, *2*, 714. (c) Butler, I. R.; Cullen, W. R.; Kim, T.-J.; Jones, T.; Einstein, F. W. B. *J. Chem. Soc. Chem. Commun.* **1984**, 719. (d) Cullen, W. R.; Kim, T.-J.; Einstein, F. W. B.; Jones, T. *Organometallics* **1985**, *4*, 346. (e) Allgeier, A. M.; Singewald, E. T.; Mirkin, C. A.; Stern, C. L. *Organometallics* **1994**, *13*, 2928. (f) Singewald, E. T.; Mirkin, C. A.; Stern C. L. Submitted.
7. (a) Hayashi, T.; Mise, T.; Mitachi, S.; Yamamoto, K.; Kumada, M. *Tetrahedron Lett.* **1976**, 1133. (b) Hayashi, T.; Mise, M.; Kumada, M. *Tetrahedron Lett.* **1976**, 4351. (c) Cullen, W. R.; Yeh, E.-S. *J. Organomet. Chem.* **1977**, *139*, C13. (d) Cullen, W. R.; Einstein, F. W. B.; Huang, C.-H.; Willis, A. C.; Yeh, E.-S. *J. Am. Chem. Soc.* **1980**, *102*, 988. (e) Hayashi, T.; Mise, T.; Fukushima, M.; Kagotani, M.; Nagashima, N.; Hamada, Y.; Matsumoto, A.; Kawakami, S.; Konishi, M.; Yamamoto, K.; Kumada, M.

- Bull Chem. Soc. Jpn.* **1980**, *53*, 1138. (f) Hayashi, T.; Kumada, M. *Acc. Chem. Res.* **1982**, *15*, 395. (g) Hayashi, T. In *Organic Synthesis: An Interdisciplinary Challenge*; Streith, J., Prinzbach, H., Schill, G., Eds.; Blackwell: 1985; 35. (h) Hayashi, T.; Kumada, M. In *Asymmetric Synthesis*; Morrison, J. D., Ed.; Academic Press: Orlando, FL, 1985; Vol. 5, 147. (i) Hayashi, T. *Pure Appl. Chem.* **1988**, *60*, 7. (j) Togni, A.; Breutel, C.; Schnyder, A.; Spindler, F.; Landert, H.; Tijani, A. *J. Am. Chem. Soc.* **1994**, *116*, 4062.
8. Trouve, G.; Broussier, R.; Gautheron, B.; Kubicki, M. M. *Acta Cryst.* **1991**, *C47*, 1966.
9. Rudie, A. W.; Lichtenberg, D. W.; Katcher, M. L.; Davison, A. *Inorg. Chem.* **1978**, *17*, 2859.
10. Dubois, D. L.; Eigenbrot, C. W., Jr.; Miedaner, A.; Smart, J. C.; *Organometallics* **1986**, *5*, 1405.
11. (a) Aggarwal, R. P.; Connelly, N. G.; Crespo, M. C.; Dunne, B. J.; Hopkins, P. M.; Orpen, A. G. *J. Chem. Soc., Dalton Trans.* **1992**, 655. (b) Atkinson, F. L.; Christofides, A.; Connelly, N. G.; Lawson, H. J.; Lowyns, A. C.; Orpen, A. G.; Rosair, G. M.; Worth, G. H. *J. Chem. Soc., Dalton Trans.* **1993**, 1441. (c) Carriedo, G. A.; Connelly, N. G.; Perez-Carreno, E.; Orpen, A. G.; Rieger, A. L.; Rieger, P. H.; Riera, V.; Rosair, G. M. *J. Chem. Soc., Dalton Trans.* **1993**, 3031. (d) Boyd, D. C.; Connelly, N. G.; Herbosa, G. G.; Hill, M. G.; Mann, K. R.; Mealli, C.; Orpen, A. G.; Richardson, K. E.; Rieger, P. H. *Inorg. Chem.* **1994**, *33*, 960. (e) Sato, M.; Shintate, H.; Kawata, Y.; Sekino, M. *Organometallics* **1994**, *13*, 1956.
12. Holmes, J. L.; McGillivray, D. *Org. Mass Spectrom.* **1971**, *5(12)*, 1349.
13. (a) Coulson, D. R. *J. Am. Chem. Soc.* **1969**, *91*, 200. (b) Stille, J. K.; Hines, L. F. *J. Am. Chem. Soc.* **1970**, *92*, 1798. (c) Hughes, R. P.; Powell, R. P. *J. Organomet. Chem.* **1972**, *34*, C51. (d) Kampmeier, J. A.; Harris, S. H.; Wedegaertner, D. K. *J. Org. Chem.* **1980**, *45*, 315. (e) Nakayama, T.; Kanai, H. *Bull. Chem. Soc.*

- Jpn.* **1985**, *58*, 16. (f) Kanai, H.; Watabe, Y.; Nakayama, T. *Bull. Chem. Soc. Jpn.* **1986**, *59*, 1277.
14. Lorkovic, I. M.; Christ, C. S.; Wrighton, M. S. Unpublished results.
15. (a) Schrock, R. R.; Osborn, J. A. *J. Chem. Soc. Chem. Commun.* **1970**, 567. (b) Vastag, S.; Heil, B.; Marko, L. *J. Mol. Cat.* **1979**, *5*, 189. (c) Tani, K.; Suwa, K.; Tanigawa, E.; Yoshida, T.; Okano, T.; Otsuka, S. *Chem. Lett.* **1982**, 261. (d) Tani, K.; Suwa, K.; Yamagata, T.; Otsuka, Sei. *Chem. Lett.* **1982**, 265. (e) Tani, K.; Suwa, K.; Tanigawa, E.; Otsuka, Sei. *ACS Symposium Series*, **1982**, *185*, 283. (f) Toros, S.; Kollar, L.; Heil, B.; Marko, J. *J. Organomet. Chem.* **1983**, *253*, 375.
16. (a) Sivak, A. J.; Muetterties, E. L. *J. Am. Chem. Soc.* **1979**, *101*, 4878. (b) Werner, H.; Wolf, J. *Angew. Chem., Int. Ed. Engl.* **1982**, *21*, 296. (c) Meier, E. B.; Burch, R. R.; Muetterties, E. L. *J. Am. Chem. Soc.* **1982**, *104*, 2661. (d) Fryzuk, M. D. *Can. J. Chem.* **1983**, *61*, 1347. (e) Butler, I. R.; Cullen, W. R.; Kim, T.-J.; Einstein, F. W. B.; Jones, T. *J. Chem. Soc., Chem. Commun.* **1984**, 719.
17. (a) Halpern, J.; Riley, D. P.; Chan, A. S. C.; Pluth, J. J. *J. Am. Chem. Soc.* **1977**, *99*, 8055. (b) Halpern, J.; Chan, A. S. C.; Riley, D. P.; Pluth, J. J. *Adv. Chem. Ser.* **1979**, *No. 173*, 16. (c) Fairlie, D. P.; Bosnich, B. *Organometallics* **1988**, *7*, 936. (d) Fairlie, D. P.; Bosnich, B. *Organometallics* **1988**, *7*, 946. (e) Singewald, E. T.; Mirkin, C. A.; Levy, A. D. *Angew. Chem., Int. Ed. Engl.* In press.

Chapter 4

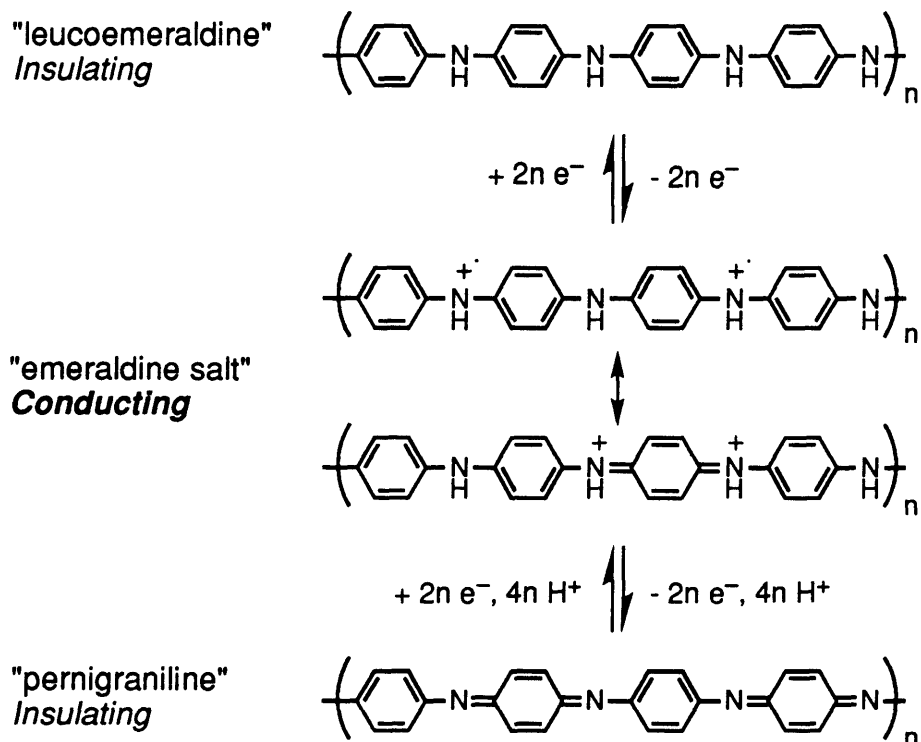
The Potential Dependent Nucleophilicity of Polyaniline

Introduction

In this chapter results are presented which demonstrate electrochemical potential control over the nucleophilicity of the conjugated organic conductor polyaniline. Polyaniline reacts with trifluoroacetic anhydride resulting in partial *N*-trifluoroacetylation. In this reaction, polyaniline displays a continuum of states of nucleophilicity determined by the degree of oxidation of the polymer, allowing electrochemical potential control of the rate of trifluoroacetylation, and thus control of polymer conductivity and electroactivity. In addition, the *N*-trifluoroacetamide moieties may be hydrolyzed to re-form the original conducting polymer.

Polyaniline,¹⁻⁵ while insulating in its colorless polybenzenoid "leucoemeraldine" reduced state, becomes conducting in acidic media when partially oxidized. The "emeraldine salt" state of polyaniline, corresponding to oxidation by 0.5 electrons per repeat unit, exhibits maximum

Scheme 1



conductivity. Further oxidation to 1 electron per repeat unit gives the insulating blue-black polyquinoid “pernigraniline” state, which in all but the most anhydrous non-nucleophilic media is deprotonated.⁶⁻¹² Polyaniline is therefore conducting over a specific range of electrochemical potential. This finite window of high conductivity is typical of conjugated organic conductors.^{9,14} An interesting and unique electrical characteristic, it is the basis of a family of novel microelectrochemical devices, and workers in this laboratory have demonstrated the preparation of a push-pull amplifier based on two different conducting polymers with partially overlapping windows of high conductivity as the device-active materials.¹⁵ It is therefore of great interest to develop methods for introducing controllable well-defined changes in conducting polymer electrochemical properties. A common route to tailoring the properties of conducting polymers is chemical modification of the monomer prior to polymerization. This approach suffers from the complication that the observed polymer properties arise from the influence of a substituent not only on polymer stereoelectronic properties but also on the polymerization reaction.^{16,17} Poor polymerization in turn may result in lower conductivity. There are relatively few reports of altering conducting polymer properties by chemical modification *after* polymerization¹⁸⁻²⁶ and even fewer of which are electrochemically controlled.²⁷ The relative insolubility of most conducting polymers complicates the study of their reactivity and modification. However, when chemical modification is successful, controllable and well-defined changes in polymer behavior may be achieved which are different from those observed after electropolymerization of an analogously modified monomer.^{28,29} In this approach, by controlling the extent of substitution on the backbone it is possible to introduce the changes in polymer properties effected by the substituent to a greater or lesser extent. It is also possible to functionalize the polymer backbone with substituents which are detrimental to, or incompatible with polymerization. Electrochemical potential control of the oxidation state of a conducting polymer allows the electron density along the backbone to be varied

continuously leading to the possibility of tuning reactivity of the polymer substrate by means of an applied voltage. Chris McCoy and I became interested in the nucleophilicity of polyaniline upon observing that its peak conductivity decayed in the presence of trifluoroacetic anhydride if the polymer was held reduced. As part of our research program to develop methods to rationally control materials properties at the molecular level and to study materials possessing electrochemically tunable reactivity, we set out to better characterize the potential dependent reaction of polyaniline with trifluoroacetic anhydride using a combination of electrochemistry and infrared spectroscopy.

Experimental

All starting materials and solvents (reagent grade or better) were purchased from commercial sources and used as received except for aniline, which was distilled from CaH_2 . All infrared spectroscopy was performed on a Nicolet 60SX FTIR spectrometer equipped with a liquid nitrogen cooled $\text{Hg}_x\text{Cd}_{1-x}\text{Te}$ detector. Solution spectra were obtained in 0.2 mm pathlength CaF_2 or NaCl solution cells. UV-Vis spectra were recorded on an HP-8452A diode array spectrophotometer. Electrochemical measurements were performed using a Pine Instruments RDE4 bipotentiostat with a saturated calomel reference electrode and platinum counterelectrode, and a Kipp and Zonen BD90 XY recorder. X-ray photoelectron spectroscopy (XPS) was performed using a Surface Science Instruments (Fisons) SSL-100 spectrometer with an $\text{Al K}_{\alpha 1,2}$ source and a quartz monochromator.

Oligomers. Rates of reaction of **I**, **III** and **V** with trifluoroacetic anhydride were measured at 25.0 °C in 0.2 M $\text{CF}_3\text{CO}_2\text{H}/\text{CH}_3\text{CN}$ by monitoring UV absorbance changes with an Applied Photophysics RX-1000 stopped flow apparatus. Since under these conditions the reaction of **II** to form **V** displayed no spectral change the rate was deduced from a competition experiment where $(\text{CF}_3\text{CO})_2\text{O}$ (150 mg) was added under Ar to a rapidly stirred solution of **I** (190 mg) and **II** (260 mg) in 0.2 M $\text{CF}_3\text{CO}_2\text{H}/\text{CH}_3\text{CN}$ (10 ml) at 25 °C. After evacuation of all volatiles, including $\text{CF}_3\text{CO}_2\text{H}$, the residue was

redissolved in CH₃CN. Using an appropriate calibration solution containing **III** and **V**, the ratio of **III** to **V** formed was measured using GC/MS, integrating ions 280 and 356, respectively, and the rate constant for the trifluoroacetylation of **II** deduced from that for **I**. Electrochemistry of **II**, **V**, and **VI** were performed in a 0.2 M CF₃CO₂H/0.1 M LiClO₄/CH₃CN solution with a 0.07 cm² glassy carbon electrode purchased from Bioanalytical Systems, Inc. XPS Spectra of **V** and **VI** were obtained by casting films from CH₂Cl₂ solutions onto Au-coated Si substrates.

Infrared Spectroscopy and Reactivity Under Electrochemical Potential Control.

Polycrystalline Au films for RIR were prepared by electron beam deposition of a 50 Å Ti adhesion layer followed by 1000 Å of Au on Si₃N₄ coated Si wafers. Electrodes were sonicated in acetone followed by isopropanol prior to use. Polyaniline was electrodeposited onto the bottom 2 cm of 4X1.5 cm pieces of these wafers by cycling the potential of the immersed electrode from 0 to 0.9 V vs SCE at 100 mV/s in a freshly prepared aqueous solution of aniline (0.1 M), NaHSO₄ (0.25 M), and H₂SO₄ (0.5 M) until the peak anodic current at 0.2 V reached 20 mA. After cyclic voltammetric characterization of the polyaniline film by potential cycling between -0.2 and 0.4 V, an RIR spectrum of the fuzzy light green film on the electrode was obtained after emmersion, copious rinsing with water, and drying under a stream of nitrogen. RIR spectra of the polyaniline films on Au were acquired with a 74° angle of incidence at 4 cm⁻¹ resolution. The spectra were linearly (binomial) baseline corrected, first between 2000 and 1400 cm⁻¹, forcing the region between 2000 and 1750 cm⁻¹ to follow the baseline and then between 2000 to 700 cm⁻¹. By this method a constant is added to the absorbance at the frequencies outside the baseline correction window to retain spectral continuity. Prior to exposure to trifluoroacetic anhydride, the electrode was held briefly at the electrochemical potential to be studied in 0.1 M LiClO₄/CH₃CN acidified with F₃CCO₂H to set the oxidation state of the polymer prior to any opportunity to react with the anhydride. The electrode was then quickly immersed under potential control in a solution, temperature controlled to 25.0° C, containing 1.0 M

trifluoroacetic anhydride in a 0.2 M trifluoroacetic acid/0.1 M LiClO₄/CH₃CN solution. After the desired immersion interval, the electrode was removed from the cell and immediately washed thoroughly with water to quench residual anhydride. The cyclic voltammogram of the electrode was recorded in the aqueous deposition solution and an RIR spectrum of the rinsed, dried electrode was obtained. The electrode was then subjected to repeated cycles of exposure to trifluoroacetic anhydride and characterization allowing the progress of the reaction to be followed. The rise in CO absorbance at potentials 0.35 V and more negative was fit to a single exponential. The curves for 0.4 and 0.5 V were fit to a line. All curves were fit excluding the time zero point, since the initial absorbance rise is potential independent. Optically transparent Au films for Transmission FTIR were prepared by electron beam deposition of a 50 Å Cr adhesion layer followed by 100 Å of Au onto a Si wafer. a Cu wire lead was attached to one border of 2 X 2 cm squares of such a wafer using silver epoxy, which was also applied around the entire perimeter of the square. After curing, the silver epoxy border was covered with insulating white epoxy, leaving an effective electrode of dimensions 14 X 14 mm. Polyaniline deposition and reaction under potential control was performed as described above for the reflectance electrodes.

Trifluoroacetamide cleavage reactions were carried out by immersion of the trifluoroacetylated polyaniline-coated electrode in 7% K₂CO₃/5:2 CH₃OH:H₂O at room temperature. Over the course of the reaction the polymer gradually turned deep purple. After exposure to the cleavage reagent, the electrode was rinsed with water and characterized in 0.5 M H₂SO₄ where the normal electrochromic response expected for polyaniline was observed.

Microelectrochemistry. Arrays of 8 individually addressable, platinum band microelectrodes, 1.5 X 80 μm separated by 1.5 μm were fabricated by conventional photolithographic and metallization techniques.^{30,31} The electrodes were cleaned prior to derivitization by cycling in 0.5 M H₂SO₄ from -0.3 to 1.2 V vs SCE. Polyaniline was

deposited onto pairs of adjacent electrodes as described above until current for the polymer oxidation wave reached 12 nA. I_D - V_G characteristics were obtained by sweeping the potential of the two adjacent polyaniline-coated microelectrodes (hooked up to K1 and K2 leads of the RDE4 bipotentiostat) between 0 and +1.1 V vs SCE with a 25 mV drain voltage applied as a negative offset on K2. Polyaniline deposited onto microelectrodes was trifluoroacetylated and subsequently hydrolyzed under the same conditions as the macroelectrodes.

Synthesis.

N-trifluoroacetyl-N'-phenylphenylenediamine (III). Trifluoroacetic anhydride (2.10 g, 10.0 mmol) was added dropwise to a rapidly stirred solution of N-phenylphenylenediamine (1.84 g, 10.0 mmol), **I**, in CH_3CN (20 ml). Volatiles were removed, the residue redissolved in CH_2Cl_2 , and chromatographed on a short silica column, eluting with CH_2Cl_2 . Calcd for $\text{C}_{14}\text{H}_{11}\text{N}_2\text{OF}_3$: C, 60.00; H, 3.96; N, 9.99. Found: C, 59.31; H, 3.81; N, 9.86. IR, CH_3CN , cm^{-1} (ϵ , $\text{M}^{-1}\text{cm}^{-1}$): 3365 (180, NH), 3318 (140, NH), 1722 (670, CO, relative oscillator strength per CO = 1), 1599 (480), 1558 (220), 1519 (720), 1497 (450), 1319 (250), 1289 (290), 1252 (300), 1237 (230, CF_3), 1201 (360, CF_3), 1154 (860, CF_3). $^1\text{H-NMR}$, acetone- d_6 , δ : 10.09, b, 1H ((CO)NH); 7.59, d (8.8 Hz), 2H; 7.48, b, 1H (PhNHPh), 7.23, t (7.4 Hz), 2H, 7.13, m, 4H, 6.85, t (7.2 Hz), 1H. UV-Vis, CH_3CN : 302 nm (23000).

N,N'-bis(trifluoroacetyl)-N-phenylphenylenediamine (IV). Trifluoroacetic anhydride (6 g, 29 mmol) was added to a stirred solution of **I** (2 g, 11 mmol). After 5 minutes the volatiles were removed and the residue taken up in CH_2Cl_2 and chromatographed on a short column of silica, eluting with CH_2Cl_2 . The product was isolated as an amorphous glassy solid. Calc. for $\text{C}_{16}\text{H}_{10}\text{N}_2\text{O}_2\text{F}_6$: C, 51.07; H, 2.68; N, 7.44; F, 30.30. Found: C, 50.41; H, 2.74; N, 7.44; F, 28.93. IR, CH_3CN , cm^{-1} (ϵ , $\text{M}^{-1}\text{cm}^{-1}$): 3301 (120, NH), 1736 (560, CONH), 1726 (620, CONH), 1709 (920, CONAr_2), relative oscillator strength per CO = 1.11, 1610 (160), 1594 (130), 1553 (360), 1513

(470), 1493 (270), 1286 (240), 1231 (880, CF₃), 1205 (1130, CF₃), 1157 (1500, CF₃). ¹H-NMR, CDCl₃, δ: 8.76, b, 1H (NH); 7.6-7.2, m, 9H. UV-Vis, CH₃CN: 254 nm (17000).

N-trifluoroacetyl-N,N'-diphenylphenylenediamine (V). Trifluoroacetic anhydride (2.10 g, 10.0 mmol) was added to a rapidly stirred solution of N,N'-diphenylphenylenediamine (2.60 g, 10.0 mmol) in CH₃CN and the product worked up as for **III**. An analytical sample was prepared by recrystallization from CH₃OH/H₂O. Calcd. for C₂₀H₁₅N₂O₂F₃: C, 67.41; H, 4.24; N, 7.86. Found: C, 67.59; H, 4.57; N, 7.89. IR, CH₃CN, cm⁻¹ (ε, M⁻¹cm⁻¹): 3386 (180, NH), 1705 (800, CO, relative oscillator strength per CO = 1.20), 1597 (540), 1519 (620), 1498 (550), 1323 (310), 1232 (640, CF₃), 1203 (660, CF₃), 1159 (510, CF₃), 1140 (530, CF₃). ¹H-NMR, CDCl₃, δ: 7.4-7.0, m, 14H; 5.88, b, 1H (NH). UV-Vis, CH₃CN: 294 nm (23000).

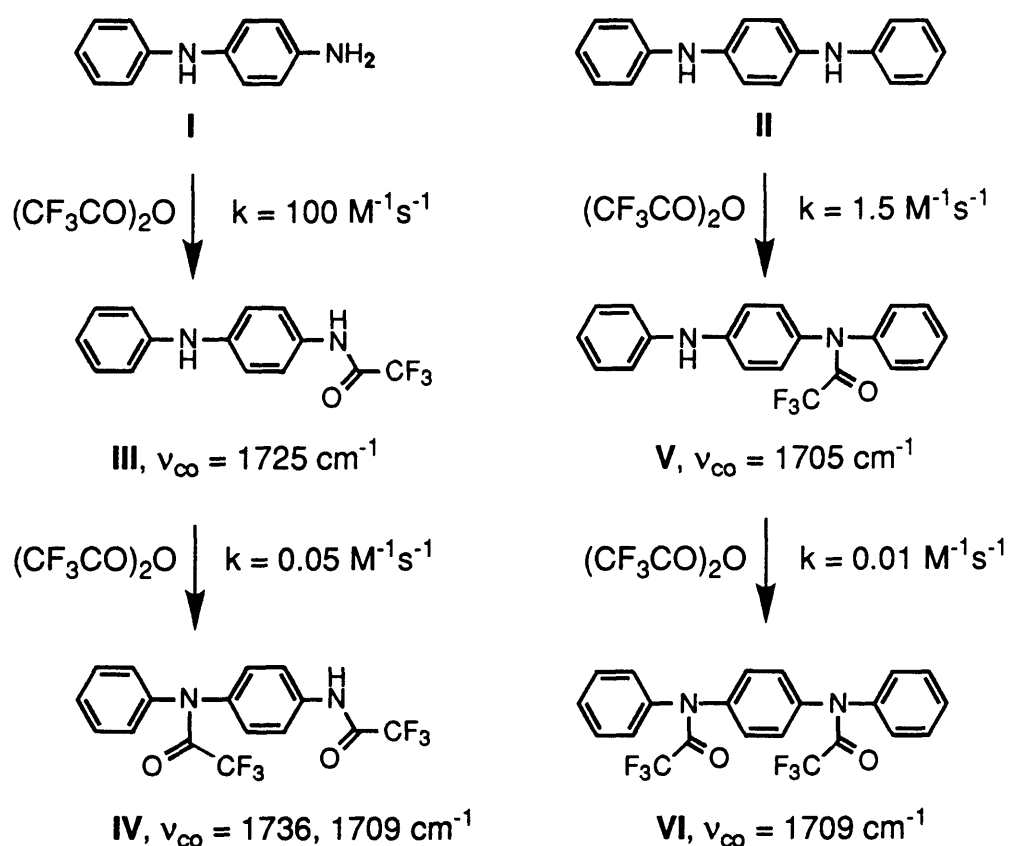
N,N'-bis(trifluoroacetyl)-N,N'-diphenylphenylenediamine (VI).

Trifluoroacetic anhydride (6 g, 29 mmol) was added to a stirred solution of N,N'-diphenylphenylenediamine (2.6 g, 10 mmol) in CH₃CN and the product worked up as for **IV**. An analytical sample was prepared by recrystallization from EtOH. Calcd. for C₂₂H₁₄N₂O₂F₆: C, 58.41; H, 3.12; N, 6.19. Found: C, 58.29; H, 3.24; N, 6.19. IR, CH₃CN, cm⁻¹ (ε, M⁻¹cm⁻¹): 1709 (1390, CO, relative oscillator strength per CO = 1.06), 1594 (200), 1507 (400), 1492 (500), 1229 (1130, CF₃), 1205 (1230, CF₃), 1161 (960, CF₃), 1146 (720, CF₃). ¹H-NMR, CDCl₃, δ: 7.45 - 7.3, m. UV-Vis, CH₃CN: 276 nm (6400), s, 236 nm (18000).

Results and Discussion

Reactivity of aniline oligomers. In order to better interpret the spectroscopic and electrochemical data for the reaction between polyaniline and trifluoroacetic anhydride, first examined was the reactivity towards trifluoroacetic anhydride of two simple oligomeric analogues to polyaniline, *N*-phenylphenylenediamine, **I**, and *N,N'*-diphenylphenylenediamine, **II**. The results are summarized in Scheme 2.

Scheme 2



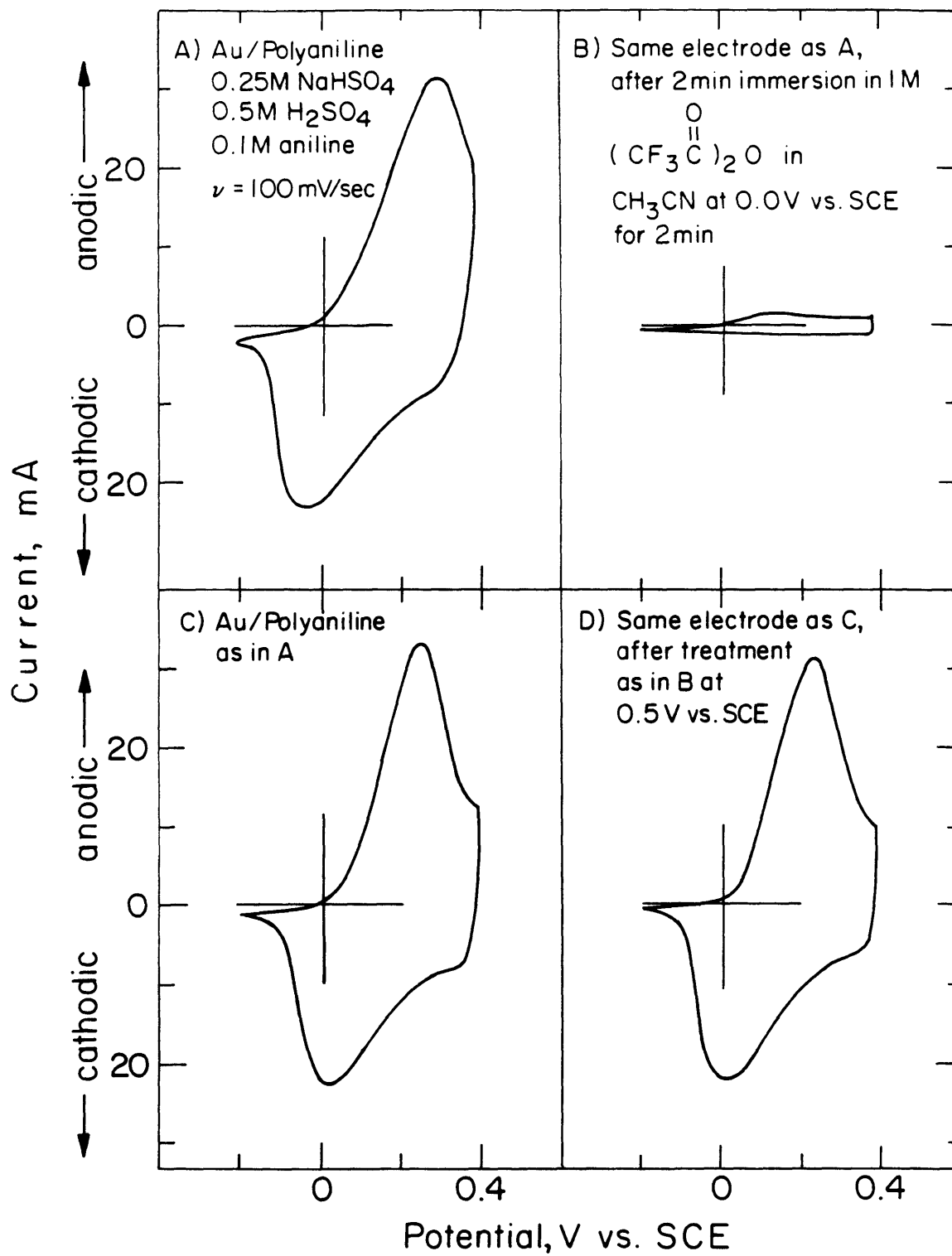
The analogs react quantitatively with trifluoroacetic anhydride at nitrogen to give amides which have characteristic absorptions in the IR at 1705 (internal amide CO), 1725 (terminal amide CO), 1230, 1200, 1160, and 1140 cm^{-1} (CF_3). At 25°C the reaction of **I** with an excess of trifluoroacetic anhydride in a 0.2 M CH_3CN solution of trifluoroacetic acid proceeds stepwise to give *N*-phenyl-*N'*-trifluoroacetylphenylenediamine, **III**, and *N,N'*-bis(trifluoroacetyl)-*N*-phenylphenylenediamine, **IV**, respectively. When 1 equivalent of

trifluoroacetic anhydride is added to a CH_3CN solution of 1 equivalent of **I**, the only product detected, by NMR, IR and GC/MS is **III**, consistent with the terminal amino group of **I** being at least twenty times more reactive than the internal amine, as is confirmed by comparison of the rate constant for initial trifluoroacetylation between **I** and **II**. The reaction of **II** with excess trifluoroacetic anhydride also proceeded stepwise to give *N,N'*-diphenyl-*N*-trifluoroacetylphenylenediamine, **V**, and *N,N'*-diphenyl-*N,N'*-bis(trifluoroacetyl)phenylenediamine, **VI**. In contrast to the reactivity of pyrrole and polypyrrole towards trifluoroacetic anhydride under similar conditions,²⁹ there were no products detected resulting from electrophilic aromatic substitution at carbon.

Having established that polyaniline-like species in solution react with trifluoroacetic anhydride at nitrogen, the reaction of electrode confined polyaniline itself with trifluoroacetic anhydride was studied. To accomplish this, polyaniline was deposited electrochemically onto flat gold macroelectrodes and onto microelectrode arrays. The resulting electrode-confined polymer allowed potential control of the oxidation state of polyaniline during reaction with trifluoroacetic anhydride, and characterization of the reaction product by cyclic voltammetry, specular reflectance FTIR (RIR), and microelectrochemical conductivity measurements.

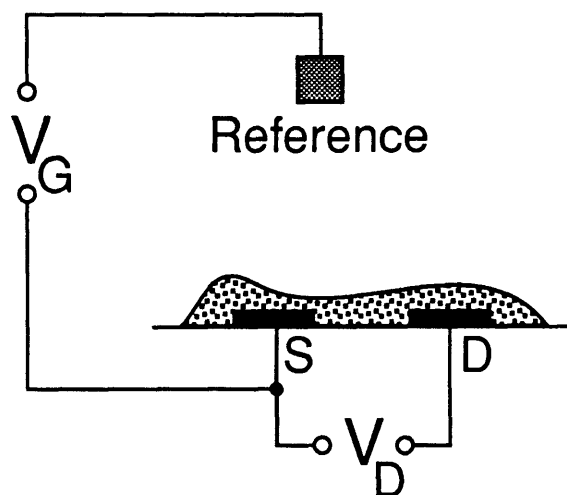
Figure 1 shows cyclic voltammetry of polyaniline electrodeposited onto two Au macroelectrodes before and after immersion under potential control into a 0.1 M $\text{LiClO}_4/0.2$ M $\text{CF}_3\text{CO}_2\text{H}/\text{CH}_3\text{CN}$ solution containing 1.0 M trifluoroacetic anhydride. The polyaniline held at 0.2 V vs SCE shows loss of most of its voltammetric response (without polymer loss, as demonstrated by RIR (*vide infra*)), consistent with loss of polymer conductivity. The polyaniline held at 0.5 V shows virtually no loss in response. While cyclic voltammetry of macroelectrodes provides a guide to the loss of electroactivity of the polyaniline films, characterization of the polymer by I_D - V_G response is more definitive and revealing. Microelectrode arrays have proven useful in the electrochemical characterization

Figure 1. Cyclic voltammetry of polyaniline deposited onto flat gold electrodes ($\Gamma = 1 \times 10^{-6}$ moles of aniline cm^{-2}) before and after exposure to trifluoroacetic anhydride. The electrode at the top was held at 0.2 V vs SCE during exposure to trifluoroacetic anhydride while the bottom electrode was poised at 0.5 V vs SCE.



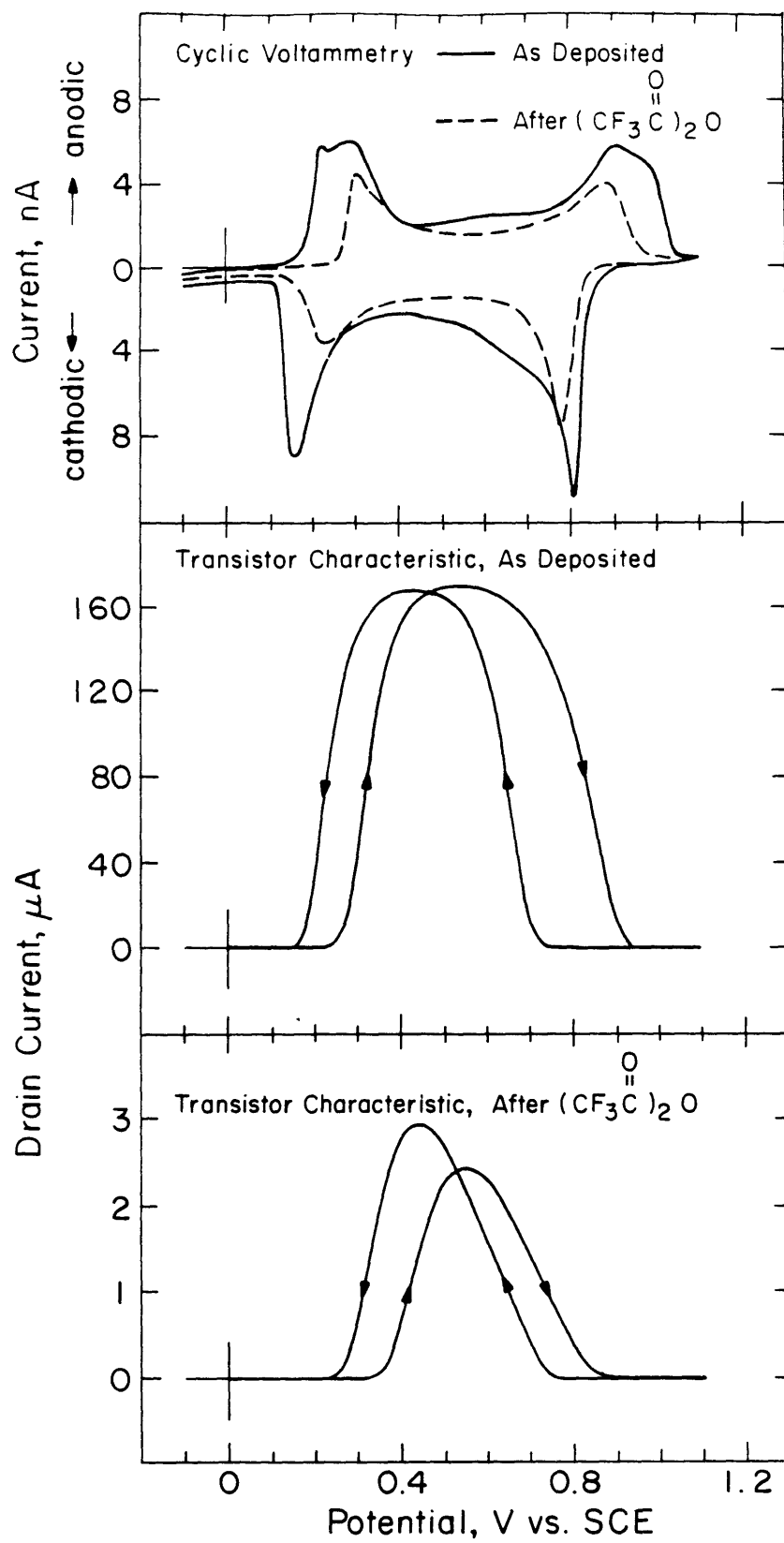
of conducting polymers.^{6,8,13,30,31} The experimental configuration, a microelectrochemical transistor, is shown in Scheme 3. The oxidation state of the polymer

Scheme 3



is controlled by application of gate voltage, V_G , using standard electrochemical potentiostatic control. A small drain voltage, V_D , is applied between two electrodes which serve as source and drain and drain current, I_D , flows when the polymer is in its partially oxidized, conducting state. By scanning V_G and monitoring I_D a profile of conductivity as a function of polymer oxidation state, the transistor characteristic, or I_D - V_G , is obtained. The remarkable durability of polyaniline allows characterization of the full window of conductivity beyond the point of oxidative turn-off in a conventional electrolyte medium without serious degradation, a behavior not shared by other conducting polymers.⁶ Figure 2 shows the cyclic voltammetry and I_D - V_G of a microelectrode array derivatized with electrodeposited polyaniline before and after treatment of the reduced polymer with trifluoroacetic anhydride. Changes in the cyclic voltammogram are not as dramatic as those observed in Figure 1 owing to a lesser degree of trifluoroacetylation; there is a contraction of the electroactive region of the polymer by about 100 mV and some loss in total charge passed. The I_D - V_G , however, is more dramatically affected; the peak conductivity

Figure 2. Cyclic voltammetry and I_D - V_G characteristics for polyaniline deposited onto three adjacent electrodes on a microelectrode array before and after treatment of the derivatized array with 1.0 M trifluoroacetic anhydride in 0.2 M F_3CCO_2H / 0.1 M $LiClO_4$ / CH_3CN .



decreases by a factor of fifty, and the conductive region narrows by about 200 mV without shifting in potential. The greater sensitivity of the I_D - V_G characteristic is not surprising as it has been observed that in many other conducting polymers the I_D - V_G characteristic is effected long before any interpretable change appears in the cyclic voltammogram.³² The changes in polyaniline electrochemistry upon reaction at N with trifluoroacetic anhydride are in stark contrast to those of polypyrrole upon reaction with trifluoroacetic anhydride and poly(3-methylthiophene) with Cl_2 . In both of the latter cases, reaction of the electrophile with the polymer results in potential shifts of up to 0.8 V in the potential of conductivity onset but a comparatively small loss in conductivity (<50%) and no loss in cyclic voltammetric response.^{28,29}

The evolution of RIR spectra for reaction of macroelectrode-confined polyaniline at 0.2 and 0.4 V vs SCE is shown in Figure 3. Bands at 1700 (CO) and 1225, 1200, and 1155 cm^{-1} (CF_3) grow in consistent with N-trifluoroacetylation of polyaniline. Trifluoroacetylation for 150 s at 0.2 V vs SCE is accompanied by a decline in cyclic voltammetric response equivalent to that seen in section B of Figure 1. Note that while the reaction proceeds relatively quickly at 0.2 V vs SCE, acetylation is an order of magnitude slower at 0.4 V vs SCE where polyaniline is partially oxidized. Despite the fact that the RIR spectra in Figure 3 were taken after full electrochemical reduction of the surface confined polyaniline, the spectra resemble those of emeraldine from other reports on the basis of the broad featureless absorbance, increasing at higher frequency (removed by baseline correction for Figure 3), and the high relative intensity of the peak at 1600 cm^{-1} .³³⁻³⁶ Spectra of fully reduced polyaniline have a flat baseline and a very weak absorbance at 1600 cm^{-1} . Some oxidation of the polyaniline is likely to occur rapidly upon taking the electrode out of potential control, by exposure to oxygen during rinsing and drying of the electrode.^{37,38} There was no noticeable evolution of the RIR spectra over 30 min once the electrode was placed in the FTIR sample chamber. Figure 4 shows plots of the trifluoroacetamide carbonyl peak absorbance as a function of trifluoroacetic anhydride

Figure 3. Reflectance IR spectra for electrodeposited polyaniline on flat Au electrodes over the course of exposure to 1.0 M trifluoroacetic anhydride in 0.2 M $\text{F}_3\text{CCO}_2\text{H}$ / 0.1 M LiClO_4 / CH_3CN . The top electrode was poised at 0.2 V vs SCE, while the bottom electrode was poised at 0.4 V vs SCE. Spectral changes corresponding to nitrogen trifluoroacetylation can be seen in both spectra.

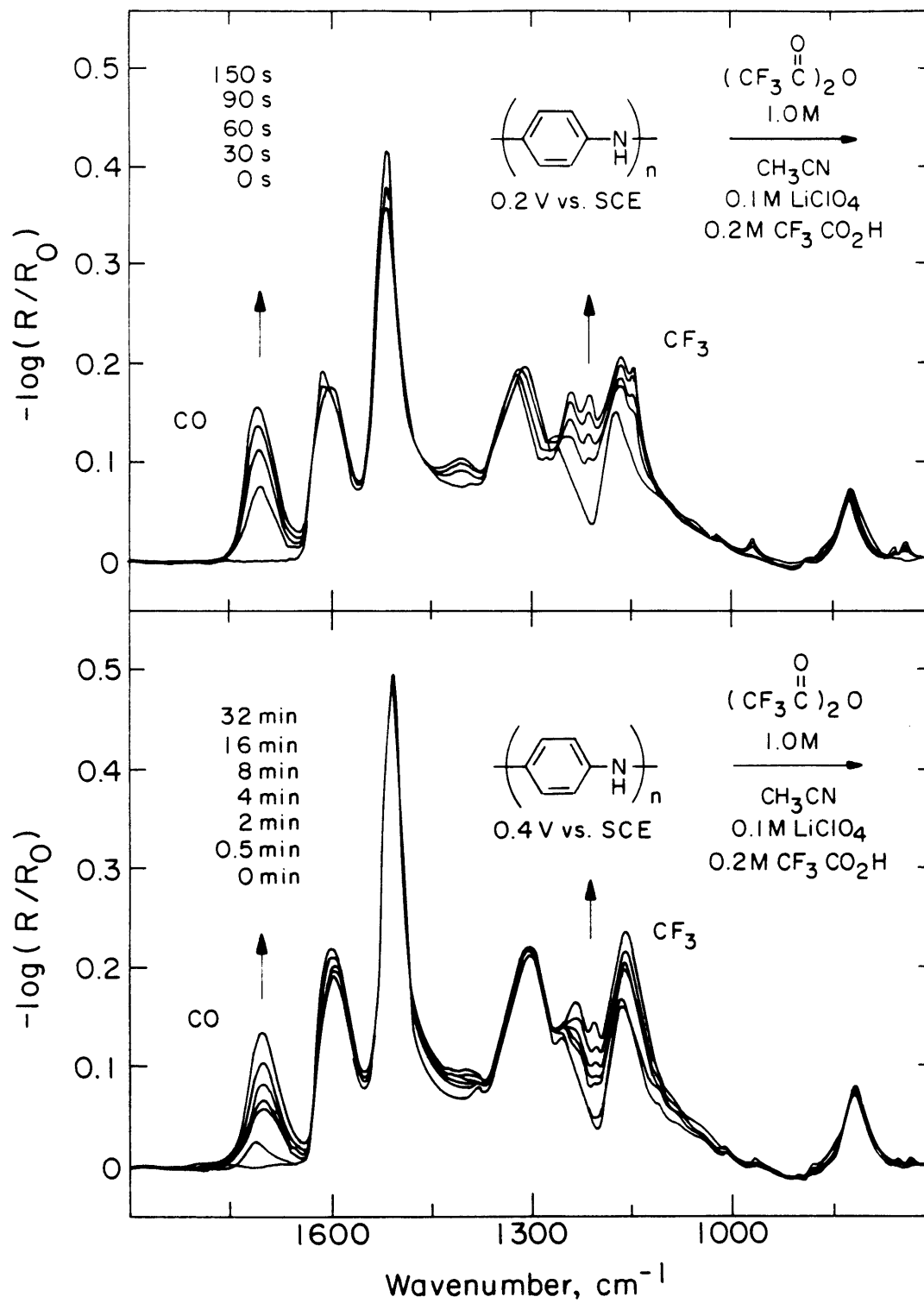
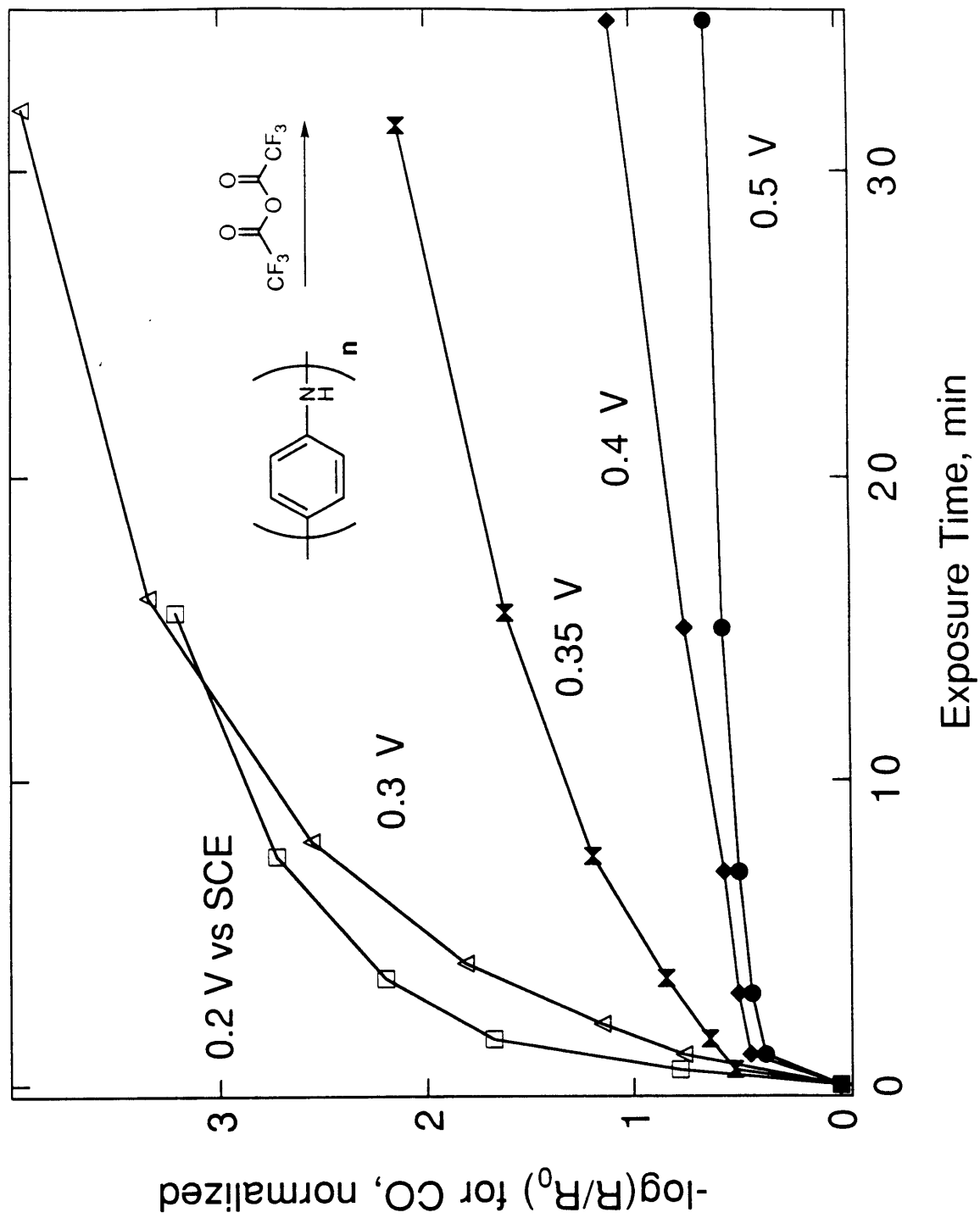


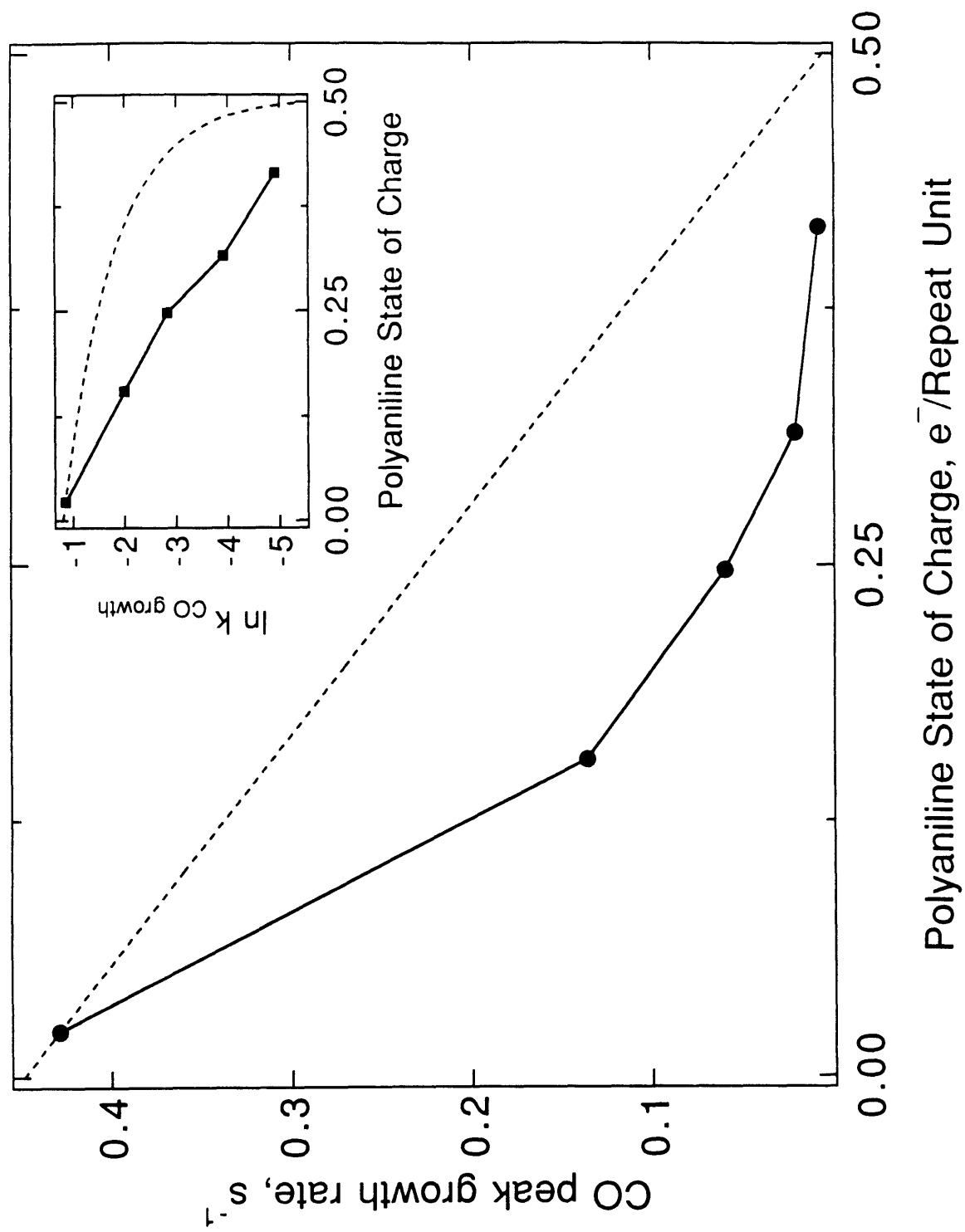
Figure 4. Evolution of $-\log(R/R_0)$ for the reaction of polyaniline on Au electrodes with trifluoroacetic anhydride while poised at different potentials. The carbonyl band "absorbance" is shown as normalized to the absorbance of the unchanging polyaniline 818 cm^{-1} band.



exposure time over a range of electrochemical potentials. There are clearly multiple states of polyaniline reactivity with trifluoroacetic anhydride; the more polyaniline is oxidized the less reactive it becomes. The most obvious changes in reactivity on the laboratory timescale occur at potentials near 0.35 V vs SCE. Since the absorbance of radiation reflected from the films varied from sample to sample, the absorbance of the peak at 818 cm^{-1} (para-substituted arene CH "flapping" mode) was used as an internal standard for the degree of polyaniline trifluoroacetylation, since, as Figure 3 demonstrates, absorbance of this peak changes very little over the course of trifluoroacetylation. Hence the carbonyl absorbance is shown as normalized absorbance, or the ratio of the carbonyl absorbance to that of the peak at 818 cm^{-1} .

There is some confusion as to whether polyaniline, when partially oxidized in acidic media, is best described as having access to a continuum of states of charge on a molecular level, ranging from 0 to 1 electrons per aniline repeat unit, or whether there are only three states: leucoemeraldine, emeraldine salt (0.5 electrons per repeat unit), or pernigraniline (1 electron per repeat unit), and "phase separated" mixtures thereof.^{7,34,39-46} The nucleophilicity of polyaniline may shed some light on this problem. Figure 5 shows the relative rate of CO absorbance rise in Figure 4 plotted as a function of the polyaniline state of charge. The dashed curve showing hypothetical initial reaction rate linearly dependent on degree of oxidation is included for comparison. Polyaniline reactivity with trifluoroacetic anhydride has a higher than first order dependence on polyaniline state of charge. A complication encountered in generating Figure 5 is that polyaniline at a given potential becomes more reduced with a higher degree of trifluoroacetylation, especially at potentials in the vicinity of the peak current of the first redox process, as seen in Figure 2, due to anodic shift in the oxidation potential of the polymer over the course of the reaction. The fractional oxidation state of polyaniline was estimated using the dashed cyclic voltammogram, representing trifluoroacetylated polymer, of Figure 2 since it was deemed

Figure 5. Plot of the rate of CO absorbance growth from Figure 4 versus polyaniline state of charge, in electrons per repeat unit. The polyaniline state of charge was obtained by averaging the anodic and cathodic current of the dashed CV in Figure 3 integrated to the potentials at which the samples were held. It was assumed that the degree of oxidation after the second anodic wave is 1 electron per repeat unit. The dashed line is a hypothetical reaction rate which is linearly dependent on the polyaniline oxidation state.



to best represent an average of degrees of trifluoroacetylation which are followed in Figure 4.

If the discrete states picture of the electronic structure of polyaniline at fractional oxidation states were better, the rate of reaction between trifluoroacetic anhydride and polyaniline would be roughly linearly dependent on the mole fraction of leucoemeraldine, assuming no mass-transport limitations. That is, polyaniline oxidized to 0.25 electrons per repeat unit, "protoemeraldine,"³ should initially react 1/2 as rapidly with trifluoroacetic anhydride as fully reduced leucoemeraldine. If, on the other hand, the degree of polymer oxidation is distributed evenly over the nitrogens of each monomer unit, the state-of-charge dependence of reaction rate should be more logarithmic, and therefore more sensitive to fractional oxidation state. Our results are therefore more consistent with the view that partially oxidized polyaniline in acidified CH₃CN has access to a continuum of charge states, rather than mixtures of the three shown in Scheme 1.

In a set of experiments carried out under identical conditions to the RIR study, the change in conductivity of polyaniline upon exposure to trifluoroacetic anhydride as a function of time was determined for a series of electrochemical potentials of the polymer. Although at potentials where the polyaniline is reduced the conductivity "decay time" is faster than the CO absorbance "rise time," the transition from quick to sluggish reactivity occurs over the 0.3 to 0.4 V range and at 0.6 V >99.9% of the original conductivity was preserved even after 40 min immersion in the trifluoroacetic anhydride solution.¹

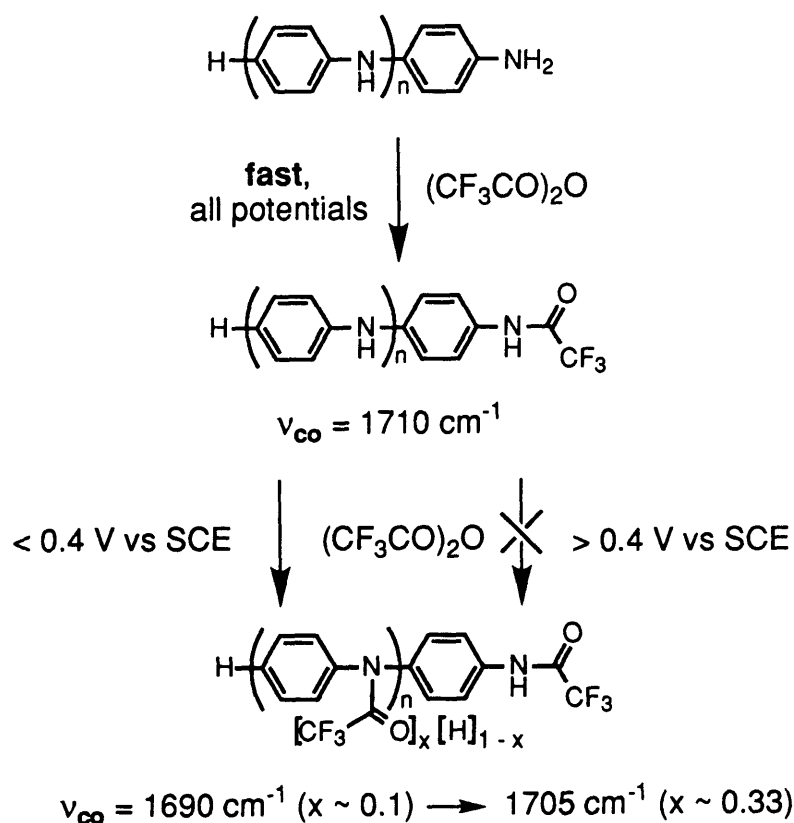
The cyclic voltammetry and I_D - V_G for polyaniline shown in Figure 2 display pronounced hysteresis, another feature typical of conjugated organic polymers which, unlike sluggish kinetics or other sources of quasi-reversibility, is essentially independent of scan rate and arises from an evolution of electronic states upon oxidation.^{4,8,44,45,47} On the return scan, it is necessary to go to a more negative potential to achieve the fully reduced state of the polymer. With thick films there is also the expected normal kinetic component to response which does vary with scan rate. For polyaniline, in acidified

CH₃CN, the hysteresis approaches a lower limit of about 100mV at scan rates down to 0.2 mV/s. For all of the potential dependent reactivity reported here, the potential was approached from the positive side, that is, during polymer re-reduction, where more negative potentials are required for full reduction of polyaniline. Hysteresis was expected to cause polyaniline held at 0.35 V, the potential with the greatest observable change in reactivity for potential change, approached from the reduced (negative) side, to have a more negative state of charge, and therefore higher nucleophilicity, than a polymer held at 0.35 V approached from the oxidized side. It was observed, contrarily, that two polyaniline derivatized electrodes held at 0.35 V vs SCE, one brought to that potential cathodically and one anodically, have indistinguishable reactivity with trifluoroacetic anhydride over periods of up to 10 min. The implication is that, contrary to the slow scan rate cyclic voltammetry results, on the timescale of a few minutes the oxidation state of polyaniline equilibrates to a single level from the initially different states of charge arising from the hysteresis observed in the normal regime of electrochemical scan rates. Charge integration of the cyclic voltammograms in Figure 2 before and after trifluoroacetylation reveal that maximal hysteresis of 0.15 electrons per repeat unit occurs at 0.2 to 0.25 V for the freshly deposited polyaniline, and at 0.25 to 0.3 V for the partially trifluoroacetylated polymer, while hysteresis at 0.35 V is lower, 0.02 and 0.09 electrons per repeat unit for the polymer before and after trifluoroacetylation, respectively. Thus, polyaniline reactivity with a less reactive anhydride such as dichloroacetic anhydride may yet display hysteresis effects since the potentials for maximum observable change in reactivity for potential shift are lower, and overlap more with the region of maximum polyaniline hysteresis, where trifluoroacetic anhydride reacts too rapidly to permit examination of hysteresis effects.¹

An interesting difference between the RIR and microelectrode conductivity data is the fact that IR reveals a rapid, but only partial, reaction with trifluoroacetic anhydride under all conditions, but conductivity declines only when the polymer is in the more reduced states. In RIR an initial, comparatively rapid appearance of a carbonyl band at

$\sim 1710\text{ cm}^{-1}$ is observed in the IR spectra of polyaniline electrodes which does not appear to depend on the electrochemical potential of the polymer. The expectation from a microelectrochemical measurement of conductivity would be a rapid, initial loss of drain current, and yet this is not observed. Instead, polyaniline shows only a slight and gradual loss of conductivity at 0.5 V and no loss whatsoever at 0.6 V even after 40 min. It is proposed that the initial potential-independent trifluoroacetylation is occurring at terminal amino groups of polyaniline, Scheme 4, and this proposition is supported with the following observations.

Scheme 4



First, reaction of **I** with 1 equivalent of trifluoroacetic anhydride produces only **III**, suggesting that terminal amino groups in polyaniline are also more reactive nucleophiles than their internal counterparts. Second, v_{CO} for the terminally trifluoroacetylated

polyaniline analogue **III** is 1725 cm^{-1} , about 20 cm^{-1} higher than for **IV**. Figure 6 shows a plot of trifluoroacetamide carbonyl peak frequency versus “normalized absorbance” for every data point in Figure 4. When the degree of trifluoroacetylation is low, either for short trifluoroacetic anhydride exposure periods of polyaniline held reduced or for longer periods with polyaniline held oxidized, the peak frequency is high, about 1710 cm^{-1} . Intermediate degrees of trifluoroacetylation give a lower peak frequency, down to 1692 cm^{-1} , while more extensive trifluoroacetylation, accompanied by complete loss of polymer electroactivity, yields gradually higher peak frequencies. Consideration of the reactivity towards trifluoroacetic anhydride of **I** and **II** and the spectral features of **III-VI** leads us to conclude that the initial rapid trifluoroacetylation resulting in a higher ν_{CO} is occurring at terminal nitrogens only, and that the subsequent trifluoroacetylation of internal nitrogens in polyaniline gives initially low and gradually increasing peak frequency as trifluoroacetylation makes the polyaniline backbone when fully reduced progressively more electron withdrawing.

In partially oxidized polyaniline most of the charge associated with the polymer oxidation is supported on the nitrogen atom, as depicted in Scheme 1.⁴⁸ Substitution at nitrogen is therefore expected to have a powerful effect on the conducting properties of the polymer. The drastic loss of conductivity upon trifluoroacetylation of nitrogen is much greater than the effect of substitution observed in *N*-alkyl or ring substituted polyanilines.⁴⁹⁻⁶⁰ Table 1 shows solution electrochemical data for oligomers **I-VI**. The greater the degree of trifluoroacetylation of the oligomeric analogues, the more positive and irreversible their electrochemical oxidations. The fully trifluoroacetylated oligomers have redox potentials about 1.5 V more positive of their protonated precursors. The data indicate that oxidation of trifluoroacetylated polyaniline nitrogen gives a much higher energy cation radical than a protonated, or methylated nitrogen cation radical, and thus presents a barrier to hole transport, resulting in lower conductivity than results from *N*-alkylation or ring substitution. This line of reasoning, along with the fact that **I**, which

Figure 6. Peak carbonyl stretching frequency for polyaniline treated with trifluoroacetic anhydride as a function of extent of trifluoroacetylation. Data taken from results shown in Figure 4.

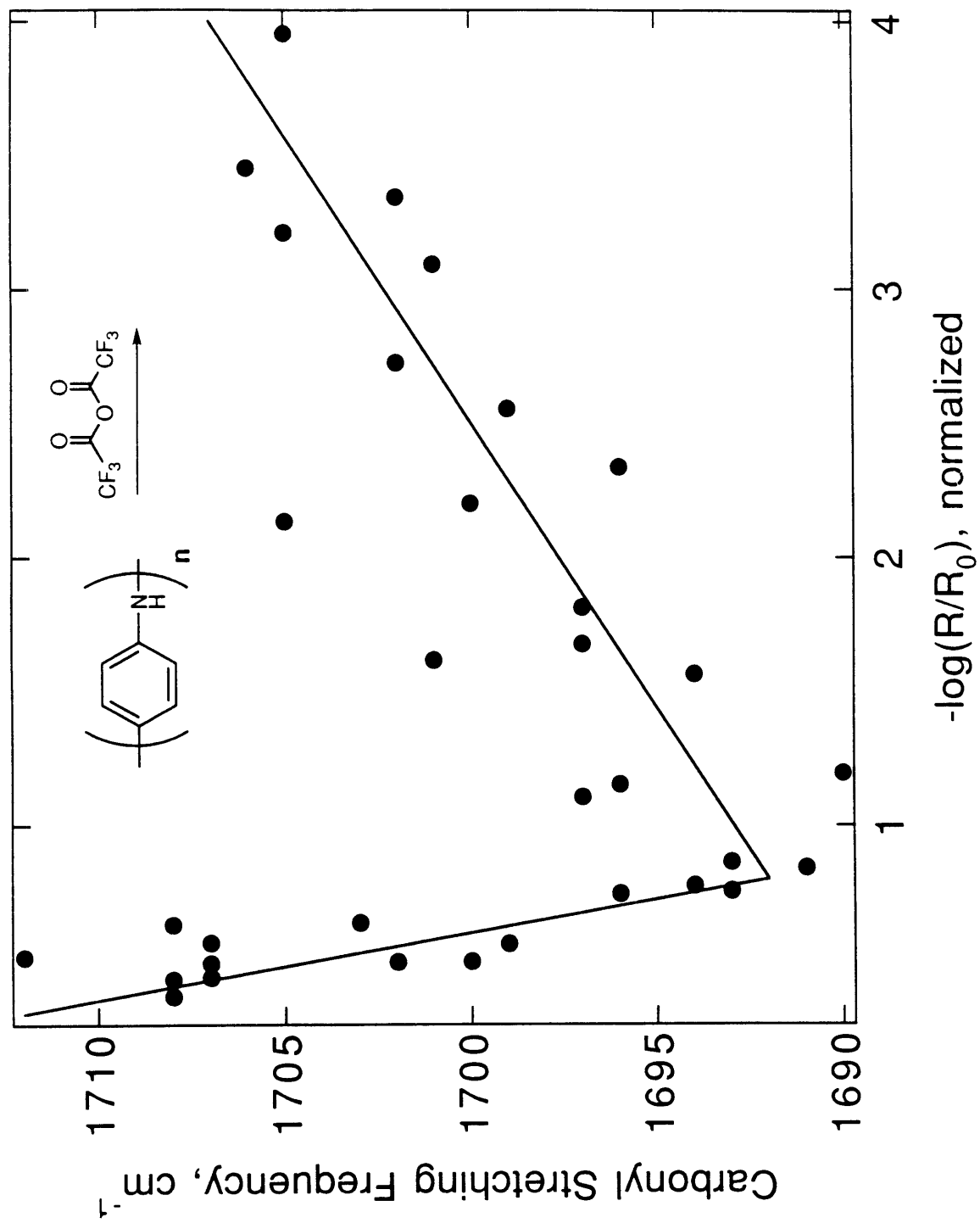


Table 1. Electrochemistry of I-VI.^a

	Potential, V vs SCE ^b	n ^c
I	0.64	1
	0.82	1
II	0.94 (E _{pa})	2
	1.34	1
	1.52	1
	0.80 (2nd scan)	<0.5
	0.70 (2nd scan)	1
III	1.93 (E _{pa})	4
	2.10 (E _{pa})	1
IV	0.48	1
	0.79	1
	1.90 (E _{pa})	4
V	1.00 (E _{pa})	2
	1.45 (E _{pa})	<1
	1.73 (E _{pa})	4
	2.07 (E _{pa})	2
	0.77 (2nd scan)	1
VI	1.95 (E _{pa})	4

^a1 mM analyte in 0.2 M CF₃CO₂H/0.1 M LiClO₄/CH₃CN at 200 mV/s at 23±2° C.

^bE_{1/2} except as noted

^cRelative peak current.

contains a terminal amine, has a higher redox potential than II, may also explain the potential independence of what is proposed to be the initial trifluoroacetylation of polyaniline terminal amino groups and the insensitivity of conductivity to terminal amine trifluoroacetylation. A partially oxidized polyaniline chain with a terminal iminium or aminium radical cation represents a less important resonance form than a chain with an internal aminium radical cation. The terminal amine group is therefore less coupled to the overall degree of oxidation of the polymer chain, retaining charge density and therefore nucleophilicity even when the polymer is partially oxidized. For the same reason, then, since a terminal nitrogen is not an important part of the charge delocalization in partially oxidized polyaniline, terminal amine trifluoroacetylation is not likely to affect polymer conductivity, as is observed.

An interesting question of broad relevance to conduction in organic polymers is what fraction of the nitrogens are trifluoroacetylated at the point at which the polymer has lost most of its electroactivity. This question was first addressed by X-Ray photoelectron spectroscopy, XPS. Results are shown in Table 2. Compounds V and VI were used as standards since they have similar chemical structure to trifluoroacetylated polyaniline. The samples "0.2 V" and "0.5 V" are the same ones studied by RIR in Figure 4, and were held in the trifluoroacetic anhydride for 16 and 32 min, respectively. By comparison with the oligomeric standards, the degree of trifluoroacetylation for the samples held at 0.2 V and 0.5 V vs SCE is found to be about 60% to 20%, respectively.

One limitation of XPS analysis for studying the composition of relatively thick films is that the electron mean free path limits quantitation to only the top 10-50 Å of the surface.⁶¹ A more unambiguously quantitative technique for coverage measurement is transmission IR. Use of electrodes bearing a very thin layer (50-100 Å) of gold allows transmission IR,⁶² but the resistance of the electrode itself gives rise to a voltage drop which results in a gradient of film thickness evident to the naked eye. Beer's law therefore does not obtain. To deposit polyaniline more uniformly, electrodes were prepared with a

Table 2. X-Ray Photoelectron Spectroscopy Data for **V**, **VI**, and for polyaniline trifluoroacetylated at 0.2 V and 0.5 V vs SCE.

XPS			
Integrations^a			
sample	C _{1s} (expected)	N _{1s}	F _{1s} (expected)
V^b	13.0 (10.0)	1	1.24 (1.5)
VI^b	14.3 (11.0)	1	2.26 (3.0)
0.2 V	11.4, 10.3 ^c	1	1.44, 1.36
0.5 V	11.0, 7.8 ^c	1	0.56, 0.40

^a Corrected for element sensitivity.

^b Average of two runs.

^c Not including CO and CF₃ carbons.

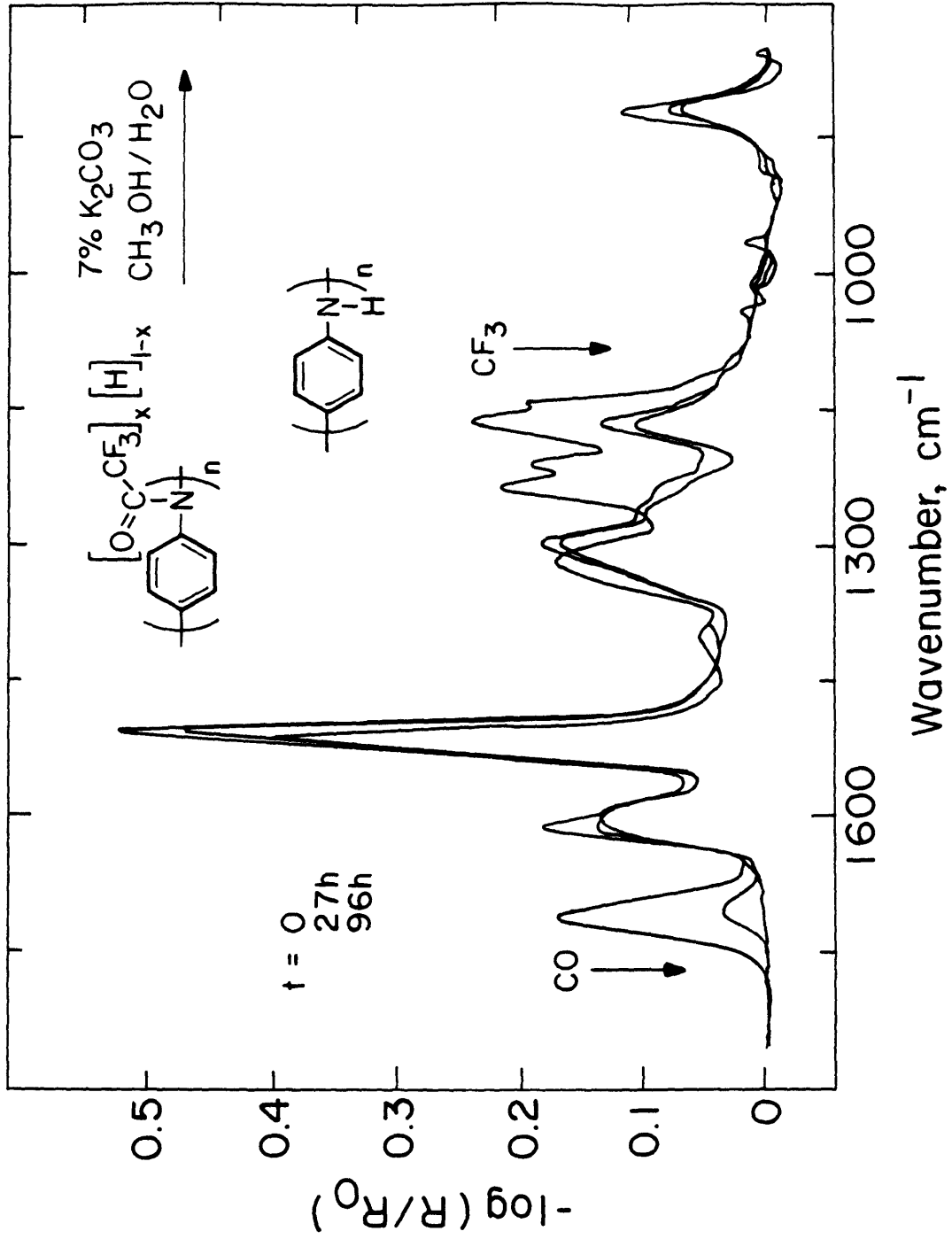
border of conductive silver epoxy to minimize voltage drop. Polyaniline coverage was determined by cyclic voltammetry, and the electrode confined polymer was subsequently trifluoroacetylated as above until >85% of the voltammetric response disappeared. The trifluoroacetyl coverage groups was determined by integrating the absorbance of the trifluoroacetyl peak and dividing by the average integrated extinction coefficient per carbonyl of **III-VI** (determined in CH₃CN) in the same frequency region. The results for 2 experiments were that 20 and 33% of the nitrogens in polyaniline are trifluoroacetylated when the electrochemical response is <15% of the non-trifluoroacetylated polyaniline. Since the transmission IR is sampling the entire thickness of the film, while XPS is sampling only the top 10-50 Å, the coverage calculated based on cyclic voltammetry and transmission IR is considered to be more reliable. One possible reason for the larger percentage trifluoroacetylation calculated by XPS is the greater concentration of terminal amino groups near the surface of the polyaniline, all of which are likely to be trifluoroacetylated. While the comparison of XPS and IR data seem to point to a depth-dependent gradient in extent of trifluoroacetylation, preliminary RIR experiments on polyaniline derivatized macroelectrodes having different thicknesses of electrodeposited polyaniline ranging over a factor of four, showed essentially the same potential dependent rate of normalized CO absorbance rise shown in Figure 4, independent of thickness. The conclusion is that loss of >99% of conductivity occurs when ≈25% of the nitrogens are trifluoroacetylated.

According to Figure 4, the "normalized" value for $-\log(R/R_0)_{CO}$ is five times larger for polyaniline films held reduced for extended periods in the presence of trifluoroacetic anhydride than for those held oxidized. Using the trifluoroacetyl coverage calculated above, and assuming that all of the terminal amino and no internal amino groups are trifluoroacetylated, it is estimated that 5-6% of the nitrogens in polyaniline as prepared here are terminal. It is proposed that reaction of oxidized polyaniline of known molecular weight and polydispersity in an acidic medium with trifluoroacetic anhydride followed by

IR could serve as a good assay for branching,⁶³⁻⁶⁶ since only terminal amino groups will react under these conditions.

While trifluoroacetylation of polyaniline results in nearly complete loss of electroactivity and conductivity of the polymer, the trifluoroacetyl group can be chemically removed to regenerate polyaniline. Amines are often protected as their trifluoroacetamide derivatives.⁶⁷ Trifluoroacetamide hydrolysis can be accomplished with potassium carbonate in 30% aqueous methanol.⁶⁸ This reagent was found to cleave the carbon-nitrogen bond in trifluoroacetylated polyaniline and return the polymer to its initial state displaying a typical I_D - V_G characteristic and cyclic voltammetry for polyaniline. Figure 7 shows the RIR spectral changes accompanying the cleavage reaction on a trifluoroacetylated polyaniline-coated electrode. The RIR spectrum prior to immersion in the cleavage reagent ($t = 0$) shows the CO and CF_3 bands as seen in Figure 3. At the times noted, the electrode was removed from the cleavage solution, rinsed, dried, and characterized by RIR. Note that over the course of exposure to the cleavage reagent the carbonyl and trifluoromethyl absorptions disappear completely, while the cyclic voltammetric response returns. When the trifluoroacetylated polyaniline hydrolysis reaction has proceeded to >80% completion, ν_{CO} remains at a low frequency (1689 cm^{-1}), indicating that only internal trifluoroacetamides remain after longer hydrolysis periods and that the terminal amide groups are therefore hydrolyzed at least as rapidly as internal amides. The recovery of conductivity in polyaniline rendered insulating by trifluoroacetylation is interesting in the context of a device known as an EPROM, or erasable-programmable-read-only-memory, the function of which is to provide semi-permanent set of information to be read and used as required but with the option of erasing and re-writing.⁶⁹ Selective introduction of trifluoroacetyl groups to polyaniline microelectrochemical transistors, several of which may be fabricated in a small area, provides a means of shutting off conductivity of any combination of specific devices allowing electrochemical "writing" of any configuration of states. The device is "read"

Figure 7. RIR spectra following the hydrolysis of trifluoroacetylated polyaniline on flat Au electrodes, showing the regeneration of polyaniline.



electrically and immersion in the cleavage reagent "erases" the device, by restoring conductivity to the acetylated transistors.

In summary, reaction of trifluoroacetic anhydride with the conducting polymer polyaniline confined to electrode surfaces gives trifluoroacetylation of nitrogen. The effect of polyaniline trifluoroacetylation is a drastic loss of conductivity accompanied by a narrowing of the potential window of conductivity, with no significant shift in its potential. The rate of trifluoroacetylation can be attenuated over a range of reactivities by partial oxidation of polyaniline, with a much higher than first order dependence of reactivity on polymer state of charge. Only terminal amine trifluoroacetylation, which has no effect on conductivity, is observed if polyaniline is held oxidized to 0.5 electrons per repeat unit. The trifluoroacetylated polyaniline may be hydrolyzed by base to reform the original polymer with its conductivity and electroactivity restored.

References

1. McCoy, C. H.; Lorkovic, I. M.; Wrighton, M. S. Manuscript submitted.
1. Letheby, H. *J. Chem. Soc.* **1862**, 161-3.
2. Willstätter, R.; Dorogi, S. *Chem. Ber.* **1909**, *42*, 2147.
3. Willstätter, R.; Dorogi, S. *Chem. Ber.* **1909**, *42*, 4118.
4. Green, A. G.; Woodhead, A. E. *J. Chem. Soc.* **1910**, 2388
5. Green, A. G.; Woodhead, A. E. *J. Chem. Soc.* **1912**, 1117.
6. Mohilner, D. M.; Adams, R. N.; Argersinger, W. J., Jr. *J. Am. Chem. Soc.* **1962**, *84*, 3618.
7. Paul, E. W.; Ricco, A. J.; Wrighton, M. S. *J. Phys. Chem.* **1985**, *89*, 1441.
8. Huang, W.-S.; Humphrey, B. D.; MacDiarmid, A. G. *J. Chem. Soc. Faraday Trans. 1* **1986**, *82*, 2385.
9. Ofer, D.; Crooks, R. M.; Wrighton, M. S. *J. Am. Chem. Soc.* **1990**, *112*, 7869.
10. Focke, W. W.; Wnek, G. E.; Wei, Y. *J. Phys. Chem.* **1987**, *91*, 5813.
11. Salanack, W. R.; Lundström, I.; Huang, W.-S.; MacDiarmid, A. G. *Synth. Met.* **1986**, *13*, 291.
12. Genies, E. M.; Boyle, A.; Lapkowski, M.; Tsintavis, C. *Synth. Met.* **1990**, *36*, 139.
13. MacDiarmid, A. G.; Chiang, J.-C.; Halpern, M.; Huang, W.-S.; Mu, S.-L.; Somasiri, N. L. D.; Wu, W.; Yaniger, S. I. *Mol. Cryst. Liq. Cryst.* **1985**, *121*, 173.
14. Ofer, D.; Park, L. Y.; Schrock, R. R.; Wrighton, M. S. *Chem. Mat.* **1991**, *3*, 573.
15. McCoy, C. H. and Wrighton, M. S. *Chemistry of Materials*, **1993**, *5*, 914
16. Diaz, A. F.; Bargon, J. In *Handbook of Conducting Polymers*; Skotheim, T. A., Ed.; Marcel Dekker: New York, 1986; Chapter 3.
17. Roncali, J. *Chem. Rev.* **1992**, *92*, 711.
18. Rubinstein, I. *J. Electrochem. Soc.* **1983**, *130*, 1506.

19. Manohar, S. K.; MacDiarmid, A. G.; Cromack, K. R.; Ginder, J. M.; Epstein, A. J. *Synth. Met.* **1989**, *29*, E349.
20. Yue, J.; Wang, Z. H.; Cromack, K. R.; Epstein, A. J.; MacDiarmid, A. G. *J. Am. Chem. Soc.* **1991**, *113*, 2665.
21. Yue, J.; Gordon, G.; Epstein, A. J. *Polymer* **1992**, *33*, 4410.
22. Patil, A. O.; Ikenoue, Y.; Wudl, F.; Heeger, A. J. *J. Am. Chem. Soc.* **1987**, *109*, 1858.
23. Fabre, P.-L.; Dolger, A. *J. Chem. Res.* **1991**, (S) 16, (M) 0255.
24. Wolf, M.; Wrighton, M. S. *Chem. Mat.* **1994**, *6*, 1526.
25. Wolf, M.; Wrighton, M. S. Submitted
26. Ochmanska, J. Pickup, P. *Can. J. Chem.* **1991**, *69*, 653.
27. Sato, M.; Fushimi, I.; Takahashi, K.; Nakaya, J. *J. Chem. Soc., Chem. Commun.* **1994**, 2373.
28. McCoy, C. H.; Rozsnyai, L. F.; Wrighton, M. S. Submitted.
29. McCoy, C. H.; Wrighton, M. S. Manuscript in preparation.
30. White, H. S.; Kittleson, G. P.; Wrighton, M. S. *J. Am. Chem. Soc.* **1984**, *106*, 5375.
31. Thackeray, J. W.; White, H. S.; Wrighton, M. S. *J. Phys. Chem.* **1985**, *89*, 5133.
32. McCoy, C. H.; Wrighton, M. S. Unpublished results.
33. Lu, F.-L.; Wudl, F.; Nowack, M.; Heeger, A. J. *J. Am. Chem. Soc.* **1986**, *108*, 8311.
34. Shacklette, L. W.; Wolf, J. F.; Gould, S.; Baughman, R. H. *J. Chem. Phys.* **1988**, *88*, 3955.
35. Tang, J.; Jing, X.; Wang, B.; Wang, F. *Synth. Met.* **1988**, *24*, 231.
36. Quillard, S.; Louarn, G.; Buisson, J. P.; Lefrant, S.; Masters, J.; MacDiarmid, A. G. *Synth. Met.* **1993**, *55-57*, 475.

37. Mengoli, G.; Musiani, M. M.; Zotti, G.; Valcher, S. *J. Electroanal. Chem.* **1986**, *202*, 217.
38. Wei, Y.; Hsueh, K.-F.; Jang, G.-W. *Macromolecules* **1994**, *27*, 518.
39. Wudl, F.; Angus, R. O., Jr.; Lu, F. L.; Allemand, P. M.; Vachon, D. J.; Nowack, M.; Liu, Z. X.; Heeger, A. J. *J. Am. Chem. Soc.* **1987**, *109*, 3677.
40. Baughman, R. H.; Wolf, J. F.; Eckhardt, H.; Shacklette, L. W. *Synth. Met.* **1988**, *25*, 121.
41. Javadi, H. H. S.; Treat, S. P.; Ginder, J. M.; Wolf, J. F.; Epstein, A. J. *J. Phys. Chem. Solids* **1990**, *51*, 107.
42. Travers, J. P.; Genoud, F.; Menardo, C.; Nechtschein, M. *Synth. Met.* **1990**, *35*, 159.
43. Shacklette, L. W.; Baughman, R. H. *Mol. Cryst Liq. Cryst.* **1990**, *189*, 193.
44. Glarum, S. H.; Marshall, J. H. *J. Phys. Chem.* **1986**, *90*, 6076.
45. Genies, E. M.; Lapkowski, M. *Synth. Met.* **1987**, *21*, 117.
46. MacDiarmid, A. G.; Chiang, J. C.; Richter, A. F.; Epstein, A. J. *Synth. Met.* **1987**, *18*, 285.
47. Brédas, J.-L.; Street, G. B. *Accs. Chem. Res.* **1985**, *18*, 309
48. Kaplan, S.; Conwell, E. M.; Richter, A. F.; MacDiarmid, A. G. *J. Am. Chem. Soc.* **1988**, *110*, 7647.
49. Wang, S.; Wang, F.; Ge, X. *Synth. Met.* **1986**, *16*, 99.
50. Snauwaert, P. H.; Lazzaroni, R.; Riga, J.; Verbist, J. J. *Synth. Met.* **1987**, *21*, 181.
51. Comisso, N.; Daolio, S.; Mengoli, G.; Salmaso, R.; Zecchin, S.; Zotti, G. *J. Electroanal. Chem.* **1988**, *255*, 97.
52. Dao, L. H.; LeClerc, M.; Guay, J.; Chevalier, J. W. *Synth. Met.* **1989**, *29*, E377.
53. Leclerc, M.; Guay, J.; Dao, L. H. *Macromolecules*, **1989**, *22*, 649.
54. MacDiarmid, A. G.; Epstein, A. J. *Farad. Discuss. Chem. Soc.*, **1989**, *88*, 317.

55. Wang, Z. H.; Ehrenfreund, E.; Ray, A.; MacDiarmid, A. G.; Epstein, A. J. *Mol. Cryst. Liq. Cryst.* **1990**, *189*, 263.
56. Wei, Y.; Hariharan, R.; Patel, S. A. *Macromolecules* **1990**, *23*, 758.
57. Yue, J.; Wang, Z. H.; Cromack, K. R.; Epstein, A. J.; MacDiarmid, A. G. *J. Am. Chem. Soc.* **1991**, *113*, 2665.
58. D'Aprano, G.; Leclerc, M.; Zotti, G. *Macromolecules* **1992**, *25*, 2145.
59. D'Aprano, G.; Leclerc, M.; Zotti, G. *J. Electroanal. Chem.* **1993**, *351*, 145.
60. Storrier, G. D.; Colbran, S. B.; Hibbert, D. B. *Synth. Met.* **1994**, *62*, 179.
61. Seah, M. P.; Dench, W. A. *Surf. Interface Anal.* **1979**, *83*, 391.
62. Kang, D.; Wrighton, M. S. *Langmuir* **1991**, *7*, 2169.
63. Genies, E. M.; Tsintavis, C. *J. Electroanal. Chem.* **1985**, *195*, 109.
64. Genies, E. M.; Lapkowski, M. *J. Electroanal. Chem.* **1987**, *220*, 67.
65. Lapkowski, M. *Synth. Met.* **1990**, *35*, 169.
66. Toshima, N.; Yan, H.; Ishiwatari, M. *Bull. Chem. Soc. Jpn.* **1994**, *67*, 1947
67. L. Greene, T. W.; Wuts, P. G. W. *Protecting Groups in Organic Synthesis* Wiley: New York, 1991 pp. 353-354.
68. Newman, H. *J. Org. Chem.* **1965**, *30*, 1287.
69. N. Horowitz, P.; Hill, W. *The Art Of Electronics*; Cambridge University Press: New York, **1989**. pp. 816-817.